

Lateral string stability of automated vehicle platoons

J. Allelein

DC 2015.075

Master Thesis

Coaches: dr. ir. S. Öncü (TNO)
dr. ir. J. Ploeg (TNO)

Supervisors: prof. dr. ir. N. van de Wouw (TU/e)
prof. dr. H. Nijmeijer (TU/e)

Eindhoven University of Technology
Department of Mechanical Engineering
Dynamics & Control

TNO
Technical Sciences
Department Integrated Vehicle Safety



Eindhoven, October, 2015

Summary

In a world where traffic becomes more congested every year, Intelligent Transport System (ITS) technologies, such as Cooperative Adaptive Cruise Control (CACC), have shown promising results when it comes to providing an environmentally friendly alternative to increase traffic throughput without the construction of more roads. To be able to utilize the potential benefits of platooning to its full extent, it is necessary to fully automate the vehicle, i.e. automated braking/accelerating *and* automated steering. When the preceding vehicle is used as a reference for the lateral control objective, the vehicles become dynamically coupled. When vehicles are coupled in such a way it is necessary to attenuate the effect of disturbances throughout the string of vehicles, such that the lateral stability of a string of vehicles or platoon is guaranteed. In the literature, however, lateral string stability is only guaranteed for a string of finite length. This limits the applicability of these methods.

The goal of this master thesis is to develop a steering controller for vehicles in a platoon, which guarantees stable vehicle following behavior in lateral direction and lateral string stability for a platoon of infinite length. For that purpose, a linearized model is developed which describes the lateral and rotational dynamics of the vehicle. Based on this model, a lateral control strategy is proposed guaranteeing lateral vehicle following and robustness in terms of a wide operating region of different velocities and look-ahead distances. Using the vehicle dynamics model and the developed controller, a closed-loop platoon model is constructed which is used for further (string stability) analysis. The string-stability properties of the platoon are evaluated in the frequency domain by analysing the so-called string stability complementary sensitivity and in time-domain by performing simulations of a lane change maneuver with a platoon consisting out of four vehicles, driving with a constant velocity and different look-ahead distances. It is shown that the proposed control method results in lateral string-stable behavior when used in a platoon of infinite length.

Finally, the controller is implemented in the experimental setup involving real-life vehicles, equipped with the proposed control strategy, and the performance is assessed using a two vehicle platoon. The results of the experiments show that the performance of the platoon in practice is significantly lower than the performance obtained in the model-based study. In particular, lateral string stability could not be achieved within the maximum inter-vehicle distance set by the longitudinal spacing policy. Reasons, for such decreased performance are, firstly, actuator dynamics and delay and sensing delay not accounted for in the models and, secondly, the fact that the controller was manually tuned to deal with sensor inaccuracies in the experimental setup. It is recommended to incorporate the actuator dynamics and delay, and the sensor delay such that the controller design and model-based analysis can be improved. Furthermore, the quality of the measured signals can be improved such that it is possible to achieve a higher performance of the system.

Acknowledgements

After eleven years the day has finally arrived, the day that was inevitable, the day I stop studying and have to start working. This master thesis is the final product of this long journey. A journey which was at times, quite challenging. However, I gained incredible experiences and I met some extraordinary people. These people helped me achieve what I am today and I want to take this opportunity to thank them. First, I would like to thank my supervising professors Henk Nijmeijer and Nathan van de Wouw for their guidance, critical view and support during my thesis. My supervisors at TNO, Jeroen Ploeg and Sinan Öncü. Jeroen, while working with you during my HBO internship, you showed me how interesting and exiting the field of automated vehicles is. Your knowledge about dynamics and control, humor and no nonsense approach made it very pleasant to work with you. Sinan, during my thesis you spent many hours on discussions, testing and reviewing an almost endless stream of reports. Thank you for the many rides back to Eindhoven and sharing your knowledge and experiences about life and lateral control, it was a great pleasure working together with you on this challenging topic. Next, I want to thank a very long list of people: my colleagues and fellow students at TNO, for the great time during my internship and master thesis; the guys of "Tafel 1", who reminded me that it is also important to have a life outside university; my roommates, for making the Boschdijk one of the best places to live in Eindhoven; my family for all the support they gave me over the last couple of years, especially, my brother and sister. Finally, I want to thank the one person who gave me the energy, love and support to keep on going when things got tough, the person that puts a smile on my face every morning, my girlfriend Liana.

Nomenclature

Roman symbols

A	system matrix	n	length of the platoon
\underline{A}	direction cosine matrix	P	plant model
\bar{A}	system matrix interconnected string	S	sine
B	input vector	\mathcal{S}	set of velocities
\bar{B}	input vector interconnected string	\mathcal{T}	set of look-ahead distances
C	cornering stiffness, cosine	T	transformation matrix
C_{L_a}	transformation matrix	V	velocity
I	moment of inertia	\bar{V}	linearized velocity
K	controller gains matrix	x	state vector, longitudinal direction
\mathcal{K}	set of vehicles	\bar{x}	state vector interconnected system
l	distance to center of mass of the vehicle	y	lateral direction
L_a	look-ahead distance	\bar{y}	global linearized lateral position
m	mass	\dot{y}	global linearized lateral velocity

Greek symbols

δ	steer input
$\bar{\delta}$	linearized steer input
Γ	string stability complementary sensitivity
ψ	heading angle
$\bar{\psi}$	linearized heading angle
$\dot{\psi}$	yaw-rate
$\dot{\bar{\psi}}$	linearized yaw-rate

Subscripts

el	errors at the look-ahead point
e	errors at the center of mass
e_i	errors of vehicle i
f	front axle
fb	feedback
ff	feedforward
$i; j$	indices
r	rear axle, reference point
r_l	rear bumper
v_i	lateral direction of vehicle i
v_l	look-ahead point
y_i	lateral direction of vehicle i

Miscellaneous

cm	center of mass
LQR	Linear Quadratic Regulator
\vec{r}	position vector
\vec{V}	velocity vector
$\dot{\vec{V}}$	acceleration vector
$\ \cdot\ _{\mathcal{H}_\infty}$	\mathcal{H}_∞ system norm

Contents

Summary	iii
Acknowledgements	v
Nomenclature	vii
1 Introduction	1
1.1 Background	1
1.2 Design approach	2
1.3 Problem statement and approach	4
1.4 Outline	5
2 Modelling of the lateral dynamics	7
2.1 Lateral vehicle dynamics	7
2.2 Lateral error dynamics derivation	9
2.2.1 Linearized error dynamics	14
2.3 Linearized lateral error dynamics with look-ahead distance	15
2.4 Conclusion	17
3 Lateral vehicle control	19
3.1 Controller requirements	19
3.2 Controller synthesis	20
3.3 Pole location analysis	23
3.4 Time-domain simulation results to a step input	24
3.5 Conclusion	27

4 Lateral string stability analysis	29
4.1 Interconnected vehicle string model	29
4.2 String stability analysis	33
4.3 Feed-forward design	34
4.4 Time-domain simulation results of a lane change manoeuver	37
4.5 Conclusion	42
5 Experimental results	45
5.1 Experimental setup	45
5.2 Implementation challenges	46
5.3 Experimental results	48
5.4 Conclusion	50
6 Conclusions & Recommendations	53
6.1 Conclusions	53
6.2 Recommendations	54
Bibliography	57
Appendix A Single-track vehicle model	59
Appendix B Error dynamics derivation with look-ahead distance	67
Appendix C Tuning LQR weighting gains	75
Appendix D Error dynamics between two vehicles	93
Appendix E Time-domain simulation results of a lane change manoeuver	101

Chapter 1

Introduction

In a world in which traffic becomes more congested every year, governments, research institutes and automotive OEM's are searching for solutions which minimize the economic and environmental affects of traffic jams. While a fast and often adopted method is the construction of more roads, in heavily populated areas, for example in The Netherlands, this is not always feasible. A more worthwhile and environmentally friendly alternative is to make use of Intelligent Transport System (ITS) technologies such as cooperative automated driving. Thereby, it is possible to drive with smaller inter-vehicle distances and therewith make better use of the available road network (Arem et al., 2006). TNO and others have already shown that promising results can be achieved in reducing shockwaves and increasing throughput by exploiting longitudinal automation (Naus et al., 2010; Ploeg, 2014). To be able to utilize the potential benefits of platooning to its full extent, the next step is to fully automate the vehicle, i.e. automated braking/accelerating *and* automated steering. This provides the possibility to automatically perform more complex manoeuvres such as merging or lane changes.

1.1 Background

Since the 1990's, research has been conducted to increase traffic flow by enabling vehicles to drive in an automated a fashion (Shladover et al., 1991). Already in the 1970's (Peppard, 1974) the observation was made that, when it is possible to attenuate the longitudinal shockwave propagation along a string of vehicles, it would be possible to increase traffic flow. This notion of shockwave attenuation is known as string stability (Swaroop and Hedrick, 1996; Swaroop, 1997). Extensive research has been conducted in understanding and developing control methods with guaranteed string stability in longitudinal direction. However, the absence of a controller design method which also assesses the string stability properties of the controller in lateral direction indicates that there are opportunities for further research in this area.

Bergenhem et al. (2012) provide an overview of research projects conducted on the control of vehicle platoons, in both, longitudinal and lateral direction. Five different projects are presented: SARTRE - a European platooning project; PATH - a California traffic automation program that includes platooning; Grand Cooperative Driving Challenge (GCDC) - a cooperative driving initiative; SCANIA platooning and; Energy ITS - a Japanese truck platooning project. Of these five

projects SARTRE, PATH and Energy ITS focus on both longitudinal and lateral control. PATH and Energy ITS use systems which are highly depending on the infrastructure, either via a reference signal embedded in the road or via lane markers on the road. This dependability on the infrastructure makes the systems expensive and vulnerable to weather influences such as snow or mist. Furthermore, situations could occur in which vehicles are driving with such small inter-vehicle spacings that it is not possible to detect the lane markings on the road anymore, for example when the platoon consists of large commercial vehicles such as trucks or buses. Within in the SARTRE project, a vehicle in the platoon follows its preceding vehicle. When a vehicle is following its predecessor, the vehicles become dynamically coupled by the underlying control law. This coupling makes it necessary to be able to attenuate the effect of lateral disturbances through the platoon in order to prevent safety critical situations and ensure proper following behavior when vehicles form a platoon. The study of such lateral string stability properties of platooning systems is the topic of this thesis.

1.2 Design approach

When designing a controller for regulating the lateral movement of a vehicle, several choices have to be made regarding, for example, the sensing method, the vehicle model and the control method.

For lateral control there are two types of sensing methods which can be used, namely, look-down and look-ahead sensing. When look-down sensing is used, a sensor is positioned at the front or at the front and the rear of the vehicle. The lateral deviation with respect to the center line of the road is measured by the sensor, using inductive lines or magnets embedded in the road surface. This sensing method is mainly used in the 90's (Shladover et al., 1991; Hingwe and Tomizuka, 1997). This sensing method relies heavily on the infrastructure which makes it expensive and sensitive to weather conditions. With the reduction in price of radar/LIDAR's and the improvement of camera sensors, the use of sensors shifted in the 2000's to the look-ahead type of sensors (White and Tomizuka, 2001; Papadimitriou et al., 2003; Solyom and Coelingh, 2013). A look-ahead sensor mounted in front of the vehicle is used to detect another vehicle or lane markings on the road (when a camera with image recognition software is used). These sensors can make use of currently available infrastructure, which makes them significantly more cost efficient and flexible compared to look-down sensors. In this thesis, the choice is made to use a look-ahead type of sensor, as this sensor can be used in combination with the existing infrastructure.

Based on the preferred sensing method, a choice has to be made on the type of reference which is going to be used. A look-down sensor can only follow the reference signal on road, while a look-ahead sensor, for example a camera with image recognition software, can be used to follow the lane-markings on the road or a preceding vehicle. When it is desired to only follow a preceding vehicle, the choice can also be made to use a radar or LIDAR. When using a look-ahead sensor to track a reference, which can be on the road or a preceding vehicle, the dynamics between the reference and the vehicle are influenced by the inter-vehicle distance or look-ahead distance, as is shown in White and Tomizuka (2001); Lu and Tomizuka (2003); Solyom et al. (2013). Therefore, depending on the chosen sensing method, the inter-vehicle distance can have an influence on the error dynamics. As mentioned at the end of the previous paragraph, a look-ahead type of sensor is used, in combination with the control objective of following a preceding vehicle. Due to the use of a look-ahead type of sensor, the look-ahead distance has to be incorporated into the dynamical model.

The next step is to choose which type of lateral vehicle model is used, being either kinematic or dynamic. When a kinematic model is used, it is assumed that the tires can always instantaneously

generate the required force needed to achieve a certain lateral acceleration (Rajamani, 2011). Although this is a reasonable assumption at low velocities ($< 5\text{m/s}$), where the deflection of the tire is minimum, at higher velocities, the tire dynamics have a significant influence on the generated lateral forces. The generation of the tire forces can be a highly non-linear process. However, under the condition that the vehicle operates within a region where the side slip angles of the tires are small ($< 0.5^\circ$), the generated tire forces can still be determined based on a linear relation between the cornering stiffness of the tire and side-slip angle of tire (Pacejka, 2005). The side-slip angle is the angle between desired heading of the tire and the actual heading of the tire. The dynamical model of vehicle using this tire model provides a proper representation of the vehicle dynamics in a wide range of different velocities, under the conditions that the side slip angles are small ($< 0.5^\circ$). The lateral controller developed in this thesis, will be designed to operate in a wide range of different velocities, therefore a dynamical model of the vehicle is used.

Now, a choice has to be made on the type of controller which is going to be used and which error(s) are going to be regulated. For example, the choice could be made to only regulate the lateral error and ignore rotational errors, or regulate both the lateral and rotational errors simultaneously. There are a significant number of control methods and approaches available when considering the lateral control of vehicles. Lu and Tomizuka (2003), Papadimitriou et al. (2003) and Hingwe et al. (2000) use a linearized vehicle dynamics model in combination with a loop-shaping method to control the lateral error between two vehicles or two tractor/trailer combinations. In Snider (2009) an extensive comparison study is conducted on different type of lateral control methods, which use either a kinematic or a dynamic vehicle model. This overview includes the lateral control methods and vehicle models used by the teams which reached the first en second place in the 2005 DARPA Grand Challenge and the winner of the 2007 DARPA Urban Challenge. The first three lateral control methods presented are based on a kinematic vehicle model, and reduce the angular error between the desired arc and real arc of the rear axle or regulate the lateral and rotational errors between a point on the desired path and the center of mass of the vehicle, where both linear and non-linear control methods are utilized. The other two methods use a linearized vehicle dynamics model and in combination with a Linear Quadratic Regulator (LQR). Both methods uses the same error dynamics model. However, one application, uses a feed-forward input based on the curvature of the road to improve the response of the system, while the other method uses an output function such that the errors at a look-ahead point in front of the vehicle are regulated. Solyom et al. (2013) presented a method which regulates the lateral error between two vehicles by using a PD-controller with feed-forward input, where the latter employs information obtained via inter-vehicle communication. By using inter-vehicle communication, a two vehicle look-ahead topology can be achieved. In this thesis, a LQR-controller design approach will be used. This method provides the ability to be robust against a wide operating region of the different velocities and inter-vehicle distances.

The performance of a platoon can be assessed by evaluating the stability of the string of vehicles. In literature there are various definitions available on string stability. However, in general, string stability is used to quantify if the value of a certain signal, e.g. accelerations, velocities or errors, amplify while traveling upstream through a string of interconnected systems. Over the years a significant amount of attention is spent on the development of methods for determining longitudinal string stability of vehicle platoons (Peppard, 1974; Swaroop, 1997; Ploeg et al., 2014). When vehicles are following the road, lateral string stability is not an issue. All vehicles in the platoon control their lateral position based on the lane-markers on the road, and thereby, there is no coupling between the vehicles in terms of the lateral dynamics. Due to the absence of coupling, the lateral error from one vehicle does not propagate to the next. However, when the preceding vehicle is used as a reference, lateral string stability becomes an issue. The movement of one vehicle

in the platoon directly influences the behavior of the next. Lateral string stability has received an increasing attention by researchers over the last couple of years. There are several definitions available for determining lateral string stability of interconnected systems. Seiler et al. (2003) investigate lateral string stability of bird V-formations using the \mathcal{H}_∞ norm of the complementary sensitivity between bird i and bird $i - 1$. Papadimitriou and Tomizuka (2004) are one of the first to evaluate whether their developed approach results into laterally string stable behavior of a platoon of vehicles using the \mathcal{L}_∞ gain of the lateral error. Khatir and Davison (2005) assess string stability of the platoon by evaluating the maximum singular values of the transfer function matrices of the lateral or rotational position between two consecutive vehicles. Solyom et al. (2013) determine \mathcal{L}_2 string stability of the lateral error between two consecutive vehicles. Due to the use of two-vehicle look-ahead control topology, their definition for string stability depends on which vehicle in the platoon is considered. The string stability definition for the first three vehicles is different compared to the other vehicles in the platoon. The methods presented until now only determine string stability in lateral direction. However, it is also possible to simultaneously consider longitudinal and lateral string stability, which is known as mesh stability. Pant et al. (2001) investigate mesh stability for a set of point masses for a cluster of unmanned aerial vehicles using the \mathcal{L}_1 -norm of the impulse response which is the equivalent of the \mathcal{L}_∞ -gain. For the analysis of string-stability properties of the platoon the work of Ploeg (2014) is used and strict \mathcal{L}_2 string stability is evaluated.

Of the five platooning projects presented in Section 1.1, only the SARTRE project addresses the issue of the lateral string stability, in relation to the dynamic coupling between the vehicles. In Solyom et al. (2013), the lateral string stability properties of the platoon in the SARTRE project are assessed. However, within SARTRE, lateral string stability is only guaranteed for a finite length of the platoon. This obstructs the scalability of the lateral controller method used and imposes a significant limitation when it comes its practical use. Therefore, a new lateral control method is necessary which guarantees lateral string stability for a platoon on infinite length such that scalability of the control method can be guaranteed.

1.3 Problem statement and approach

The aim of this master thesis is to develop a steering controller for vehicles in a platoon, which guarantees stable vehicle following behavior in lateral direction and lateral string stability for a platoon of infinite length. This steering controller should be, in a wide operating region, robust against changing velocity and changing look-ahead distances, while respecting actuator bandwidth and have a velocity depending steer input for safe driving behavior.

For the development of the steering controller, the following step-wise approach is used:

- modelling of the lateral vehicle dynamics;
- synthesizing the steering controller based on this model;
- modelling of the closed-loop platoon dynamics using the steering controller;
- model-based analysis of the closed-loop platoon dynamics to evaluate if the developed steering controller results in lateral string stability of the platoon;
- experimental analysis of the closed-loop platoon dynamics to evaluate the performance of the developed steering controller in an experimental setup;

1.4 Outline

This master thesis report is organized as follows. In Chapter 2, the dynamic models used in this master thesis are presented, Chapter 3 focusses on synthesizing the steering controller and analyzing the influence of velocity and look-ahead distance on the transient response of one vehicle. In Chapter 4, a closed-loop model of a platoon or interconnected string is presented and the lateral string-stability properties are investigated. Chapter 5 presents experimental results obtained by implementing the developed controller in a platoon consisting of two experimental vehicles. Finally, Chapter 6 contains the conclusion and recommendations of this master thesis.

Chapter 2

Modelling of the lateral dynamics

To utilize the potential benefits of platooning, a vehicle needs to be fully automated, i.e. incorporating both automated accelerating/braking and automated steering. In this chapter, the dynamic models are presented which are used for the synthesis and analysis of the steering controller proposed in Chapter 3. TNO uses a Toyota Prius as prototype platform for the development of ITS technologies; this vehicle is equipped with a radar and a camera such that it can detect the lane markers on the road or a preceding vehicle. The error-dynamics model should be representative for both situations, irrespective of whether the road or a vehicle is being followed. This chapter is organized as follows. In Section 2.1, the linearized vehicle model is presented and in Section 2.2 the error dynamics are derived between the center of mass of a vehicle and a reference point. In Section 2.3 the error dynamics model is extended such that the look-ahead distance is incorporated into the model and Section 2.4 contains the conclusion of this chapter.

2.1 Lateral vehicle dynamics

One of the first steps in the design process of a lateral controller is to obtain a model of the lateral vehicle dynamics. Therefore, in this section a model of the lateral vehicle dynamics is presented. The lateral dynamics of vehicle can be derived using a so-called single-track vehicle model. A single-track vehicle model is a simplified vehicle where both tires of the front or rear axle are lumped together into an 'equivalent' tire. Furthermore, it is assumed that the height of the center of mass of the vehicle is zero and that the tires are positioned flat on the road surface. In Appendix A, the single track vehicle model is used to obtain a linearized lateral vehicle dynamics model. In Figure 2.1, the linearized single track vehicle model for vehicle i is presented, where \bar{V}_{x_i} and \bar{V}_{y_i} are the longitudinal and lateral velocity of the vehicle, where index i indicates the vehicle number. Both velocities are defined with respect to vehicle frame $\bar{\epsilon}^i$ and (\cdot) notation refers here to the linearized states. $\bar{\psi}_{v_i}$ is the rotation angle of the vehicle frame $\bar{\epsilon}^i$ with respect to the global frame $\bar{\epsilon}^0$ and $\bar{\delta}_i$ is the steering angle of the vehicle, respectively. l_f and l_r are the distances from the center of mass (abbreviated from hereon with *cm*) of the vehicle to the front and rear axle, respectively. For further details on the modelling, we refer to Appendix A.

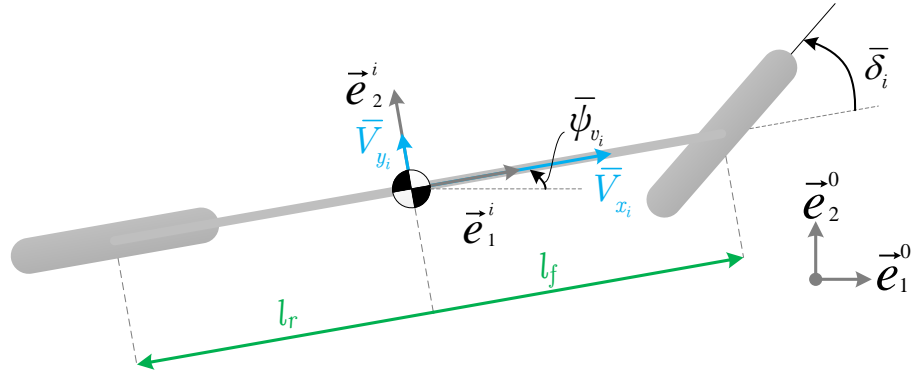


Figure 2.1: Schematic representation of a single-track vehicle model.

The linearized vehicle dynamics model, as derived in Appendix A, see Equation (A.21), is repeated here for convenience:

$$\begin{bmatrix} \dot{\bar{V}}_{y_i} \\ \ddot{\bar{V}}_{y_i} \end{bmatrix} = \begin{bmatrix} -\frac{C_f + C_r}{m\bar{V}_x} & -\frac{C_f l_f - C_r l_r}{m\bar{V}_x} - \bar{V}_x \\ -\frac{C_f l_f - C_r l_r}{I_z \bar{V}_x} & -\frac{C_f l_f^2 + C_r l_r^2}{I_z \bar{V}_x} \end{bmatrix} \begin{bmatrix} \dot{\bar{V}}_{y_i} \\ \ddot{\bar{V}}_{y_i} \end{bmatrix} + \begin{bmatrix} \frac{C_f}{C_f l_f} \\ \frac{C_f}{I_z} \end{bmatrix} \bar{\delta}_i, \quad (2.1)$$

where $\dot{\bar{V}}_{y_i}$ is the lateral acceleration of vehicle i with respect to vehicle frame \bar{e}^i and C_f and C_r are the cornering stiffness of the front and rear tire, respectively. Furthermore, $\dot{\bar{\psi}}_{v_i}$ and $\ddot{\bar{\psi}}_{v_i}$ are the angular velocity and acceleration of vehicle i , both, with respect to global frame \bar{e}^0 . To be able to use this model for simulation purposes of the platoon model, a coordinate transformation has to be performed from the vehicle frame \bar{e}^i to the global frame \bar{e}^0 . From Rajamani (2011), the following linear relations can be obtained:

$$\begin{aligned} \bar{V}_{y_i} &= \dot{\bar{y}}_{v_i} - \bar{V}_x \dot{\bar{\psi}}_{v_i}, \\ \dot{\bar{V}}_{y_i} &= \ddot{\bar{y}}_{v_i} - \bar{V}_x \dot{\bar{\psi}}_{v_i}, \end{aligned} \quad (2.2)$$

where $\dot{\bar{y}}_{v_i}$ and $\ddot{\bar{y}}_{v_i}$ are the linearized global lateral velocity and acceleration of vehicle i , respectively. Next, by substituting (2.2) into (2.1) and choosing a state vector as $x_i = [\bar{y}_{v_i} \ \dot{\bar{y}}_{v_i} \ \bar{\psi}_{v_i} \ \dot{\bar{\psi}}_{v_i}]$, the lateral vehicle dynamics model for vehicle i with respect to the global frame can be written as follows:

$$\dot{x}_i = Ax_i + B\bar{\delta}_i \quad i \in \mathcal{K}_n, \quad (2.3)$$

where $\mathcal{K}_n = \{i \in \mathbb{N} | 1 \leq i \leq n\}$ is the set of identical vehicles, which results a homogeneous platoon with length $n \in \mathbb{N}$ and with

$$A = \begin{bmatrix} 0 & 1 & 0 & 0 \\ 0 & -\frac{C_f + C_r}{m\bar{V}_x} & \frac{C_f + C_r}{m} & -\frac{C_f l_f - C_r l_r}{m\bar{V}_x} \\ 0 & 0 & 0 & 1 \\ 0 & -\frac{C_f l_f - C_r l_r}{I_z \bar{V}_x} & \frac{C_f l_f - C_r l_r}{I_z} & -\frac{C_f l_f^2 + C_r l_r^2}{I_z \bar{V}_x} \end{bmatrix} \quad \text{and} \quad B = \begin{bmatrix} 0 \\ \frac{C_f}{m} \\ 0 \\ \frac{C_f l_f}{I_z} \end{bmatrix}.$$

2.2 Lateral error dynamics derivation

The objective of the lateral controller design is for the *cm* of the vehicle (v) to follow a point of reference (r). This can be achieved by regulating the lateral and rotational errors between these two points to zero. In Figure 2.2, a schematic representation of the lateral control problem is presented, which will be used to derive the lateral and rotational errors between the center of mass of the vehicle and the reference point r . For the derivation of the error dynamics three reference frames are introduced, a global frame, a frame attached to the vehicle and, a frame attached to the reference point, respectively. The global right-hand frame is defined, with the orientation of a set $\underline{\vec{e}}^0 := [\ \vec{e}_1^0 \ \vec{e}_2^0 \ \vec{e}_3^0]^T$ of three mutually orthogonal unit vectors \vec{e}_1^0 , \vec{e}_2^0 and \vec{e}_3^0 . The *cm* of the vehicle is positioned in the origin of frame $\underline{\vec{e}}^1$, which is fixed to the vehicle body. Furthermore, frame $\underline{\vec{e}}^1$ consist, likewise to frame $\underline{\vec{e}}^0$, of a set of three mutually orthogonal unit vectors \vec{e}_1^1 , \vec{e}_2^1 and \vec{e}_3^1 , where vector \vec{e}_1^1 is oriented in the forward direction along the center axis of the vehicle. The error dynamics, between the *cm* of the vehicle and the reference point r are derived with respect to frame $\underline{\vec{e}}^2$. Frame $\underline{\vec{e}}^2$ consists, as well as frame $\underline{\vec{e}}^0$ and frame $\underline{\vec{e}}^1$, of a set of three mutually orthogonal unit vectors \vec{e}_1^2 , \vec{e}_2^2 and \vec{e}_3^2 , where vector \vec{e}_1^2 is oriented in forward direction of the velocity of reference point r . In Figure 2.2, vectors \vec{r}_r and \vec{r}_v are, respectively, the distance vectors between the origin of the global frame $\underline{\vec{e}}^0$ and the reference point r and the origin of global frame $\underline{\vec{e}}^0$ and the *cm* of the vehicle. The vectors \vec{V}_r and \vec{V}_v are the absolute velocity vectors of the reference point r and the *cm* of the vehicle, respectively. V_x and V_y are the longitudinal and lateral velocity of *cm* of the vehicle with respect to the body-fixed frame $\underline{\vec{e}}^1$. ψ_r is the angle from frame $\underline{\vec{e}}^0$ to frame $\underline{\vec{e}}^2$, ψ_v is the angle from frame $\underline{\vec{e}}^0$ to frame $\underline{\vec{e}}^1$ and β is the vehicle side-slip angle. y_e is the lateral error between the *cm* of the vehicle and the reference point r , with respect to frame $\underline{\vec{e}}^2$, which can be written as:

$$y_e = (\vec{r}_v - \vec{r}_r) \cdot \vec{e}_2^2. \quad (2.4)$$

Furthermore, it is assumed that any disturbance caused by the lateral movement on the longitudinal dynamics is compensated for by a longitudinal controller, such that longitudinal dynamics remain unaffected and the relative longitudinal velocity and distance remains constant, more specifically it is assumed that:

$$(\vec{r}_v - \vec{r}_r) \cdot \vec{e}_1^2 = 0. \quad (2.5)$$

and

$$(\vec{V}_v - \vec{V}_r) \cdot \vec{e}_1^2 = 0. \quad (2.6)$$

Finally, for notational convenience, $\cos(\alpha)$ and $\sin(\alpha)$ are denoted by $C\alpha$ and $S\alpha$, respectively, where α can be any angle.

The velocity of the reference point r can be written as follows:

$$\begin{aligned} \vec{V}_r &= \underline{V}_r^2 \underline{\vec{e}}^2, \\ &= [V_r \ 0 \ 0] \underline{\vec{e}}^2, \end{aligned} \quad (2.7)$$

where \underline{V}_r^2 contains the longitudinal and lateral velocities of point r with respect to frame $\underline{\vec{e}}^2$. The acceleration of the reference point can be obtained by taking the time derivative of (2.7). When the reference point moves in space, frame $\underline{\vec{e}}^2$, being a body-fixed frame, also moves. This means that when taking the time derivative of (2.7), the time derivative of body-fixed frame $\underline{\vec{e}}^2$ is unequal to zero, i.e. $\dot{\underline{\vec{e}}}^2 \neq 0$. Before going into further detail how to obtain $\dot{\underline{\vec{e}}}^2$, lets first introduce the direction cosine matrix \underline{A}^{ij} . The direction cosine matrix \underline{A}^{ij} can be used to perform a coordinate transformation from one frame to another such that the coordinates with respect to frame i can

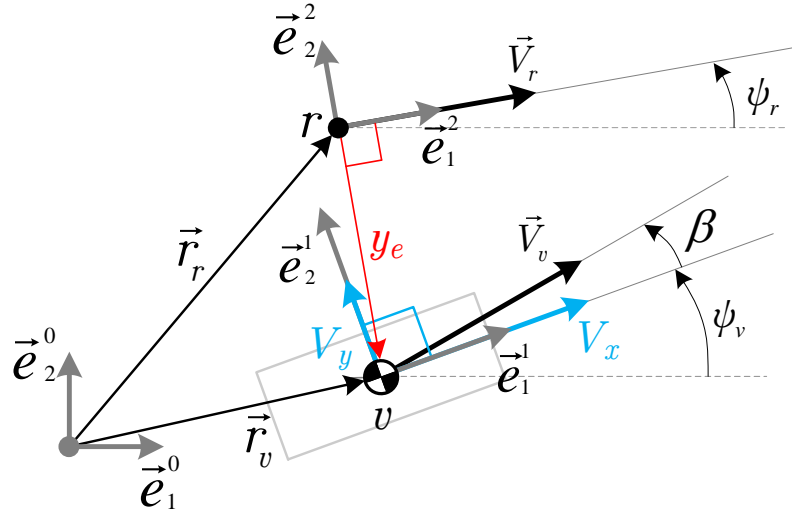


Figure 2.2: A schematic representation of the lateral control problem used to derive the lateral and rotational error dynamics between the *cm* of the vehicle (*v*) and the reference point (*r*).

be expressed in coordinates with respect to frame *j*. Now, the coordinates with respect to frame $\underline{\vec{e}}^2$ can be written with respect to frame $\underline{\vec{e}}^0$ using the following relationship:

$$\underline{\vec{e}}^2 = \underline{A}^{20} \underline{\vec{e}}^0. \quad (2.8)$$

Next, the time derivative of (2.8) can be written in following way:

$$\begin{aligned} \dot{\underline{\vec{e}}}^2 &= \dot{\underline{A}}^{20} \underline{\vec{e}}^0 + \underline{A}^{20} \dot{\underline{\vec{e}}}^0, \\ &= \dot{\underline{A}}^{20} \underline{\vec{e}}^0, \end{aligned} \quad (2.9)$$

where $\dot{\underline{\vec{e}}}^0 = 0$, due to $\underline{\vec{e}}^0$ being the fixed global frame. Furthermore, by using the Poisson equation presented in van de Wouw (2010), $\dot{\underline{A}}^{20}$ can be written as follows:

$$\dot{\underline{A}}^{20} = -{}^{20}\tilde{\omega}^2 \underline{A}^{20}, \quad (2.10)$$

where ${}^{20}\tilde{\omega}^2$ is a skew-symmetric matrix related to the angular velocity of frame $\underline{\vec{e}}^2$ with respect to frame $\underline{\vec{e}}^0$, expressed in coordinates with respect to frame $\underline{\vec{e}}^2$. Furthermore, the coordinate transformation of frame $\underline{\vec{e}}^0$ to frame $\underline{\vec{e}}^2$ can be written as follows:

$$\underline{\vec{e}}^0 = \underline{A}^{02} \underline{\vec{e}}^2, \quad (2.11)$$

where $\underline{A}^{02} = \underline{A}^{20}{}^T$. Now, by substituting (2.10) and (2.11) into (2.9) the following relation for $\dot{\underline{\vec{e}}}^2$ is obtained:

$$\dot{\underline{\vec{e}}}^2 = -{}^{20}\tilde{\omega}^2 \underline{\vec{e}}^2. \quad (2.12)$$

The acceleration of the reference point can now be calculated by taking the time derivative of (2.7) and substituting (2.12) for $\dot{\underline{e}}^2$, which results in the following:

$$\begin{aligned}\dot{\vec{V}}_r &= \dot{\underline{V}}_r^{2T} \underline{\vec{e}}^2 + \underline{V}_r^{2T} \dot{\underline{e}}^2, \\ &= \dot{\underline{V}}_r^{2T} \underline{\vec{e}}^2 - \underline{V}_r^{2T} {}^{20} \tilde{\omega}^2 \underline{\vec{e}}^2, \\ &= \begin{bmatrix} \dot{\underline{V}}_r \\ 0 \\ 0 \end{bmatrix}^T \underline{\vec{e}}^2 - \begin{bmatrix} \underline{V}_r \\ 0 \\ 0 \end{bmatrix}^T \begin{bmatrix} 0 & -\dot{\psi}_r & 0 \\ \dot{\psi}_r & 0 & 0 \\ 0 & 0 & 0 \end{bmatrix} \underline{\vec{e}}^2, \\ &= [\dot{\underline{V}}_r \quad \underline{V}_r \dot{\psi}_r \quad 0] \underline{\vec{e}}^2.\end{aligned}\tag{2.13}$$

For the derivation of the error dynamics it is necessary to express the velocities and accelerations of the vehicle and the reference point with respect to the same frame, in this case frame $\underline{\vec{e}}^2$, respectively. This can be accomplished by using the direction cosine matrix, as presented previously. In Figure 2.2, only the orientation of frame $\underline{\vec{e}}^1$ with respect to frame $\underline{\vec{e}}^0$ (ψ_v) and the orientation of frame $\underline{\vec{e}}^2$ with respect to frame $\underline{\vec{e}}^0$ (ψ_r) are known. However, both orientations can be used to derive the direction cosine matrix which describes the orientation of frame $\underline{\vec{e}}^1$ with respect to frame $\underline{\vec{e}}^2$, this results in the following matrix:

$$\begin{aligned}\underline{A}^{12} &= \underline{A}^{10} \underline{A}^{02}, \\ &= \begin{bmatrix} C(\psi_r - \psi_v) & -S(\psi_r - \psi_v) & 0 \\ S(\psi_r - \psi_v) & C(\psi_r - \psi_v) & 0 \\ 0 & 0 & 1 \end{bmatrix}.\end{aligned}\tag{2.14}$$

The time derivative of the direction cosine matrix \underline{A}^{12} is determined by taking the time derivative of (2.14) and is written as follows:

$$\dot{\underline{A}}^{12} = (\dot{\psi}_r - \dot{\psi}_v) \begin{bmatrix} -S(\psi_r - \psi_v) & -C(\psi_r - \psi_v) & 0 \\ C(\psi_r - \psi_v) & -S(\psi_r - \psi_v) & 0 \\ 0 & 0 & 0 \end{bmatrix}.\tag{2.15}$$

The velocity vector \vec{V}_v consists of the longitudinal (V_x) and lateral (V_y) velocity of the *cm* of the vehicle, both velocities are defined with respect to the body-fixed frame $\underline{\vec{e}}^1$. Now, by using (2.14) the velocity coordinates of the *cm* with respect to frame $\underline{\vec{e}}^1$ can be expressed in coordinates with respect to frame $\underline{\vec{e}}^2$, which leads to the following result:

$$\begin{aligned}\vec{V}_v &= \underline{V}_v^{1T} \underline{A}^{12} \underline{\vec{e}}^2, \\ &= [V_x \quad V_y \quad 0] \begin{bmatrix} C(\psi_r - \psi_v) & -S(\psi_r - \psi_v) & 0 \\ S(\psi_r - \psi_v) & C(\psi_r - \psi_v) & 0 \\ 0 & 0 & 1 \end{bmatrix} \underline{\vec{e}}^2, \\ &= \begin{bmatrix} V_x C(\psi_r - \psi_v) + V_y S(\psi_r - \psi_v) \\ V_y C(\psi_r - \psi_v) - V_x S(\psi_r - \psi_v) \\ 0 \end{bmatrix}^T \underline{\vec{e}}^2,\end{aligned}\tag{2.16}$$

where \underline{V}_v^1 contains the longitudinal and lateral velocities of the *cm* with respect to frame $\underline{\vec{e}}^1$. The acceleration of the *cm* of the vehicle can be calculated by taking the time derivative of equation

(2.16), i.e. $\dot{\vec{V}}_v$ is determined as follows:

$$\begin{aligned}
\dot{\vec{V}}_v &= \underline{\dot{V}_v}^{1T} \underline{A}^{12} \underline{\vec{e}}^2 + \underline{V_v}^{1T} \underline{\dot{A}}^{12} \underline{\vec{e}}^2 + \underline{V_v}^{1T} \underline{A}^{12} \dot{\underline{\vec{e}}}^2, \\
&= \underline{\dot{V}_v}^{1T} \underline{A}^{12} \underline{\vec{e}}^2 + \underline{V_v}^{1T} \underline{\dot{A}}^{12} \underline{\vec{e}}^2 - \underline{V_v}^{1T} \underline{A}^{1220} \tilde{\omega}^2 \underline{\vec{e}}^2, \\
&= \begin{bmatrix} \dot{V}_x \\ \dot{V}_y \\ 0 \end{bmatrix}^T \begin{bmatrix} C(\psi_r - \psi_v) & -S(\psi_r - \psi_v) & 0 \\ S(\psi_r - \psi_v) & C(\psi_r - \psi_v) & 0 \\ 0 & 0 & 1 \end{bmatrix} \underline{\vec{e}}^2 \\
&\quad + \begin{bmatrix} V_x \\ V_y \\ 0 \end{bmatrix}^T (\dot{\psi}_r - \dot{\psi}_v) \begin{bmatrix} -S(\psi_r - \psi_v) & -C(\psi_r - \psi_v) & 0 \\ C(\psi_r - \psi_v) & -S(\psi_r - \psi_v) & 0 \\ 0 & 0 & 0 \end{bmatrix} \underline{\vec{e}}^2 \\
&\quad - \begin{bmatrix} V_x \\ V_y \\ 0 \end{bmatrix}^T \begin{bmatrix} C(\psi_r - \psi_v) & -S(\psi_r - \psi_v) & 0 \\ S(\psi_r - \psi_v) & C(\psi_r - \psi_v) & 0 \\ 0 & 0 & 1 \end{bmatrix} \begin{bmatrix} 0 & -\dot{\psi}_r & 0 \\ \dot{\psi}_r & 0 & 0 \\ 0 & 0 & 0 \end{bmatrix} \underline{\vec{e}}^2, \\
&= \begin{bmatrix} \dot{V}_x C(\psi_r - \psi_v) + \dot{V}_y S(\psi_r - \psi_v) - V_y \dot{\psi}_v C(\psi_r - \psi_v) + V_x \dot{\psi}_v S(\psi_r - \psi_v) \\ \dot{V}_y C(\psi_r - \psi_v) - \dot{V}_x S(\psi_r - \psi_v) + V_x \dot{\psi}_v C(\psi_r - \psi_v) + V_y \dot{\psi}_v S(\psi_r - \psi_v) \\ 0 \end{bmatrix}^T \underline{\vec{e}}^2. \tag{2.17}
\end{aligned}$$

As presented previously in (2.4), the lateral error y_e is defined as the difference between \vec{r}_v and \vec{r}_r in the \vec{e}_2^2 -direction. The first- and second-order time derivatives of (2.4) can be obtained as follows:

$$\begin{aligned}
\dot{y}_e &= (\dot{\vec{r}}_v - \dot{\vec{r}}_r) \cdot \vec{e}_2^2 + (\vec{r}_v - \vec{r}_r) \cdot \dot{\vec{e}}_2^2, \\
&= (\vec{V}_v - \vec{V}_r) \cdot \vec{e}_2^2 - (\vec{r}_v - \vec{r}_r) \cdot \dot{\psi}_r \vec{e}_1^2, \tag{2.18}
\end{aligned}$$

$$\begin{aligned}
\ddot{y}_e &= (\dot{\vec{V}}_v - \dot{\vec{V}}_r) \cdot \vec{e}_2^2 + (\vec{V}_v - \vec{V}_r) \cdot \dot{\vec{e}}_2^2 - (\dot{\vec{r}}_v - \dot{\vec{r}}_r) \cdot \dot{\psi}_r \vec{e}_1^2 - (\vec{r}_v - \vec{r}_r) \cdot \ddot{\psi}_r \vec{e}_1^2 - (\vec{r}_v - \vec{r}_r) \cdot \dot{\psi}_r \dot{\vec{e}}_1^2, \\
&= (\dot{\vec{V}}_v - \dot{\vec{V}}_r) \cdot \vec{e}_2^2 - (\vec{V}_v - \vec{V}_r) \cdot \dot{\psi}_r \vec{e}_1^2 - (\vec{V}_v - \vec{V}_r) \cdot \dot{\vec{e}}_1^2 - (\vec{r}_v - \vec{r}_r) \cdot \ddot{\psi}_r \vec{e}_1^2 - (\vec{r}_v - \vec{r}_r) \cdot \dot{\psi}_r \dot{\vec{e}}_1^2, \tag{2.19}
\end{aligned}$$

where $\dot{\vec{e}}_2^2$ is substituted with $-\dot{\psi}_r \vec{e}_1^2$ and $\dot{\vec{e}}_1^2$ is substituted with $\dot{\psi}_r \vec{e}_2^2$, using the Poisson equation presented in van de Wouw (2010). As mentioned in the beginning of this section, it is assumed that all disturbances caused by the lateral movement of the vehicle on the longitudinal dynamics are compensated by the longitudinal controller, such that the dynamics in the \vec{e}_1^2 direction remain unaffected. This assumption results in all errors in the \vec{e}_1^2 -directions being equal to zero, i.e. $(\vec{r}_v - \vec{r}_r) \cdot \vec{e}_1^2 = 0$ and $(\vec{V}_v - \vec{V}_r) \cdot \vec{e}_1^2 = 0$ for all time. When this assumption is applied to (2.18) and (2.19) the following equations are obtained for the first- and second-order time derivatives of (2.4):

$$\dot{y}_e = (\vec{V}_v - \vec{V}_r) \cdot \vec{e}_2^2, \tag{2.20}$$

$$\ddot{y}_e = (\dot{\vec{V}}_v - \dot{\vec{V}}_r) \cdot \vec{e}_2^2 - (\vec{r}_v - \vec{r}_r) \cdot \dot{\psi}_r^2 \vec{e}_2^2. \tag{2.21}$$

Substituting (2.7) and (2.16) into (2.20) and (2.4), (2.13) and (2.17) into (2.21), results in the following non-linear lateral error dynamics:

$$\dot{y}_e = V_y C(\psi_r - \psi_v) - V_x S(\psi_r - \psi_v), \quad (2.22)$$

$$\ddot{y}_e = \dot{V}_y C(\psi_r - \psi_v) - \dot{V}_x S(\psi_r - \psi_v) + V_x \dot{\psi}_v C(\psi_r - \psi_v) + V_y \dot{\psi}_v S(\psi_r - \psi_v) - V_r \dot{\psi}_r - y_e \dot{\psi}_r^2. \quad (2.23)$$

The control problem is formulated in the \mathbb{R}^2 space, which implies that all rotations occur around the z -axis of each frame and that the z -axis of all frames are orientated in the same direction. Therefore, the rotational error and its derivatives can therefore be written as follows:

$$\psi_e = \psi_v - \psi_r, \quad (2.24)$$

$$\dot{\psi}_e = \dot{\psi}_v - \dot{\psi}_r, \quad (2.25)$$

$$\ddot{\psi}_e = \ddot{\psi}_v - \ddot{\psi}_r. \quad (2.26)$$

Now, equation (2.24) can be substituted in (2.22) and (2.23), which results in the following lateral error dynamics:

$$\dot{y}_e = V_y C\psi_e + V_x S\psi_e, \quad (2.27)$$

$$\ddot{y}_e = \dot{V}_y C\psi_e + \dot{V}_x S\psi_e + V_x \dot{\psi}_v C\psi_e - V_y \dot{\psi}_v S(\psi_e) - V_r \dot{\psi}_r - y_e \dot{\psi}_r^2. \quad (2.28)$$

Furthermore, (2.27) can be used to obtain an expression for V_y :

$$V_y = \frac{\dot{y}_e - V_x S\psi_e}{C\psi_e}, \quad (2.29)$$

and (2.25) is used to obtain an expression for $\dot{\psi}_v$:

$$\dot{\psi}_v = \dot{\psi}_e + \dot{\psi}_r. \quad (2.30)$$

Next, the non-linear single-track vehicle model, as derived in Appendix A, see Equation (A.20), is presented:

$$\dot{V}_y = -\frac{1}{m} \left(C\delta C_f \text{atan} \left(\frac{-V_x S\delta + (V_y + l_f \dot{\psi}_v) C\delta}{V_x C\delta + (V_y + l_f \dot{\psi}_v) S\delta} \right) + C_r \text{atan} \left(\frac{V_y - l_r \dot{\psi}_v}{V_x} \right) \right) - V_x \dot{\psi}_v, \quad (2.31)$$

$$\ddot{\psi}_v = -\frac{1}{I_z} \left(l_f C\delta C_f \text{atan} \left(\frac{-V_x S\delta + (V_y + l_f \dot{\psi}_v) C\delta}{V_x C\delta + (V_y + l_f \dot{\psi}_v) S\delta} \right) - l_r C_r \text{atan} \left(\frac{V_y - l_r \dot{\psi}_v}{V_x} \right) \right). \quad (2.32)$$

When (2.29), (2.30), (2.31) are substituted in (2.28) and based on (2.6) (i.e. the velocity error in \vec{e}_1^2 -direction is equal to zero which results in $V_r = V_x$), the following equation for the second-order

time derivative of the non-linear lateral error dynamics is obtained:

$$\ddot{y}_e = \left(-\frac{C\delta C_f \tan\left(\frac{-V_x S \delta + (\dot{y}_e - V_x S \psi_e + l_f(\dot{\psi}_e + \dot{\psi}_r)) C \delta}{V_x C \delta + (\dot{y}_e - V_x S \psi_e + l_f(\dot{\psi}_e + \dot{\psi}_r)) S \delta}\right) + C_r \tan\left(\frac{\dot{y}_e - V_x S \psi_e - l_r(\dot{\psi}_e + \dot{\psi}_r)}{V_x}\right)}{m} \right. \\ \left. - V_x (\dot{\psi}_e + \dot{\psi}_r) \right) C \psi_e + \dot{V}_x S \psi_e + V_x (\dot{\psi}_e + \dot{\psi}_r) C \psi_e - \frac{\dot{y}_e - V_x S \psi_e}{C \psi_e} (\dot{\psi}_e + \dot{\psi}_r) S \psi_e \\ - V_x \dot{\psi}_r - y_e \dot{\psi}_r^2. \quad (2.33)$$

Furthermore, when (2.29), (2.30) and (2.32) are substituted in (2.26), the following equation for the second-order time derivative of the non-linear rotational error dynamics is obtained:

$$\ddot{\psi}_e = -\frac{l_f C \delta C_f \tan\left(\frac{-V_x S \delta + (\dot{y}_e - V_x S \psi_e + l_f(\dot{\psi}_e + \dot{\psi}_r)) C \delta}{V_x C \delta + (\dot{y}_e - V_x S \psi_e + l_f(\dot{\psi}_e + \dot{\psi}_r)) S \delta}\right) - l_r C_r \tan\left(\frac{\dot{y}_e - V_x S \psi_e - l_r(\dot{\psi}_e + \dot{\psi}_r)}{V_x}\right)}{I_z} \\ - \ddot{\psi}_r. \quad (2.34)$$

2.2.1 Linearized error dynamics

For analysis purposes, it is desired to obtain a linearized model of the lateral and rotational error dynamics. An equilibrium for (2.33) and (2.34) can be obtained by setting all time derivatives in (2.33) and (2.34) to zero. Equation (2.33) and (2.34) are then equal to zero when also $\psi_e = 0$ and $\delta = 0$, i.e. the origin is an equilibrium for (2.33) and (2.34). Next, a state vector and input vector are chosen as $\zeta_1 = [y_e \ \dot{y}_e \ \psi_e \ \dot{\psi}_e]^T$ and $\gamma_1 = [\delta \ \dot{\psi}_r \ \ddot{\psi}_r]^T$, respectively. Equations (2.33) and (2.34) are linearized by choosing zero for all states (ζ_1) and inputs (γ_1) as a linearization point. Furthermore, linearization also relies on the assumption that all inputs will be small ($< 10^\circ$). Moreover, in Appendix A, see Equation (A.20), the linearized vehicle model is presented. The linearized vehicle model is a Linear Parametric Varying model (LPV), with V_x as varying parameter. A consequence of this fact is that for the linearized vehicle model and thereby the model of the error dynamics to be valid, it is necessary that $\dot{V}_x = 0$. Linearizing (2.33) results in the following:

$$\ddot{y}_e = \left. \frac{\partial \ddot{y}_e}{\partial y_e} \right|_{\zeta_1=0, \gamma_1=0} (\bar{y}_e - 0) + \left. \frac{\partial \ddot{y}_e}{\partial \dot{y}_e} \right|_{\zeta_1=0, \gamma_1=0} (\dot{\bar{y}}_e - 0) + \left. \frac{\partial \ddot{y}_e}{\partial \psi_e} \right|_{\zeta_1=0, \gamma_1=0} (\bar{\psi}_e - 0) + \left. \frac{\partial \ddot{y}_e}{\partial \dot{\psi}_e} \right|_{\zeta_1=0, \gamma_1=0} (\dot{\bar{\psi}}_e - 0) \\ + \left. \frac{\partial \ddot{y}_e}{\partial \delta} \right|_{\zeta_1=0, \gamma_1=0} \bar{\delta} + \left. \frac{\partial \ddot{y}_e}{\partial \dot{\psi}_r} \right|_{\zeta_1=0, \gamma_1=0} \dot{\bar{\psi}}_r + \left. \frac{\partial \ddot{y}_e}{\partial \ddot{\psi}_r} \right|_{\zeta_1=0, \gamma_1=0} \ddot{\bar{\psi}}_r, \\ = -\frac{C_f + C_r}{m \bar{V}_x} \dot{\bar{y}}_e + \frac{C_f + C_r}{m} \bar{\psi}_e - \frac{C_f l_f - C_r l_r}{m \bar{V}_x} \dot{\bar{\psi}}_e + \frac{C_f}{m} \bar{\delta} - \left(\frac{C_f l_f - C_r l_r}{m \bar{V}_x} + \bar{V}_x \right) \dot{\bar{\psi}}_r, \quad (2.35)$$

where \bar{V}_x is the longitudinal velocity for which $\dot{V}_x = 0$ and \bar{y}_e , $\dot{\bar{y}}_e$ and so forth are the linearized states and inputs. When (2.34) is linearized, the following equation is obtained:

$$\begin{aligned}\ddot{\psi}_e &= \frac{\partial \ddot{\psi}_e}{\partial y_e} \Big|_{\substack{\zeta_1 = \underline{\varrho} \\ \gamma_1 = \underline{\varrho}}} (\bar{y}_e - 0) + \frac{\partial \ddot{\psi}_e}{\partial \dot{y}_e} \Big|_{\substack{\zeta_1 = \underline{\varrho} \\ \gamma_1 = \underline{\varrho}}} (\dot{\bar{y}}_e - 0) + \frac{\partial \ddot{\psi}_e}{\partial \psi_e} \Big|_{\substack{\zeta_1 = \underline{\varrho} \\ \gamma_1 = \underline{\varrho}}} (\bar{\psi}_e - 0) + \frac{\partial \ddot{\psi}_e}{\partial \dot{\psi}_e} \Big|_{\substack{\zeta_1 = \underline{\varrho} \\ \gamma_1 = \underline{\varrho}}} (\dot{\bar{\psi}}_e - 0) \\ &\quad + \frac{\partial \ddot{\psi}_e}{\partial \delta} \Big|_{\substack{\zeta_1 = \underline{\varrho} \\ \gamma_1 = \underline{\varrho}}} \bar{\delta} + \frac{\partial \ddot{\psi}_e}{\partial \dot{\psi}_r} \Big|_{\substack{\zeta_1 = \underline{\varrho} \\ \gamma_1 = \underline{\varrho}}} \dot{\bar{\psi}}_r + \frac{\partial \ddot{\psi}_e}{\partial \ddot{\psi}_r} \Big|_{\substack{\zeta_1 = \underline{\varrho} \\ \gamma_1 = \underline{\varrho}}} \ddot{\bar{\psi}}_r, \\ &= -\frac{C_f l_f - C_r l_r}{I_z \bar{V}_x} \dot{\bar{y}}_e + \frac{C_f l_f - C_r l_r}{I_z} \bar{\psi}_e - \frac{C_f l_f^2 + C_r l_r^2}{I_z \bar{V}_x} \dot{\bar{\psi}}_e + \frac{C_f l_f}{I_z} \bar{\delta} - \frac{C_f l_f^2 + C_r l_r^2}{I_z \bar{V}_x} \dot{\bar{\psi}}_r \\ &\quad - \ddot{\bar{\psi}}_r.\end{aligned}\tag{2.36}$$

Now, by choosing a state vector as $x_e = \begin{bmatrix} \bar{y}_e & \dot{\bar{y}}_e & \bar{\psi}_e & \dot{\bar{\psi}}_e \end{bmatrix}^T$, the state-space representation of the linearized error dynamics can be written as follows:

$$\begin{aligned}\dot{x}_e &= A_e x_e + B_{e_1} \bar{\delta} + B_{e_2} \dot{\bar{\psi}}_r + B_{e_3} \ddot{\bar{\psi}}_r, \\ \begin{bmatrix} \dot{\bar{y}}_e \\ \ddot{\bar{y}}_e \\ \dot{\bar{\psi}}_e \\ \ddot{\bar{\psi}}_e \end{bmatrix} &= \begin{bmatrix} 0 & 1 & 0 & 0 \\ 0 & -\frac{C_f + C_r}{m \bar{V}_x} & \frac{C_f + C_r}{m} & -\frac{C_f l_f - C_r l_r}{m \bar{V}_x} \\ 0 & 0 & 0 & 1 \\ 0 & -\frac{C_f l_f - C_r l_r}{I_z \bar{V}_x} & \frac{C_f l_f - C_r l_r}{I_z} & -\frac{C_f l_f^2 + C_r l_r^2}{I_z \bar{V}_x} \end{bmatrix} \begin{bmatrix} \bar{y}_e \\ \dot{\bar{y}}_e \\ \bar{\psi}_e \\ \dot{\bar{\psi}}_e \end{bmatrix} + \begin{bmatrix} 0 \\ \frac{C_f}{m} \\ 0 \\ \frac{C_f l_f}{I_z} \end{bmatrix} \bar{\delta} \\ &\quad + \begin{bmatrix} 0 \\ -\frac{C_f l_f - C_r l_r}{m \bar{V}_x} - \bar{V}_x \\ 0 \\ -\frac{C_f l_f^2 + C_r l_r^2}{I_z \bar{V}_x} \end{bmatrix} \dot{\bar{\psi}}_r + \begin{bmatrix} 0 \\ 0 \\ 0 \\ -1 \end{bmatrix} \ddot{\bar{\psi}}_r,\end{aligned}\tag{2.37}$$

where $\bar{\delta}$ is the control input and $\dot{\bar{\psi}}_r$ and $\ddot{\bar{\psi}}_r$ are considered as the exogenous disturbances to the system. Note that $A_e = A$ and $B_{e_1} = B$ in (2.3).

2.3 Linearized lateral error dynamics with look-ahead distance

When measurements for tracking an object, either the road or a vehicle, are obtained using a look-ahead sensor, the error-dynamics are influenced by the look-ahead or inter-vehicle distance (White and Tomizuka, 2001; Lu and Tomizuka, 2003; Solyom et al., 2013). Therefore, the look-ahead distance has to be incorporated into the error-dynamics model. The position of the look-ahead distance can be chosen freely. However, in literature (Lu and Tomizuka, 2003; Solyom et al., 2013), the choice is often made to position the look-ahead on the centerline of the vehicle, as is shown in Figure 2.3. A benefit of positioning the look-ahead onto the centerline of the vehicle is that, when the system is linearized, a state transformation can be performed such that the error states at the look-ahead point can be defined as function of the error states at the *cm* of the vehicle. The resulting error dynamics are now a function of velocity and look-ahead distance, while still being able to observe the errors at the *cm* of the vehicle. The addition of the look-ahead point also changes the objective of the lateral controller design. In this new system representation, the *cm* of the vehicle has to follow the reference point r_l by regulating the lateral and rotational errors between the reference point (r_l) and the look-ahead point (v_l) to zero. In addition to the variables

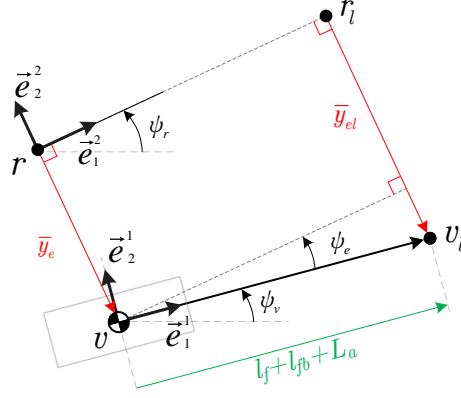


Figure 2.3: Schematic representation of the lateral control problem used to formulate the state transformation in (2.41).

already defined in Section 2.2. the following variables are introduced: \bar{y}_{el} is the linearized lateral position error between the reference r_l and the look-ahead point v_l , $\bar{\psi}_{el}$ is the linearized rotational error, l_{fb} is the distance between the front axle and front bumper and L_a is the distance between the front bumper and the look-ahead point v_l , i.e. the look-ahead distance, respectively. The errors between the reference point r_l and the look-ahead point v_l can be written as follows:

$$\begin{aligned}\bar{y}_{el} &= \bar{y}_e + (l_f + l_{fb} + L_a) \bar{\psi}_e, \\ \dot{\bar{y}}_{el} &= \dot{\bar{y}}_e + (l_f + l_{fb} + L_a) \dot{\bar{\psi}}_e, \\ \bar{\psi}_{el} &= \bar{\psi}_e, \\ \dot{\bar{\psi}}_{el} &= \dot{\bar{\psi}}_e.\end{aligned}\tag{2.38}$$

Furthermore, it is assumed, as in Section 2.2, that there is a longitudinal controller present, which compensates for the influence of the lateral movement onto the longitudinal dynamics such that the longitudinal dynamics remain unaffected and the longitudinal velocity is held constant. Suppose that the position of point r_l can be expressed in terms of vector \vec{r}_{r_l} and the position of point v_l as \vec{r}_{v_l} , i.e. the assumptions made above can be written as follows:

$$(\vec{r}_{r_l} - \vec{r}_{v_l}) \cdot \vec{e}_1^2 = 0,\tag{2.39}$$

and

$$(\dot{\vec{r}}_{r_l} - \dot{\vec{r}}_{v_l}) \cdot \vec{e}_1^2 = 0.\tag{2.40}$$

Next, by using (2.38), the following state transformation can be formulated:

$$x_{el} = C_{L_a} x_e,\tag{2.41}$$

where

$$x_{el} = \begin{bmatrix} \bar{y}_{el} & \dot{\bar{y}}_{el} & \bar{\psi}_{el} & \dot{\bar{\psi}}_{el} \end{bmatrix}^T, \quad \text{and} \quad C_{L_a} = \begin{bmatrix} 1 & 0 & l_f + l_{fb} + L_a & 0 \\ 0 & 1 & 0 & l_f + l_{fb} + L_a \\ 0 & 0 & 1 & 0 \\ 0 & 0 & 0 & 1 \end{bmatrix}.$$

Transformation matrix C_{L_a} is invertible, therefore the inverse state transformation can be written in the following way:

$$x_e = C_{L_a}^{-1} x_{el}. \quad (2.42)$$

Using the fact that C_{L_a} is invertible, a new algebraic equivalent system can be derived using the state transformation of (2.42). This new system represents the dynamics at the look-ahead point and can be obtained by substituting (2.42) into (2.37), which results in the following:

$$\begin{aligned} C_{L_a}^{-1} \dot{x}_{el} &= A_e C_{L_a}^{-1} x_{el} + B_{e_1} \bar{\delta} + B_{e_2} \dot{\bar{\psi}}_r + B_{e_3} \ddot{\bar{\psi}}_r, \\ \dot{x}_{el} &= C_{L_a} A_e C_{L_a}^{-1} x_{el} + C_{L_a} B_{e_1} \bar{\delta} + C_{L_a} B_{e_2} \dot{\bar{\psi}}_r + C_{L_a} B_{e_3} \ddot{\bar{\psi}}_r, \\ &=: A_{el} x_{el} + B_{el_1} \bar{\delta} + B_{el_2} \dot{\bar{\psi}}_r + B_{el_3} \ddot{\bar{\psi}}_r, \end{aligned} \quad (2.43)$$

where

$$A_{el} = C_{L_a} A_e C_{L_a}^{-1}, \quad B_{el_1} = C_{L_a} B_{e_1}, \quad B_{el_2} = C_{L_a} B_{e_2} \quad \text{and} \quad B_{el_3} = C_{L_a} B_{e_3}. \quad (2.44)$$

The system in (2.43) is acquired by performing a similarity transformation. However, (2.43) can also be obtained using the multibody approach of Section 2.2, both methods result in the same error-dynamics model. The results of using the multibody approach in obtaining the error dynamics with look-ahead are presented in Appendix B.

2.4 Conclusion

The first step in developing a steering controller is to obtain a model which adequately represents the lateral vehicle dynamics. Therefore, a single track vehicle model is used to obtain the linearized lateral vehicle dynamics. Next, the error dynamics between a reference point and the *cm* of a vehicle are derived using a multibody approach. The non-linear model of the error dynamics is linearized, using the origin as linearization point and the look-ahead distance is incorporated into the error-dynamics model by using a state transformation. This model will be used in the next chapter to synthesize a steering control.

Chapter 3

Lateral vehicle control

In order to follow a reference on the road or a preceding vehicle, a steering controller has to be developed which regulates the lateral and rotational errors to zero. This controller has to be robust against a wide region of different operating conditions of varying velocities and look-ahead distances. For this purpose, a steering controller is synthesized in this chapter based on the error-dynamics model derived in Chapter 2. This controller is evaluated using a pole location analysis and time-domain simulations to a step input. This chapter is organized as follows: in Section 3.1, the requirements for the steering controller are presented and in Section 3.2, the steering controller is synthesized using an LQR design approach. Section 3.3 contains the analysis of the closed-loop pole locations and Section 3.4, presents the time-domain responses of the closed-loop system to a step input for different operating conditions. Finally, Section 3.5 contains the conclusion of this chapter.

3.1 Controller requirements

Designing a controller for lateral vehicle control is not a trivial matter. Besides the controller requirements for stability, tracking performance and respecting actuator bandwidth, safety is a very important issue when considering the lateral control of a vehicle. For example, it is undesired to have a large steer input at high velocities. A large steer input at high velocities could lead to serious or fatal injuries to the occupants of the vehicle. Therefore, the limitation of the steer input with increasing velocity is required in the controller design.

The dynamic response of a vehicle to a steer input is determined by the pole locations of the system. In Figure 3.1, the open-loop pole locations of the error dynamics in (2.37) are presented for varying longitudinal velocities $\bar{V}_x \in \mathcal{S}$, where $\mathcal{S} = \{\bar{V}_x \in \mathbb{N} | 1 \leq \bar{V}_x \leq 40 \text{m/s}\}$. For the time being, it assumed that 40m/s is the maximum operating velocity of the system. The open-loop poles can be separated into two groups, one group (on the left in Figure 3.1) involve a pair of complex conjugate poles related to the dynamics of the vehicle and two poles in the origin related to the integration of \dot{y}_e and the linear dependency between row 2 and 4 in matrix A_e , Equation (2.37). To improve tracking performance, the two poles in the origin have to be shifted into the Left Half Plane (LHP) by means of feedback control. The two other closed-loop poles can be positioned at the same location as the complex conjugated pole pair related to the dynamics of

the vehicle, these poles are already located in the LHP and sufficiently damped. Additionally, the system is ill-conditioned, which means that although the system is fully controllable, certain pole locations in the LHP are not feasible or can only be achieved by applying a very large control input. Finally, to ensure proper tracking performance, it is desired to have asymptotic convergence of the errors. Now, a set of controller requirements can be formulated which will be used to evaluate the

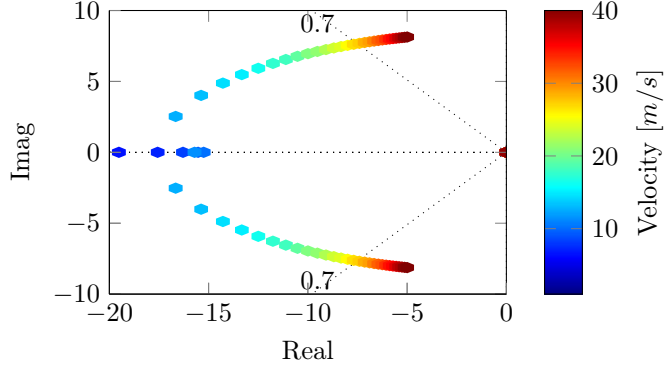


Figure 3.1: Open-loop pole locations of the error-dynamics model in (2.37).

performance of the controller:

1. The controller has to induce stable vehicle following behavior (i.e. the errors have to converge asymptotically to zero) and needs to be robust in a wide operating region against varying velocities and look-ahead distances.
2. Two closed-loop poles have to be positioned at the same location as the complex conjugated pole pair related to the dynamics of the vehicle.
3. The controller has to achieve lateral string stability for a platoon of infinite length.
4. To prevent a large steer input at high velocity, the steer input has to be limited based on the longitudinal velocity.

3.2 Controller synthesis

A reasonable choice for an approach towards controller design would be to use a pole placement technique. However, using pole placement has some drawbacks. There are two parameters which influence the dynamic behavior of the system, the longitudinal velocity (\bar{V}_x) and the look-ahead distance (L_a), both can vary within a wide range of values. In Guldner et al. (1999) the notion of Γ -stability is introduced to solve a lateral control problem which has to perform in a wide range of operating conditions. Γ -stability describes a region of the LHP where the poles of the error-dynamics in the origin can be positioned such that specifications such as settling time, damping and actuator bandwidth can be considered. In Figure 3.2, a general example is presented of the Γ -stability region, where Γ_1 can be used to set a condition for settling time, Γ_2 is used to obtain a certain amount of damping, while Γ_3 is determined by the maximum actuator bandwidth. Although, the Γ -stability region provides guidance in where to position the closed-loop poles, it does not provide the possibility to verify if controller requirement 4, limitation of the steer input

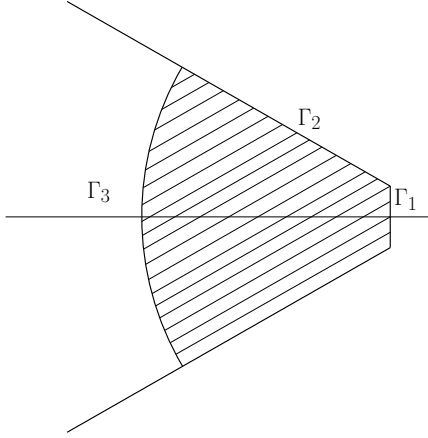


Figure 3.2: Γ -stability region presented in Guldner et al. (1999).

with increasing velocity, is fulfilled. To confirm if the requirement of limiting the steer input is satisfied; it is necessary to check for each configuration of \bar{V}_x , L_a , where the safety requirement is still fulfilled, in order to choose a pole location. This makes pole placement a time consuming and labor intensive method.

In Snider (2009), five different control methods (linear and non-linear) for lateral vehicle control are compared. Of these five control methods it is shown, by using time-domain simulations of three different scenarios performed with velocities varying from 5m/s to 20 m/s, that using LQR controller synthesis results in the smallest errors over a wide operating region of different velocities. The controller gains determined with LQR controller synthesis can be influenced by changing the weighting gains in state weighting matrix Q and control weighting matrix R . Furthermore, by using LQR, the controller input can be penalized with increasing velocity by control weighting matrix R . This results in a lower control input at higher velocities, which fulfills controller requirement 4. However, in Seiler et al. (2003), the LQR-controller is only applied in a lane-following mode and not in vehicle following mode. Furthermore, using LQR design has some drawbacks. LQR is designed to minimize the errors based on infinite time horizon and initial condition perturbation. If the minimum of the objective function is far from the origin, the corresponding gains are very small and this would lead to a very slow response of the system. Moreover, LQR controller synthesis is developed to minimize the errors based an initial condition perturbation. Using LQR to track a reference point can only be achieved by considering the behavior of the reference point as an exogenous disturbance. Which means that using LQR to follow a reference is a slight misuse of LQR controller design. This might have unexpected results, something one should be aware of when using LQR controller design for a vehicle following objective.

Although the application of LQR controller synthesis has some drawbacks compared to the use pole placement, the ease of integrating the penalization of the steering input into the controller synthesis has a significant preference. Furthermore, pole placement can be difficult to achieve when having a system of larger dimension (He and Mehrmann, 1994).

For a general state-space system:

$$\dot{\rho} = A\rho + B\gamma, \quad (3.1)$$

with state ρ and input γ , the LQR controller gain is obtained by minimizing a cost function \mathcal{J} . The cost function \mathcal{J} can be expressed as the quadratic form of state ρ , plus the quadratic form of the control input γ . The generalized form of the cost function used by LQR to calculate the

controller gains, can be written as follows:

$$\mathcal{J} = \int_0^\infty [\rho'(\tau)Q\rho(\tau) + \gamma'(\tau)R\gamma(\tau)] d\tau, \quad (3.2)$$

where Q and R are symmetric weighting matrices. A more detailed description of LQR-controller synthesis can be found in Friedland (2012). LQR design results in a static state feedback for which the cost function of (3.2) is minimized for solutions of the system in (3.1). The controller gains are calculated by solving the continuous-time Algebraic Riccati Equation (ARE):

$$0 = PA + A^T P + Q - PBR^{-1}B^T P, \quad (3.3)$$

where P is the symmetric positive definite solution of the ARE. Based on this, the following control law can be obtained:

$$\begin{aligned} \gamma &= -R^{-1}B^T P\rho, \\ &=: -K\rho. \end{aligned} \quad (3.4)$$

First, for convenience, let us present the error-dynamics model with look-ahead again (see (2.43)):

$$\dot{x}_{el} = A_{el}x_{el} + B_{el_1}\bar{\delta} + B_{el_2}\dot{\psi}_r + B_{el_3}\ddot{\psi}_r. \quad (3.5)$$

Now, the LQR-controller synthesis is performed using (3.5). The cost function \mathcal{J} can then be written as follows:

$$\mathcal{J} = \int_0^\infty [x'_{el}(\tau)Qx_{el}(\tau) + \bar{\delta}'(\tau)R\bar{\delta}(\tau)] d\tau, \quad (3.6)$$

with exogenous inputs $\dot{\psi}_r = \ddot{\psi}_r = 0$, input weighting matrix $R = 2\bar{V}_x$ and state weighting matrix

$$Q = \begin{bmatrix} q_1 & 0 & 0 & 0 \\ 0 & q_2 & 0 & 0 \\ 0 & 0 & q_3 & 0 \\ 0 & 0 & 0 & q_4 \end{bmatrix}. \quad (3.7)$$

The choice of weighting matrix Q provides the possibility to influence the transient behavior of the system based on the weighting of a state. This results in the following feedback control law:

$$\bar{\delta} = \delta_{fb} = -K_{el}x_{el}, \quad (3.8)$$

where

$$K_{el} = [k_{el_{11}} \ k_{el_{12}} \ k_{el_{13}} \ k_{el_{14}}].$$

K_{el} are the controller gains calculated by using LQR controller synthesis; this set of controller gains are depending on \bar{V}_x and L_a , since the dynamics in (2.43) depend on \bar{V}_x and L_a , and R depends on \bar{V}_x . For analysis purposes, it is desired to obtain a system which provides the possibility to investigate the error at the *cm* of the vehicle. Therefore, the state transformation of (2.41) is substituted in (3.8), such that the error states at the look-ahead point are transformed back to the error states at the *cm* of the vehicle. This results in the following control law:

$$\bar{\delta} = \delta_{fb} = -K_{el}C_{L_a}x_e, \quad (3.9)$$

Now, by substituting (3.9) for $\bar{\delta}$ in the open-loop error dynamics model without look-ahead in (2.37), a closed-loop model is obtained with controller gains which are based on \bar{V}_x and L_a , while still being able to observe the errors at the *cm* of the vehicle:

$$\dot{x}_e = (A_e - B_{e_1}K_{el}C_{L_a})x_e + B_{e_2}\dot{\psi}_r + B_{e_3}\ddot{\psi}_r. \quad (3.10)$$

The next step is to perform a pole location analysis of (3.10) to investigate how \bar{V}_x and L_a influence the closed-loop pole locations of the system and thereby the transient behavior of the system.

3.3 Pole location analysis

The controller gains in (3.9) are influenced by the values of the weighting gains in matrix Q in (3.7). The weighting gains q_1 , q_2 , q_3 and q_4 can therefore be considered to be the design parameters. In Appendix C, an extensive analysis is performed on the influence of the individual weighting coefficients on the closed-loop pole locations and time-domain response of the errors to a step input. It is shown that increasing the weighting of q_1 results in better tracking performance at the cost of oscillations, while increasing the weighting of q_3 results in adding more damping to the system. The weighting gains q_2 and q_4 have a limited positive contribution on the response of the system and mainly affect the pole locations related to the dynamics of the vehicle. Furthermore, out of a set of four different configurations for Q , the configuration is chosen which results in the smallest errors and generates the lowest control input. Based on the results in Appendix C, the weighting gains have the values presented in Table 3.1. In Figure 3.3a, the open-loop poles of the

Weighting gains	
q_1	0.25
q_2	0.01
q_3	1
q_4	0

Table 3.1: Weighting gains for matrix Q .

error dynamics model in (2.37) are presented. Figure 3.3b shows the closed-loop pole locations of (3.10) with $\bar{V}_x \in \mathcal{S}$, $L_a = 0$ and $\dot{\psi}_r = \ddot{\psi}_r = 0$. As can be observed in Figure 3.3b, the two poles in the origin are shifted into the LHP, while the two other closed-poles are located at the same positions as the complex conjugated pole pair related to the dynamic behavior of the vehicle, which fulfills controller requirement 2. However, Figure 3.3b does not provide insight into the influence of the L_a on the closed-loop pole locations. In Figure 3.4a, the closed-loop pole locations of (3.10)

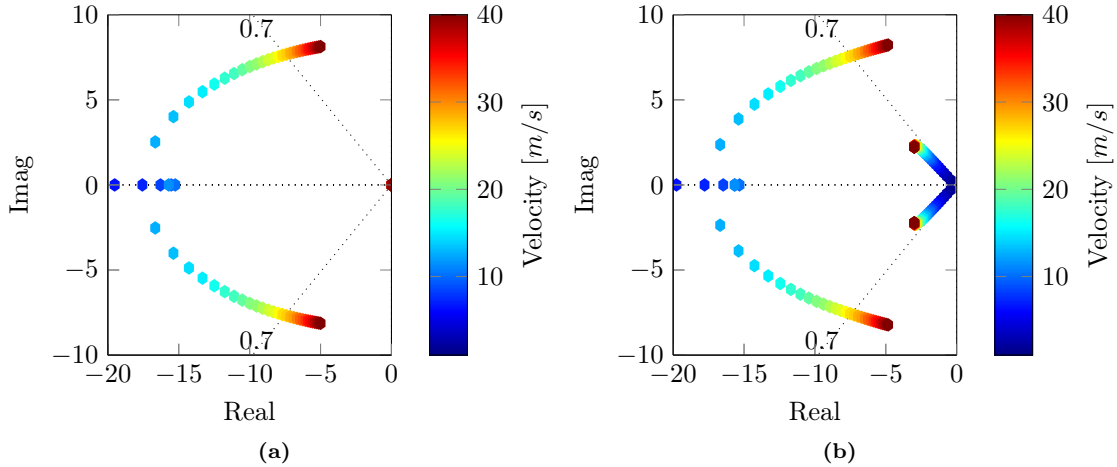


Figure 3.3: (a) Open-loop pole locations of the error dynamics in (2.37). (b) Closed-loop poles of (3.10) for $L_a = 0$ and $\dot{\psi}_r = \ddot{\psi}_r = 0$.

are presented for $\bar{V}_x \in \mathcal{S}$ and $L_a \in \mathcal{T}$, where $\mathcal{T} = \{L_a \in \mathbb{N} | 1 \leq L_a \leq 10\}$ and $\dot{\psi}_r = \ddot{\psi}_r = 0$. \mathcal{T} is chosen, such that the influence of different length of L_a onto the closed-loop pole locations of the lateral dynamics can be investigated. In practice, the look-ahead distance is not limited to the set \mathcal{T} , for example L_a could also be based on the longitudinal spacing policy. Hence, under the assumption that \bar{V}_x is constant, the distance between two vehicle, also known as the inter-vehicle distance, is also constant. It has to be noted that, when the look-ahead distance is chosen based on the longitudinal spacing policy, L_a can not be chosen freely, but is dictated by the chosen time gap and safety distance in the longitudinal spacing policy.

The pole pair in the left of Figure 3.4a is related to the dynamic behavior of the look-ahead point; changing the look-ahead distance changes the dynamics of the look-ahead point. The cyan colored arrow indicates the direction in which the pole locations are shifted when increasing L_a . The magenta colored arrow in Figure 3.4a indicates how the pole locations of the system in (3.10) are influenced when increasing \bar{V}_x . The closed-loop poles are positioned on the real axis at low velocities and change into a complex conjugate pair with increasing velocity. The poles on the left in Figure 3.4a determine the lateral dynamics of the look-ahead point. As the passenger is not positioned at the look-ahead point, the lateral dynamics of this pole pair is of less interest. However, what is of interest, is the influence of \bar{V}_x and L_a on the location of the pole pair near the origin. The location of the these poles influences the tracking performance of the system. Figure 3.4b presents the position of the closed-loop poles of (3.10) near the origin. These poles are located on the real axis at low velocities and change into a complex conjugate pair when increasing \bar{V}_x . The magenta colored arrow indicates how the pole locations are influenced when increasing \bar{V}_x . Increasing L_a results in the poles staying longer on the real axis before changing into a complex conjugated pole pair, this can be interpreted as adding more damping to the system. The cyan colored arrow indicates how the location of the poles near the origin are influenced when L_a is increased. Furthermore, when \bar{V}_x and L_a are small, both poles originate near the origin. However, when \bar{V}_x is small and L_a is increased to, for example 10m, one pole originates near the origin, while the second pole originates around -3 . When \bar{V}_x is then increased, the poles move towards each other and change into a complex conjugated pole pair. This is caused by the coupling the second and fourth row in (2.3).

To summarize, using LQR for controller synthesis results in a closed-loop system where two poles are positioned at the same locations as the complex conjugated pole pair related to the dynamics of the vehicle, which satisfies controller requirement 2, while the pole pair in origin are shifted into the LHP to improve tracking performance. It is shown that increasing \bar{V}_x results in a larger complex part of the pole pair near the origin, while increasing L_a can be used to add more damping to the system.

In the next section, the influence of the pole location on the time-domain response of the errors will be investigated. The goal is to gain more insight in the influence of a pole location on the transient response of the system.

3.4 Time-domain simulation results to a step input

In the previous section, it is shown that the velocity and look-ahead distance influences location of the poles of the closed-loop system. In this section, the influence of the look-ahead distance on the time response of the errors will be further analyzed. The goal is to investigate if a certain position of the pole pair near the origin results a more desired transient response of the errors. First, the control matrix K_{el} is presented. Matrix K_{el} consists of four controller gains and is defined as follows:

$$K_{el} = [k_1 \quad k_2 \quad k_3 \quad k_2]. \quad (3.11)$$

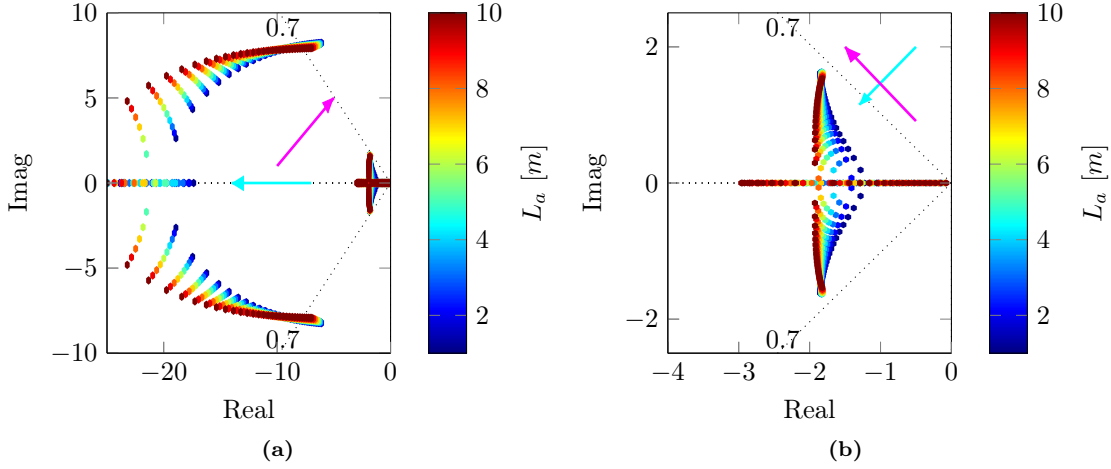


Figure 3.4: (a) Closed-loop poles of (3.10) for $\bar{V}_x \in \mathcal{S}$, $L_a \in \mathcal{T}$ and $\dot{\psi}_r = \ddot{\psi}_r = 0$. (b) Closed-loop poles of (3.10) close to the origin for $\bar{V}_x \in \mathcal{S}$, $L_a \in \mathcal{T}$ and $\dot{\psi}_r = \ddot{\psi}_r = 0$.

In Figure 3.5, the corresponding controller gains for $\bar{V}_x \in \mathcal{S}$ and $L_a \in \mathcal{T}$ are presented. The value of controller gain k_1 remains constant with increasing L_a and decreases with increasing \bar{V}_x , whereas k_2 increases with increasing L_a , while increasing \bar{V}_x results in a decrease in the controller gains of k_2 . k_3 decreases when \bar{V}_x and/or L_a is increased, while k_4 remains constant when increasing \bar{V}_x and increasing L_a at low velocities results in a decrease in the controller gain. The trend of k_1 is unexpected. Further numerical analysis shows, that the coefficients in matrix P change depending on \bar{V}_x and L_a , and the second coefficient in input vector B_{el1} in (2.43), changes only depending on L_a . The multiplication of P and B_{el1} , according to (3.4), results then in the values of k_1 only changing depending only on \bar{V}_x .

Next, a step on $\dot{\psi}_r$ will be used to perturb the system (Figure 3.6a) and time-domain simulations are performed with the following parameters: $\ddot{\psi}_r = 0$, $\bar{V}_x = 15\text{m/s}$ and $L_a \in \mathcal{T}_1$, where $\mathcal{T}_1 = \{ 2, 6, 10 \}$. The choice of \mathcal{T}_1 results in three distinct locations of the pole pair near the origin. Figure 3.6b contains the closed-loop pole locations near the origin of (3.10) for $\bar{V}_x = 15\text{m/s}$, $L_a \in \mathcal{T}_1$ and $\dot{\psi}_r = \ddot{\psi}_r = 0$. When $L_a = 2\text{m}$, the pole pair has a large complex part, than damping is added to the system by increasing L_a . This shifts the pole pair closer to the real axis until both poles are positioned on the real axis when $L_a = 10\text{m}$. The different pole locations should provide a different transient response of the system, e.g. a large complex is expected to result in a faster responds of the system at the cost of overshoot and oscillations. In Figure 3.7, the time domain response of the errors to the step input for $\bar{V}_x = 15\text{m/s}$ and $L_a \in \mathcal{T}_1$ are presented. Disturbing the system with a step on the yaw-rate results in the vehicle making a circle with a constant radius, this means that the system will have a steady state lateral error (\bar{y}_e) and rotational error ($\bar{\psi}_e$), while the derivatives of both states will converge to zero, as can be observed in Figure 3.7. When considering the transient behavior of the system, it is shown that a larger look-ahead distance adds more damping to the system, which results in a slower response of the system but less overshoot. Furthermore, the quantitative influence of choosing a larger look-ahead distance on the errors decreases when L_a is increased. This, most clearly, can be observed in Figure 3.7d, where the reduction in overshoot is significantly less when L_a is increased from 6m to 10m, compared to when L_a is increased from 2m to 6m.

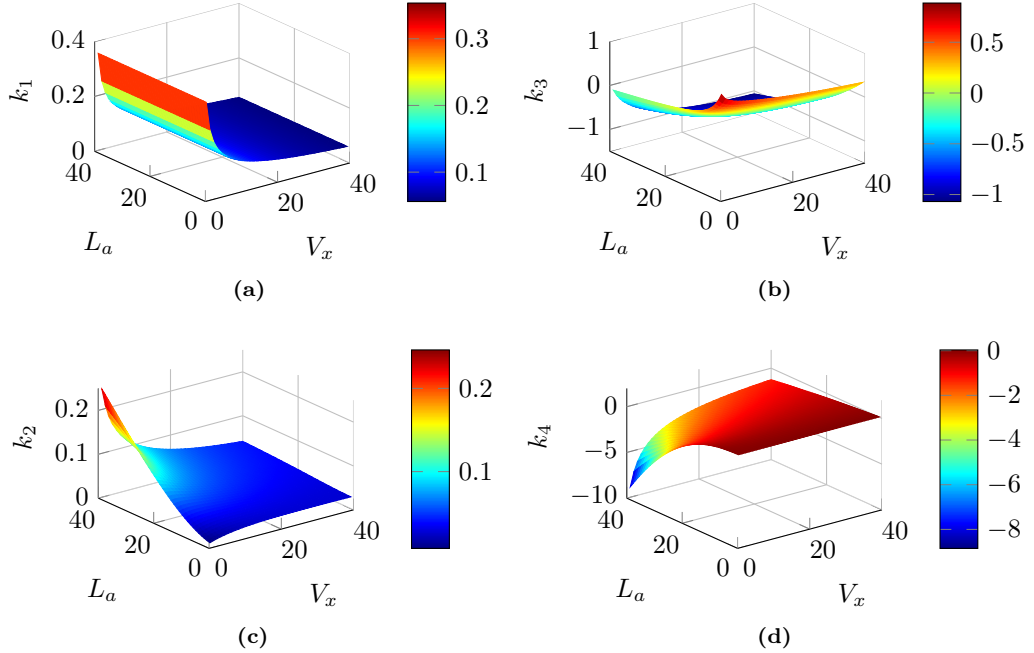


Figure 3.5: Controller gains of (3.11) for $\bar{V}_x \in \mathcal{S}$ and $L_a \in \mathcal{T}$.

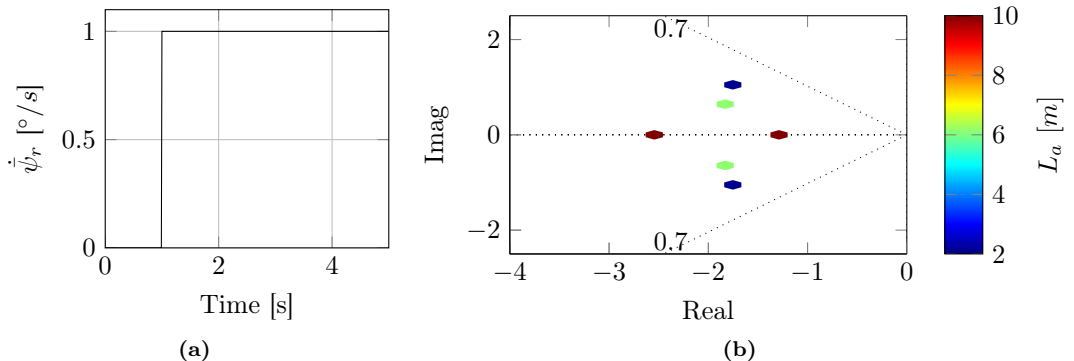


Figure 3.6: (a) Step input for $\dot{\psi}_r$. (b) Closed-loop pole locations near the origin of (3.10) for $\bar{V}_x = 15\text{m/s}$, $L_a \in \mathcal{T}_1$ and $\dot{\bar{\psi}}_r = \ddot{\bar{\psi}}_r = 0$.

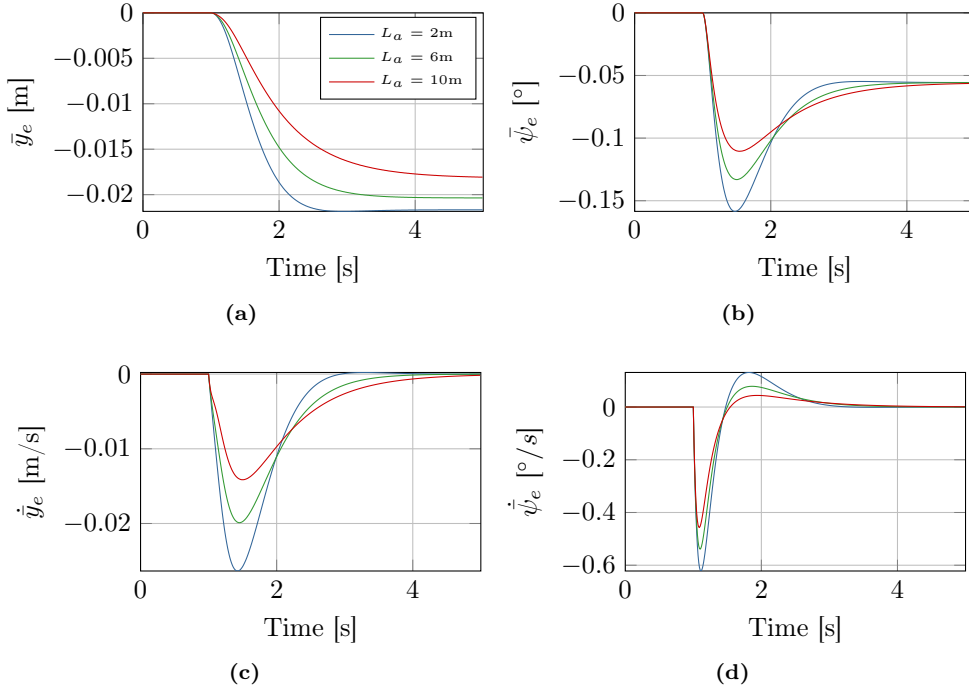


Figure 3.7: Error response to the step input for $\bar{V}_x = 15\text{m/s}$ and $L_a = [2 \quad 6 \quad 10]\text{m}$.

3.5 Conclusion

In this chapter, a steering controller is developed for lateral manoeuvering. The controller is obtained based on the linearized error dynamics between the *cm* of a vehicle and a reference point in front of the vehicle, derived in the previous chapter. A Linear Quadratic Regulator (LQR) design approach is used to synthesize a feedback controller, with controller gains which are depending on longitudinal velocity and look-ahead distance. Such optimal control approach, depending on these key parameters, ensures stable lateral tracking of a reference trajectory while limiting the steering action needed, for a range of longitudinal velocities and look-ahead distances.

Using time-domain simulations to a step input, it is shown that a larger look-ahead distance can be used to add more damping to the system. The addition of extra damping to the system, by increasing the look-ahead distance, results in a slower response of the system and less overshoot. Finally, it is not yet evaluated if the controller will result in lateral string stability of a platoon of vehicles, this will be addressed in the next chapter.

Chapter 4

Lateral string stability analysis

A platoon of vehicles can be considered as a string of interconnected systems. To assess the performance of an interconnected system, and the influence of the proposed steering controller on the platoon performance, the notion of string stability is used. In literature, many approaches, definitions and terminologies are available on this topic. However, in general, string stability is used to assess the amplification/attenuation of a certain variable in a string of interconnected systems, this variable can be, for example, velocity, error or input. There is no requirement on which variable is used, as long as the same type of variable is used for individual systems. The string stability analysis performed in this chapter is based on the work presented in Ploeg et al. (2014). This chapter is organized as follows. In Section 4.1, the model of a homogeneous interconnected string of vehicles is presented, in Section 4.2, lateral string stability is assessed based on strict \mathcal{L}_2 string stability, see Ploeg et al. (2014), and, in Section 4.3, a feedforward steering input is added to the control strategy to increase the performance of the system. In Section 4.4, time-domain simulations results for a lane change with a platoon containing four vehicles are presented and, finally, Section 4.5 contains the conclusion of this chapter.

4.1 Interconnected vehicle string model

For the string stability analysis of a homogeneous platoon of vehicles, a model of the interconnected vehicle string has to be obtained. The interconnected string model can be obtained by substituting the control law of (3.8) into the linearized lateral vehicle dynamics model of (2.3). First, the vehicle dynamics model, as derived in (2.3), is presented again:

$$\dot{x}_i = Ax_i + B\bar{\delta}_i, \quad i \in \mathcal{K}_n, \quad (4.1)$$

where $\mathcal{K}_n = \{i \in \mathbb{N} | 1 < i < n\}$ is a set of vehicles in a platoon with length $n \in \mathbb{N}$ and state vector $x_i = [\bar{y}_{v_i} \quad \dot{\bar{y}}_{v_i} \quad \bar{\psi}_{v_i} \quad \dot{\bar{\psi}}_{v_i}]^T$. The states in vector x_i are defined with respect to the global frame, while the error states \bar{y}_{el_i} and $\dot{\bar{y}}_{el_i}$ in the control law of Equation (3.8) are defined with respect to the frame of the preceding vehicle, i.e. frame \bar{e}^{i-1} . Therefore, a coordinate transformation has to be performed such that the lateral errors with respect to the global frame \bar{e}^0 can be expressed with respect to the frame of a preceding vehicle, frame \bar{e}^{i-1} . First, let us consider Figure 4.1. In

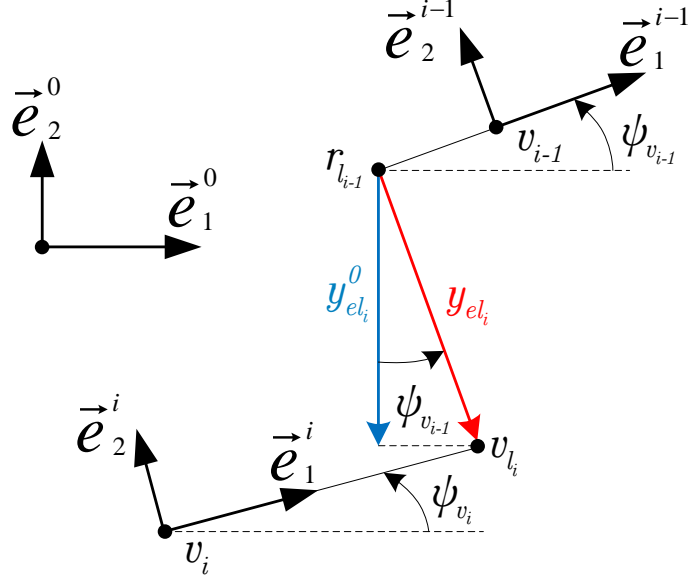


Figure 4.1: Simplified schematic representation of the coordinate transformation of the lateral error with respect to the global to the lateral error with respect to the frame of the preceding vehicle.

Figure 4.1, a simplified schematic representation of a two vehicle platoon is presented, where v_i and v_{i-1} indicate the *cm* of vehicle i and $i - 1$, respectively, v_{l_i} is the look-ahead point of vehicle i and $r_{l_{i-1}}$ is the location of the rear bumper of vehicle $i - 1$. ψ_{v_i} and $\psi_{v_{i-1}}$ are the angles between vehicle frames \bar{e}^i and the global frame \bar{e}^0 and \bar{e}^{i-1} and the global frame \bar{e}^0 , respectively. y_{el_i} is the lateral error with respect to frame \bar{e}^{i-1} and $y_{el_i}^0$ will be used to denote the lateral error with respect to the global frame \bar{e}^0 . Under the assumption that the longitudinal distance error remains constant and velocity error is equal to zero in the \bar{e}_1^{i-1} -direction (an assumption which is made previously in Chapter 2), the lateral error y_{el_i} and its derivative can be determined based on the lateral error $y_{el_i}^0$ with respective to the global frame \bar{e}^0 as follows:

$$y_{el_i} = \frac{y_{el_i}^0}{\cos(\psi_{v_{i-1}})}, \quad (4.2)$$

$$\dot{y}_{el_i} = \frac{\dot{y}_{el_i}^0}{\cos(\psi_{v_{i-1}})} - \frac{y_{el_i}^0}{(\cos(\psi_{v_{i-1}}))^2} \sin(\psi_{v_{i-1}}) \dot{\psi}_{v_{i-1}}. \quad (4.3)$$

Next, to avoid introducing non-linearities in the model, (4.2) and (4.3) are linearized around the same point as used to obtain the linearized vehicle dynamics model in Appendix A, being the origin. Using the state vector $\nu = [y_{el_i}^0 \quad \dot{y}_{el_i}^0 \quad \psi_{v_{i-1}} \quad \dot{\psi}_{v_{i-1}}]^T$, the following results are obtained (in a linearized sense):

$$\begin{aligned} \bar{y}_{el_i} &= \left. \frac{\partial y_{el_i}}{\partial y_{el_i}^0} \right|_{\nu=0} (\bar{y}_{el_i}^0 - 0) + \left. \frac{\partial y_{el_i}}{\partial \dot{y}_{el_i}^0} \right|_{\nu=0} (\dot{\bar{y}}_{el_i}^0 - 0) + \left. \frac{\partial y_{el_i}}{\partial \psi_{v_{i-1}}} \right|_{\nu=0} (\bar{\psi}_{v_{i-1}} - 0) \\ &\quad + \left. \frac{\partial y_{el_i}}{\partial \dot{\psi}_{v_{i-1}}} \right|_{\nu=0} (\dot{\bar{\psi}}_{v_{i-1}} - 0), \\ &= \bar{y}_{el_i}^0, \end{aligned} \quad (4.4)$$

and

$$\begin{aligned}\dot{\bar{y}}_{el_i} &= \frac{\partial \bar{y}_{el_i}}{\partial \bar{y}_{el_i}^0} \Big|_{\nu=0} (\bar{y}_{el_i}^0 - 0) + \frac{\partial \bar{y}_{el_i}}{\partial \dot{\bar{y}}_{el_i}^0} \Big|_{\nu=0} (\dot{\bar{y}}_{el_i}^0 - 0) + \frac{\partial \bar{y}_{el_i}}{\partial \bar{\psi}_{v_{i-1}}} \Big|_{\nu=0} (\bar{\psi}_{v_{i-1}} - 0) \\ &\quad + \frac{\partial \bar{y}_{el_i}}{\partial \dot{\bar{\psi}}_{v_{i-1}}} \Big|_{\nu=0} (\dot{\bar{\psi}}_{v_{i-1}} - 0), \\ &= \dot{\bar{y}}_{el_i}^0,\end{aligned}\tag{4.5}$$

This means that the lateral error between the look-ahead point of vehicle i and the rear bumper of vehicle $i - 1$, with respect to the frame of vehicle $i - 1$, can be determined based on the difference between the global lateral position of the look-ahead point of vehicle i and the global lateral position of the rear bumper of vehicle $i - 1$ without having to perform a coordinate transformation. In Figure 4.2, a new, more detailed, schematic representation of a linearized two vehicle platoon is presented. In addition to the variables already presented earlier, variable l_{rb} is introduced. Variable l_{rb} is distances from the rear axle to the rear bumper, respectively. Based on Figure 4.2, the lateral

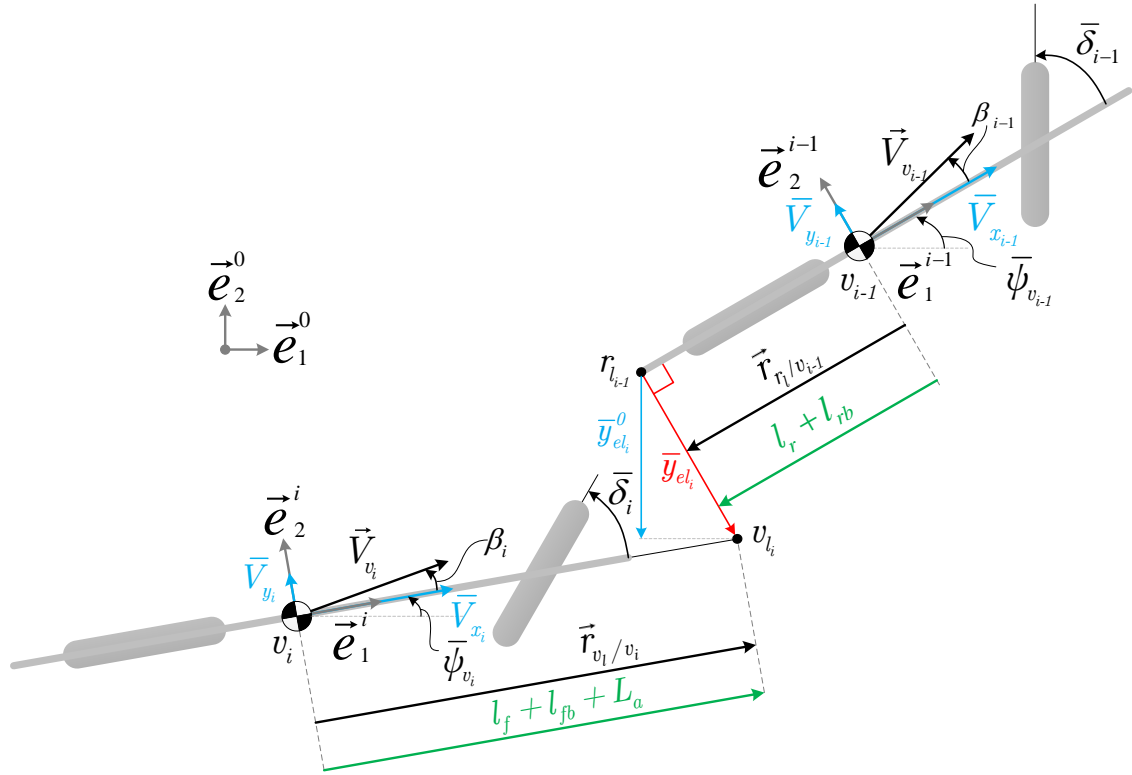


Figure 4.2: Detailed schematic representation of a two vehicle platoon used to formulate the lateral error between the rear bumper (r_l) and the look-ahead point v_l .

error $\bar{y}_{el_i}^0$ and its derivative with respect the global frame can be written as follows:

$$\bar{y}_{el_i}^0 = (\bar{y}_{v_i} + (l_f + l_{fb} + L_a) \bar{\psi}_{v_i}) - (\bar{y}_{v_{i-1}} - (l_r + l_{rb}) \bar{\psi}_{v_{i-1}}), \tag{4.6}$$

$$\dot{\bar{y}}_{el_i}^0 = (\dot{\bar{y}}_{v_i} + (l_f + l_{fb} + L_a) \dot{\bar{\psi}}_{v_i}) - (\dot{\bar{y}}_{v_{i-1}} - (l_f + l_{rb}) \dot{\bar{\psi}}_{v_{i-1}}). \tag{4.7}$$

Next, (4.4) and (4.5) can be substituted into (4.6) and (4.7) resulting in the following:

$$\bar{y}_{el_i} = (\bar{y}_{v_i} + (l_f + l_{fb} + L_a) \bar{\psi}_{v_i}) - (\bar{y}_{v_{i-1}} - (l_r + l_{rb}) \bar{\psi}_{v_{i-1}}), \quad (4.8)$$

$$\dot{\bar{y}}_{el_i} = (\dot{\bar{y}}_{v_i} + (l_f + l_{fb} + L_a) \dot{\bar{\psi}}_{v_i}) - (\dot{\bar{y}}_{v_{i-1}} - (l_f + l_{rb}) \dot{\bar{\psi}}_{v_{i-1}}). \quad (4.9)$$

Using (4.8) and (4.9), the linearized errors in state vector x_{el} can be written as follows:

$$x_{el_i} = T_{v_l} x_i - T_{r_l} x_{i-1}, \quad i \in \mathcal{K}_n, \quad (4.10)$$

with

$$T_{v_l} = \begin{bmatrix} 1 & 0 & l_f + l_{fb} + L_a & 0 \\ 0 & 1 & 0 & l_f + l_{fb} + L_a \\ 0 & 0 & 1 & 0 \\ 0 & 0 & 0 & 1 \end{bmatrix} \quad \text{and} \quad T_{r_l} = \begin{bmatrix} 1 & 0 & -(l_r + l_{rb}) & 0 \\ 0 & 1 & 0 & -(l_r + l_{rb}) \\ 0 & 0 & 1 & 0 \\ 0 & 0 & 0 & 1 \end{bmatrix}.$$

Since the first vehicle in platoon does not have a reference, a virtual reference vehicle is introduced. This virtual reference vehicle has the same lateral dynamics as a normal vehicle in the string:

$$\dot{x}_0 = Ax_0 + B\bar{\delta}_0, \quad (4.11)$$

with state vector $x_0 = [\bar{y}_{v_0} \quad \dot{\bar{y}}_{v_0} \quad \bar{\psi}_{v_0} \quad \dot{\bar{\psi}}_{v_0}]^T$ and $\bar{\delta}_0$ as input. Furthermore, due to the addition of a virtual vehicle, a uniform control structure is obtained for all vehicles in the platoon. Now, by using (4.1) and (4.11), a string of n vehicles is constructed (note that there is no interconnection between the vehicles yet):

$$\begin{aligned} \dot{x}_0 &= Ax_0 + B\bar{\delta}_0, \\ \dot{x}_1 &= Ax_1 + B\bar{\delta}_1, \\ \dot{x}_2 &= Ax_2 + B\bar{\delta}_2, \\ &\vdots \\ \dot{x}_n &= Ax_n + B\bar{\delta}_n. \end{aligned} \quad (4.12)$$

Next, the control law as derived in (3.8) is presented again:

$$\bar{\delta}_i = \delta_{fb_i} = -K_{el} x_{el_i}, \quad i \in \mathcal{K}_n, \quad (4.13)$$

where x_{el_i} can be substituted with (4.10), which results in:

$$\bar{\delta}_i = -K_{el} (T_{v_l} x_i - T_{r_l} x_{i-1}), \quad i \in \mathcal{K}_n. \quad (4.14)$$

The closed-loop interconnected vehicle string is then obtained by substituting (4.14) into (4.12):

$$\begin{aligned} \dot{x}_0 &= Ax_0 + B\bar{\delta}_0, \\ \dot{x}_1 &= (A - BK_{el}T_{v_l})x_1 + BK_{el}T_{r_l}x_0, \\ \dot{x}_2 &= (A - BK_{el}T_{v_l})x_2 + BK_{el}T_{r_l}x_1, \\ &\vdots \\ \dot{x}_n &= (A - BK_{el}T_{v_l})x_n + BK_{el}T_{r_l}x_{n-1}. \end{aligned} \quad (4.15)$$

By defining a new state vector $\bar{x}_n = [x_0^T \ x_1^T \ x_2^T \ \cdots \ x_n^T]^T$, the subsystems can be lumped together into an interconnected string model of the following form:

$$\dot{\bar{x}}_n = \bar{A}_n \bar{x}_n + \bar{B}_n \bar{\delta}_0, \quad (4.16)$$

with

$$\begin{aligned} \bar{A}_n &= \begin{bmatrix} A & 0 & 0 & \cdots & 0 \\ BK_{el}T_{r_l} & A - BK_{el}T_{v_l} & 0 & \cdots & 0 \\ 0 & BK_{el}T_{r_l} & A - BK_{el}T_{v_l} & \cdots & 0 \\ \vdots & & \ddots & \ddots & \vdots \\ 0 & \cdots & 0 & BK_{el}T_{r_l} & A - BK_{el}T_{v_l} \end{bmatrix}, \\ \bar{B}_n &= [B^T \ 0 \ 0 \ \cdots \ 0]^T, \end{aligned}$$

and $\bar{\delta}_0$ is considered as the exogenous input.

4.2 String stability analysis

The performance of the interconnected string model in (4.16) is assessed by conducting a string stability analysis. In Ploeg (2014) an extensive study is conducted on the design and analysis of longitudinal controllers for automated vehicles. Furthermore, Ploeg (2014) provides a thorough framework for assessing longitudinal string stability of platoons based on \mathcal{L}_p string stability. This framework can also be used to assess lateral string stability. First, this theoretical framework is presented, whereafter the framework is applied to the interconnected system in (4.16). In addition to the system in (4.16), consider the linear output functions according to:

$$y_i = C_i \bar{x}_n, \quad i \in \mathcal{K}_n. \quad (4.17)$$

In lateral direction, for example, $y_i = \bar{y}_{v_i}$ or $y_i = \bar{\psi}_{v_i}$ could be used to determine string stability. Then, the input-output dynamics of system (4.16), (4.17) can be formulated in the Laplace domain as follows:

$$y_i(s) = P_i(s) \bar{\delta}_0(s) + O_i(s) \bar{x}_n(0), \quad i \in \mathcal{K}_n. \quad (4.18)$$

where s is the Laplace operator with $s \in \mathbb{C}$ and $P_i(s)$ and $O_i(s)$ being the complementary sensitivity function and initial conditions transfer function, respectively, corresponding to

$$\begin{aligned} P_i(s) &= C_i (sI - \bar{A}_n)^{-1} \bar{B}_n, \\ O_i(s) &= C_i (sI - \bar{A}_n)^{-1}. \end{aligned} \quad (4.19)$$

It is assumed that $P_i(s)$ is square, i.e. $\dim(\bar{\delta}_0) = \dim(y_i) = \ell$, for all i . Next, the string stability complementary sensitivity is introduced as follows:

$$\Gamma_i(s) := P_i(s) P_{i-1}^{-1}(s), \quad (4.20)$$

assuming that $P_i(s)$ is nonsingular for all i such that $P_{i-1}^{-1}(s)$ exists. Then *Theorem 4.1* is obtained from Ploeg et al. (2014).

Theorem 4.1 *Let (4.16), (4.17) represent a linear unidirectionally-interconnected system of which the input-output behavior is described by (4.18), (4.19). Assume that the pair (C_i, \bar{A}_n) is such that*

the unstable and marginally stable modes are unobservable and that $P_i(s)$ is square and nonsingular for all $i \in \mathbb{N}$. Then the system (4.16), (4.17) is strictly \mathcal{L}_2 string stable if and only if

$$\|\Gamma_i(s)\|_{\mathcal{H}_\infty} \leq 1, \quad \forall i \in \mathbb{N} \setminus \{1\}.$$

For the analysis, the same values for \bar{V}_x and L_a are used as in Section 3.4, being $\bar{V}_x = 15\text{m/s}$ and $L_a \in \mathcal{T}_1$. Since the derivative of a state can be written in the Laplace domain as the state multiplied with the Laplace operator s , the following relations exist: $\Gamma_i(s) = \frac{\bar{y}_{v_i}(s)}{\bar{y}_{v_{i-1}}(s)} = \frac{s\bar{y}_{v_i}(s)}{s\bar{y}_{v_{i-1}}(s)}$ and $\Gamma_i(s) = \frac{\bar{\psi}_{v_i}(s)}{\bar{\psi}_{v_{i-1}}(s)} = \frac{s\bar{\psi}_{v_i}(s)}{s\bar{\psi}_{v_{i-1}}(s)}$. Therefore, the choice for \bar{y}_{v_i} or its derivative $\dot{\bar{y}}_{v_i}$ to determine lateral string stability does not influence the result of the string stability complementary sensitivity, the same holds for $\bar{\psi}_{v_i}$ and $\dot{\bar{\psi}}_{v_i}$, under the conditions that the same state is chosen for vehicle i and vehicle $i - 1$. Furthermore, after careful calculations it can be shown analytically, that $\Gamma_i(s) = \frac{\bar{y}_{v_i}(s)}{\bar{y}_{v_{i-1}}(s)}$ or $\Gamma_i(s) = \frac{\bar{\psi}_{v_i}(s)}{\bar{\psi}_{v_{i-1}}(s)}$ results in the same string stability complementary sensitivity function. In Figure 4.3, the magnitude of the string stability complementary sensitivity is presented for vehicle $i \in \mathcal{K}_n$. As can be observed, the string stability complementary sensitivity of $\Gamma_i(s) = \frac{\bar{y}_{v_i}(s)}{\bar{y}_{v_{i-1}}(s)}$ is equal to $\Gamma_i(s) = \frac{\bar{\psi}_{v_i}(s)}{\bar{\psi}_{v_{i-1}}(s)}$. Furthermore, unstable and marginally stable modes are unobservable, illustrated by the zero slope at low frequencies. The criteria for strict \mathcal{L}_2 string stability presented in *Theorem 4.1* are not met for $L_a = 2\text{m}$, which results in the system being strictly \mathcal{L}_2 string unstable. Furthermore, increasing L_a results in a lower magnitude of $|\Gamma_i|$, which results in meeting the criteria for strict \mathcal{L}_2 string stability. Hence, we have now developed a controller strategy which induces stable lateral vehicle following and induces string stable behavior for large enough look-ahead distances. However, in practice, the maximum distance between two vehicles, or inter-vehicle distance, is determined by the longitudinal spacing policy. The longitudinal spacing policy is based on a standstill distance, desired time gap and longitudinal velocity, without taking into account the minimum look-ahead distance needed to achieve string stability in lateral direction. Therefore, it is desired to increase the performance of the system such that it is possible to achieve lateral string stability, irrespective of the look-ahead distance.

4.3 Feed-forward design

To increase the performance of the system, such that it is possible to achieve lateral string stability independent of the look-ahead distance, a feedforward steering input is added. In longitudinal control of vehicle platoons, it is shown that with the addition of a feedforward input, the performance of the interconnected system can be increased such that it is possible to achieve longitudinal string stability while maintaining small inter-vehicle distances (Swaroop, 1997; Naus et al., 2010; Öncü, 2013; Ploeg, 2014). The feedforward input is obtained via wireless communication. This approach could also be applicable in the lateral control of platoons.

The first step in obtaining a feedforward input, is to derive the error dynamics between two vehicles. The error dynamics between two vehicles are derived in Appendix D, where the following error dynamics are obtained (Appendix D, Equation (D.20)):

$$\dot{x}_{el_i} = A_{el}x_{el_i} - A_{v_{i-1}}x_{i-1} + B_{v_l}\bar{\delta}_i - B_{r_l}\bar{\delta}_{i-1}, \quad i \in \mathcal{K}_n, \quad (4.21)$$

where A_{el} contains the error dynamics between the two vehicles and according to the formulation of A_{el} in (2.43). Matrix $A_{v_{i-1}}$ contains the dynamics related to the transformation of states at the

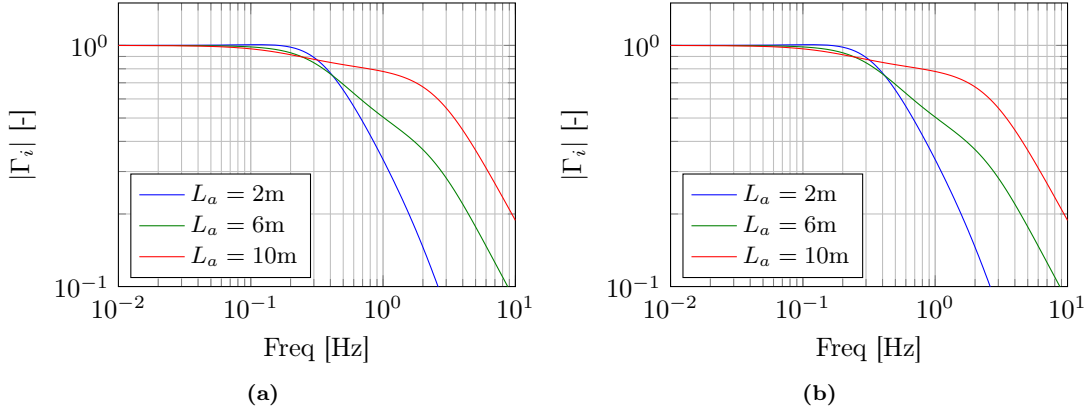


Figure 4.3: (a) Magnitude of the string stability complementary sensitivity $|\Gamma_i|$ with $i \in \mathcal{K}_n$ and $\bar{V}_x = 15\text{m/s}$, for the system with feedback and $\Gamma_i(s) = \frac{\bar{y}_{v_i}(s)}{\bar{y}_{v_{i-1}}(s)}$. (b) Magnitude of the string stability complementary sensitivity $|\Gamma_i|$ with $i \in \mathcal{K}_n$ and $\bar{V}_x = 15\text{m/s}$, for the system with feedback and $\Gamma_i(s) = \frac{\hat{\psi}_{v_i}(s)}{\hat{\psi}_{v_{i-1}}(s)}$.

cm of vehicle $i - 1$ to the rear bumper, B_{v_l} is the input vector, B_{r_l} is the disturbance vector, $\bar{\delta}_i$ is the control input and $\bar{\delta}_{i-1}$ the exogenous disturbance. The ideal feedforward input, which results in perfect following behavior when all errors are zero, does not only depend on the exogenous disturbance input $\bar{\delta}_{i-1}$ but also on the states of vehicle $i - 1$. The states in vector x_{i-1} are global states, however, obtaining global states accurately in practice can be very challenging. Therefore, an alternative feedforward is proposed, while being highly aware of the fact that this is not the ideal feedforward term based on the error dynamics. As the steer input of vehicle $i - 1$ is the exogenous disturbance, it is proposed to use this as a feedforward steer input, i.e.

$$\delta_{ff_i} = \bar{\delta}_{i-1}, \quad i \in \mathcal{K}_n. \quad (4.22)$$

The steer input $\bar{\delta}_{i-1}$ of vehicle $i - 1$ can be obtained by utilizing the wireless communication between vehicle i and $i - 1$. It has to be noted that, the communication delay between two vehicles, due to the use of wireless communication, is assumed to be equal zero. Next, a new control law is formulated for vehicle i , based on (4.14) and (4.22):

$$\bar{\delta}_i = \delta_{fb_i} + \delta_{ff_i} = -K_{el} (T_{vl} x_i - T_{rl} x_{i-1}) + \bar{\delta}_{i-1}, \quad i \in \mathcal{K}_n. \quad (4.23)$$

A consequence of choosing to use the communicated steer input of vehicle $i - 1$ as in (4.23), is that vehicle i will immediately respond to a steer input of vehicle $i - 1$. This means that vehicle i will steer at the same time as vehicle $i - 1$, rather than, from a global perspective, at the same position as vehicle $i - 1$. This will result in vehicle i making smaller corners compared to vehicle $i - 1$, which means that the practical use of this approach is limited to straight roads, for example a highway. Equation (4.23) can be substituted into (4.12), which results in the following model of

the interconnected vehicle string:

$$\begin{aligned}
 \dot{x}_0 &= Ax_0 + B\bar{\delta}_0, \\
 \dot{x}_1 &= (A - BK_{el}T_{v_l})x_1 + BK_{el}T_{r_l}x_0 + B\bar{\delta}_0, \\
 \dot{x}_2 &= (A - BK_{el}T_{v_l})x_2 + BK_{el}(T_{r_l} - T_{v_l})x_1 + BK_{el}T_{r_l}x_0 + B\bar{\delta}_0, \\
 &\vdots \\
 \dot{x}_n &= (A - BK_{el}T_{v_l})x_n + \sum_{k=1}^{n-1} (BK_{el}(T_{r_l} - T_{v_l})x_{n-k}) + BK_{el}T_{r_l}x_0 + B\bar{\delta}_0.
 \end{aligned} \tag{4.24}$$

By defining a new state vector $\bar{x}_n = [x_0^T \ x_1^T \ x_2^T \ \dots \ x_n^T]^T$, the subsystems can be lumped together into an interconnected string model of the following form:

$$\dot{\bar{x}}_n = \bar{A}_n^{ff}\bar{x}_n + \bar{B}_n^{ff}\bar{\delta}_0, \tag{4.25}$$

with

$$\begin{aligned}
 \bar{A}_n^{ff} &= \begin{bmatrix} A & 0 & 0 & \dots & 0 \\ BK_{el}T_{r_l} & A - BK_{el}T_{v_l} & 0 & \dots & 0 \\ BK_{el}T_{r_l} & BK_{el}(T_{r_l} - T_{v_l}) & A - BK_{el}T_{v_l} & \dots & 0 \\ \vdots & & \ddots & \ddots & \vdots \\ BK_{el}T_{r_l} & \dots & BK_{el}(T_{r_l} - T_{v_l}) & BK_{el}(T_{r_l} - T_{v_l}) & A - BK_{el}T_{v_l} \end{bmatrix}, \\
 \bar{B}_n^{ff} &= [B^T \ B^T \ B^T \ \dots \ B^T]^T,
 \end{aligned}$$

and $\bar{\delta}_0$ is considered as the exogenous input. A result of assuming the communication delay to be equal to zero and the choice of the vehicle states in (4.1) is that the resulting interconnected system with feedback and feedforward input, changes into a direct feed through system. In this system, every vehicle in the platoon obtains directly the disturbance input $\bar{\delta}_0$ and the errors of all the preceding vehicles. In Figure 4.4, the magnitude of the corresponding string stability complementary sensitivity is presented. As can be seen, the response is significantly different as in Figure 4.3. This difference in response is due the different structures of (4.16) and (4.25). However, adding the feedforward steer input results in achieving lateral string stability irrespective of the look-ahead distance. Note, however, that this type of feedforward causes the magnitude of the string stability complementary sensitivity to approach 1 for high frequencies, indicating a high sensitivity of vehicle i to the behavior of vehicle $i - 1$, which may vary well be undesirable in practice.

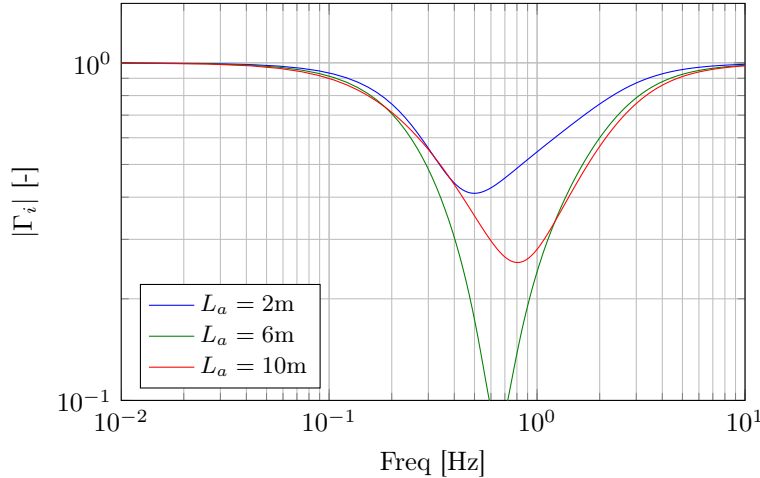


Figure 4.4: Magnitude of the string stability complementary sensitivity $|\Gamma_i|$ with $i \in \mathcal{K}_n$ and $\bar{V}_x = 15\text{m/s}$, for the system with feedback and feedforward input.

4.4 Time-domain simulation results of a lane change manoeuvre

In this section, time-domain simulations with the interconnected vehicle string or platoon are performed. For the simulations, the platoon consists of four vehicles, i.e. $n = 4$. The virtual reference vehicle will perform a lane change manoeuvre which results in lateral displacement of 3.5m and the manoeuvre will have a duration of 4 seconds. The lateral displacement is based on the road width of Dutch highways¹. For the first simulation, all vehicles in the platoon only use the feedback controller, i.e. the interconnected system in (4.16) is used for the simulation. In Figure 4.5, the resulting errors are presented when a lane change is performed by the platoon with $\bar{V}_x = 15\text{m/s}$ and $L_a = 6\text{m}$. The lateral and rotational errors decrease when traveling upstream through the platoon, which corresponds with the results seen in Figure 4.3. In Figure 4.6a, the steer inputs of the vehicles in the platoon are presented. The input response also displays string-stable behavior corresponding with the results previous section. The small steer input seen around 2 seconds is due to the outward movement of the rear bumper. This is a result of the coordinate transformation from the states of the cm of the vehicle $i - 1$ to the rear bumper. As a result of the system being string stable in this configuration, vehicle i has a smaller control input compared to vehicle $i - 1$ (as can be seen in Figure 4.6a). In Figure 4.6b, the global longitudinal (x_{v_i}) and global lateral (y_{v_i}) positions of the vehicles in the platoon are presented. As can be observed, vehicle i cuts the corners compared to vehicle $i - 1$, this is a side effect of directly responding to the movement of the preceding vehicle. This behavior can be observed in Figure 4.6b, by vehicle i starting to steer, from a global position perspective, earlier compared to vehicle $i - 1$. Next, let us present the time-domain results when a lane change is conducted with $\bar{V}_x = 15\text{m/s}$, $L_a = 2\text{m}$ and the lane change manoeuvre now has a duration of 8s. According to results presented Figure 4.3, the system in this configuration is string unstable. Conducting a lane change with a duration of 8s excites the

¹[http://www.rijkswaterstaat.nl/images/Nieuwe%20Ontwerprichtlijn%20Autosnelwegen%20\(NOA\)_tcm174-325052.pdf](http://www.rijkswaterstaat.nl/images/Nieuwe%20Ontwerprichtlijn%20Autosnelwegen%20(NOA)_tcm174-325052.pdf)

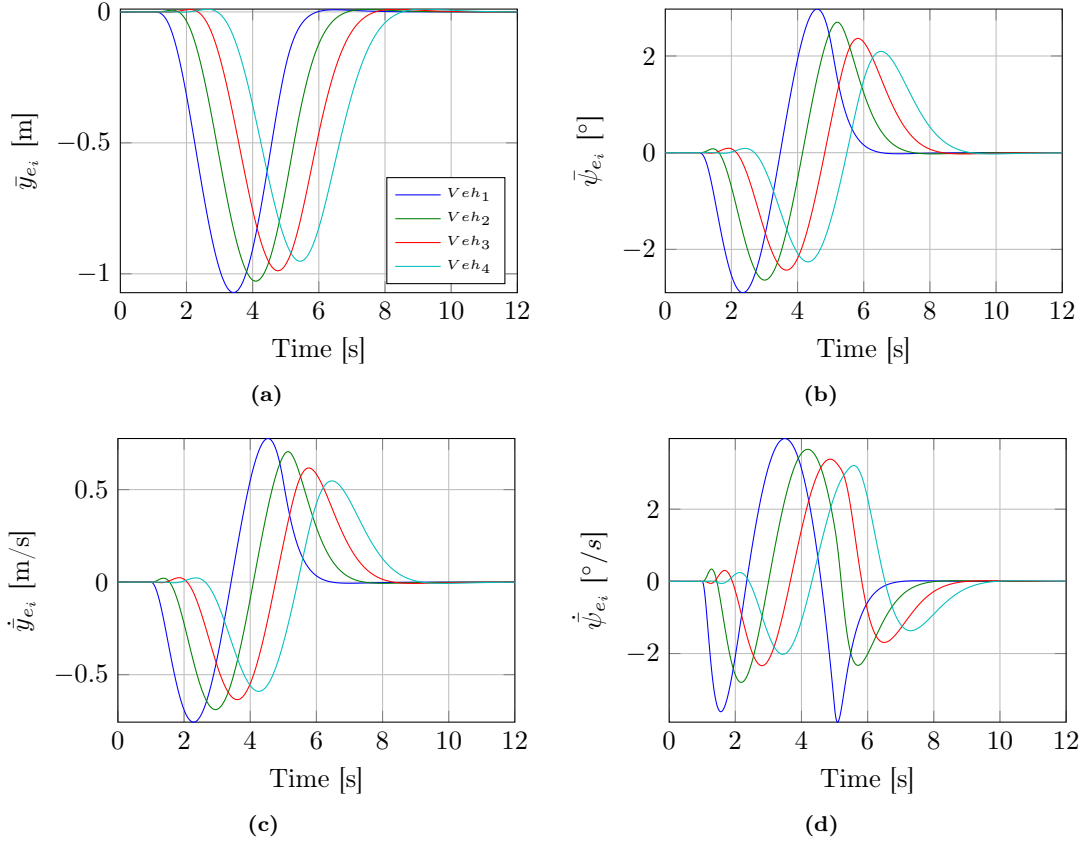


Figure 4.5: The error responses of the platoon when only the feedback controller is used with $\bar{V}_x = 15\text{m/s}$ and $L_a = 6\text{m}$.

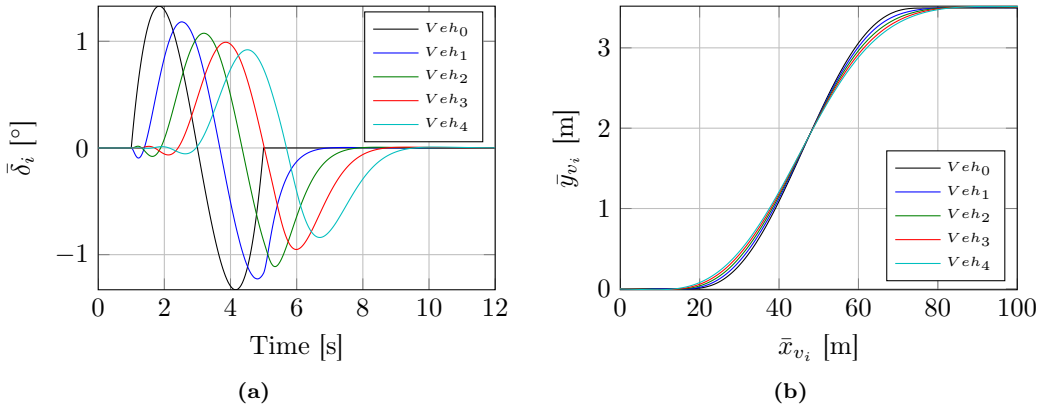


Figure 4.6: (a) Control inputs for the vehicles in the platoon when a lane change is performed. (b) Global longitudinal (x_{v_i}) and lateral (y_{v_i}) positions of the vehicles in the platoon.

system at the frequency with the largest magnitude of the string stability complementary sensitivity function in Figure 4.3. As the goal is to illustrate that the system is string unstable, only the error states are presented in Figure 4.7. The results of the steer inputs and global positions are presented in Appendix E, however, these results do not provide new information. As is shown in Figure 4.7, the system is string unstable in this configuration. Next, a simulation is performed with using feedback and feedforward control such that the effect of adding the feedforward steer input to the system can be further investigated. For this simulation the interconnected system in (4.25) is used,

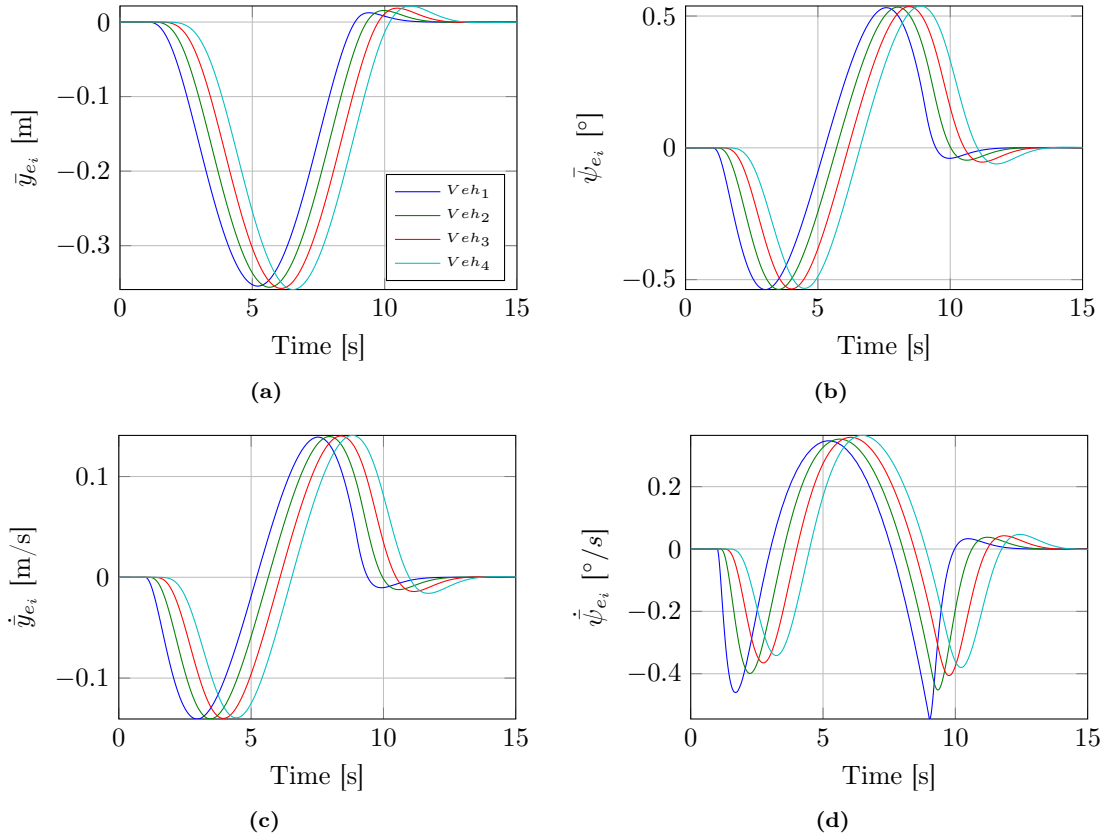


Figure 4.7: The error responses of the platoon when only the feedback controller is used with $\bar{V}_x = 15\text{m/s}$, $L_a = 2\text{m}$ and a lane change manoeuvre with a duration of 8s.

with $\bar{V}_x = 15\text{m/s}$, $L_a = 2\text{m}$ and the lane change manoeuvre has a duration of 8s. As presented previously in Figure 4.3 and in Figure 4.7, the platoon is string unstable when only feedback is used in combination with the chosen velocity and look-ahead distance. Adding feedforward results in meeting the requirements for strict \mathcal{L}_2 string stability in the frequency domain for all look-ahead distances, as is shown in Figure 4.4. The effect of adding the feedforward input, although not being the ideal feedforward, on the time-domain responses is now investigated. The platoon performs again a lane change manouevre and the corresponding errors are presented in Figure 4.8. Adding the feedforward input results, likewise to the results seen in the frequency domain, in string stable behavior of the platoon in the time domain. The errors decrease while traveling upstream through the platoon. Furthermore, adding feedforward results significantly larger errors compared to the

situation when only feedback is used and oscillations occurring around Time=1s and Time=9s of yaw-rate error response, as is shown Figure 4.8d. Next, in Figure 4.9a, the steer inputs of the

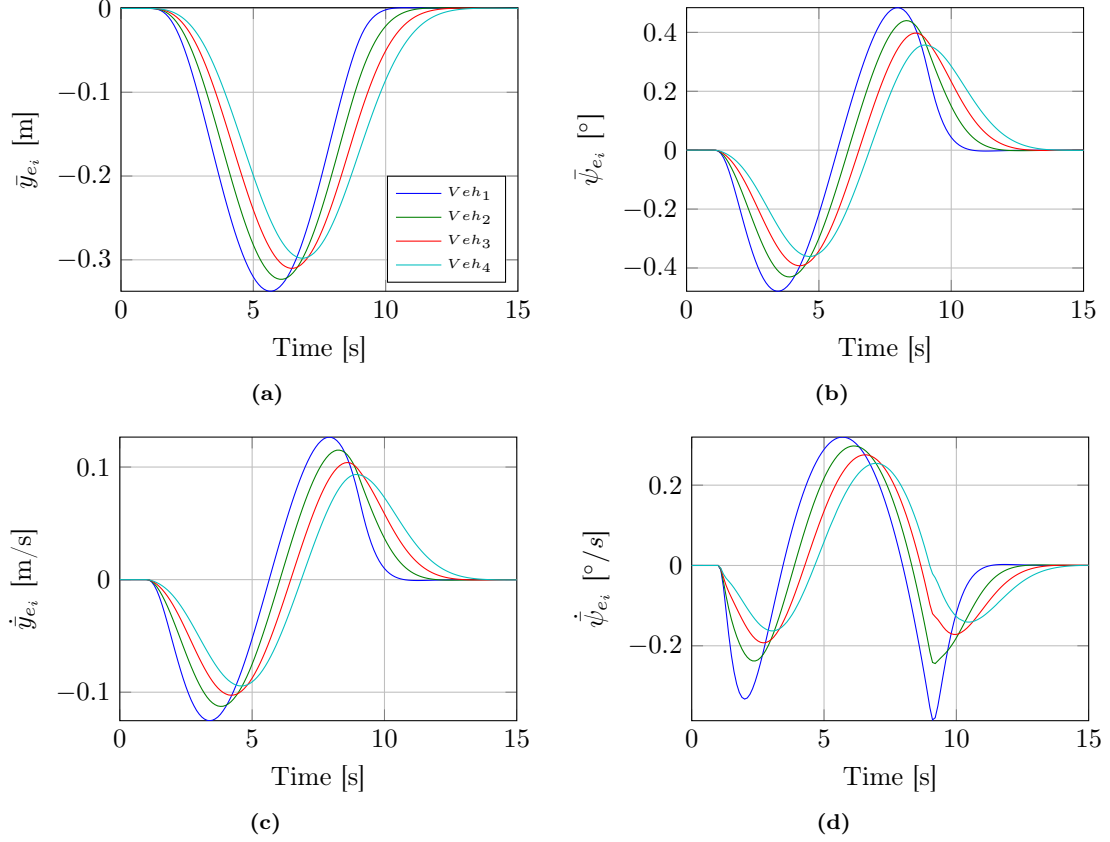


Figure 4.8: The error responses of the platoon when the feedback and feedforward controller are used with $V_x = 15\text{m/s}$ and $L_a = 2\text{m}$.

vehicles in the platoon are presented. It can be seen that the oscillations observed in Figure 4.8d, occur at the start and end of the lane change made by the virtual reference vehicle. Before going into further detail about the cause of these oscillations, let us consider the influence of adding the feedforward on the global position response of the vehicles in the platoon. In Figure 4.9b, the global longitudinal and lateral position of the vehicle in the platoon are presented. The addition of feedforward results in vehicle i obtaining preview information about the intended movement of vehicle $i - 1$. This results in vehicle i starting to steer earlier than in the situation where only feedback is used. As a result of this the corning cutting behavior is amplified by the addition of feedforward. All simulation results for $\bar{V}_x = 15\text{m/s}$ and $L_a \in \mathcal{T}_1$, when using feedback and feedback and feedforward control can be found in Appendix E. Next, let us have a closer look at the steer input $\bar{\delta}_i$ to identify the cause of the oscillations seen in Figure 4.8 and Figure 4.9a. As presented in Equation (4.23), $\bar{\delta}_i$ consist of two components, δ_{fb_i} and δ_{ff_i} . In Figure 4.10, the components δ_{fb_i} and δ_{ff_i} of $\bar{\delta}_i$ of all vehicles in the platoon are presented. Due to omitting the time delay and having a direct feed through system in (4.25), all vehicles in the platoon receive the feedforward input at the same time (indicated with the dash-dotted line in the Figure 4.10). However, the steer input of the feedback controller has a different sign compared to the feedforward

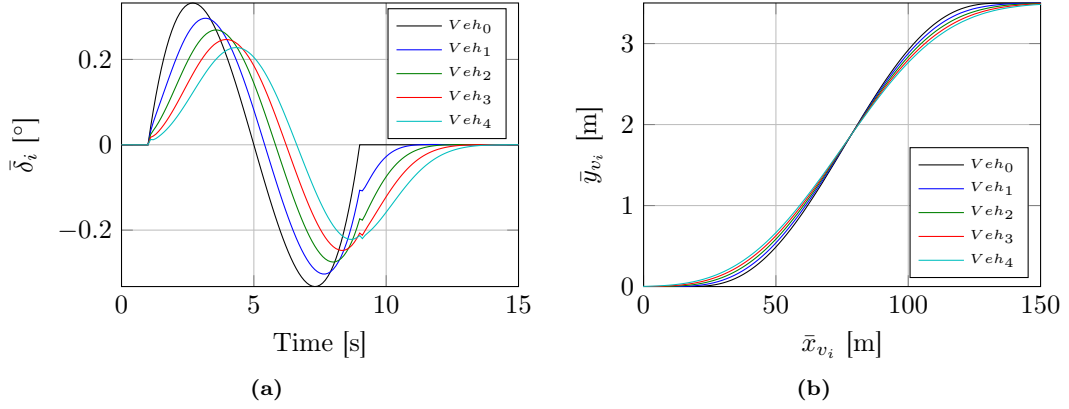


Figure 4.9: (a) Control input for the vehicles in the platoon when a lane change is performed.
(b) Global longitudinal (x_{v_i}) and lateral (y_{v_i}) positions of the vehicles in the platoon.

steer input. This means that both inputs want to steer in opposite directions rather than being complementary to each other. This is caused by the following phenomenon. In Figure 4.11, a

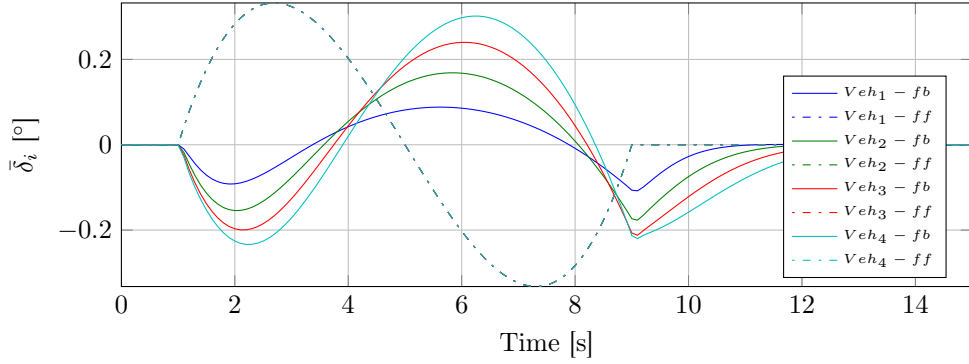


Figure 4.10: Decomposed steer input showing the contribution of the feedback and feedforward input.

schematic representation is presented of the cause of the conflicting steer input. As mentioned previously, the steer input of vehicle $i - 1$ is directly used in the control law of vehicle i , which means, for example, that vehicle i starts steering to the left when vehicle $i - 1$ starts steering to the left. However, due to the geometry of the vehicle, the rear bumper of vehicle $i - 1$ will move outwards in opposite direction. As the rear bumper is used as a reference for the determining the errors used in the feedback controller of vehicle i , this feedback controller wants to steer to the right, i.e. in opposite direction. The oscillations then occur when the feedforward input starts and stops. Finally, the response of the platoon is presented when only feedforward steer input is used. It has to be mentioned that this method can not be used in practice, due to the absence of a feedback controller, which can compensate for model inaccuracies, initial errors and disturbances, and if left out, could potentially lead to unsafe situations. In Figure 4.12a, the steer input for all vehicles in the platoon are presented. As expected, all vehicles start steering at the same time and the steer inputs have the same qualitative and quantitative properties. Furthermore, using only

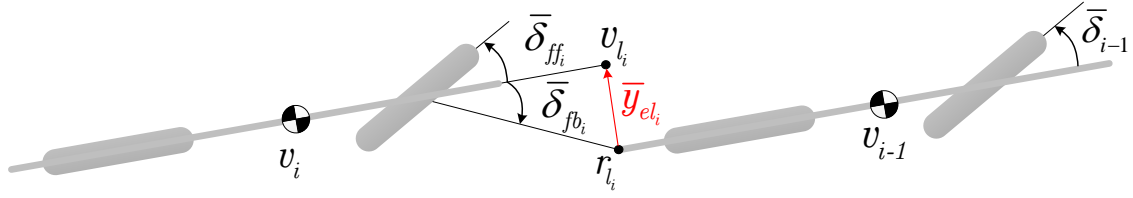


Figure 4.11: Schematic representation of the situation when the feedback and feedforward steer have an input in opposite direction.

feedforward steer input significantly increases the cornering cutting of the vehicles in the platoon, as is shown in Figure 4.12b.

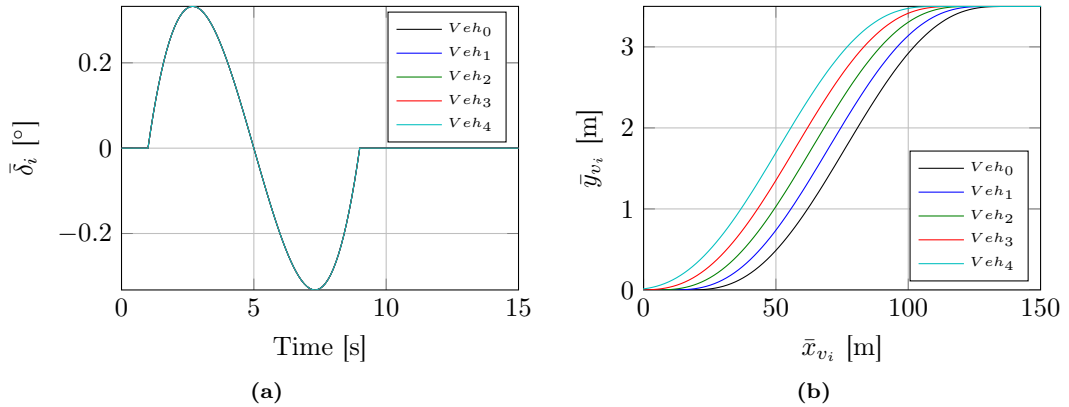


Figure 4.12: (a) Control input for the vehicles in the platoon when a lane change is performed. (b) Global longitudinal (x_{v_i}) and lateral (y_{v_i}) positions of the vehicles in the platoon.

4.5 Conclusion

In this chapter, the lateral string stability of a platoon is assessed when using the steering controller synthesized in Chapter 3. The first step in this analysis is to construct a model of an interconnected string of n vehicles. Next, criteria for assessing lateral string stability are presented based on the work in Ploeg et al. (2014). It is shown that the system with only feedback control can meet the requirements for being strictly \mathcal{L}_2 string stable if the look-ahead distance is chosen sufficiently large. Of the three different look-ahead distances presented, the system fulfills the requirements for being strictly \mathcal{L}_2 string stable when a look-ahead distance is chosen of 6m or 10m, while the system does not meet the requirements for being strictly \mathcal{L}_2 string stable when the look-ahead distance is 2m. A feedforward input is added to improve the performance of the system such that it is possible to achieve string stability, irrespective of the look-ahead distance. However, based on the error dynamics between two vehicles, it is illustrated that the ideal feedforward is depending on global coordinates of vehicle $i - 1$. As it is very challenging to obtain accurate global information in practice, the choice is made to use the steering angle of vehicle $i - 1$ as a feedforward input for vehicle i , while being aware of the fact that this is not the ideal feedforward input. The

resulting closed-loop system, using this feedforward, is laterally string stable, irrespective of the look-ahead distance. As a consequence of the choice of the system states and feedforward input, the interconnected string model with feedforward changes into a direct feed through system. This means that each vehicle directly responds to the steer input of the virtual reference vehicle. Next, time-domain simulations are performed with the interconnected system when using only feedback control and feedback and feedforward control. The system with only feedback shows lateral string stable behavior when the look-ahead distance is chosen sufficiently large, corresponding with the frequency domain results. The system with feedback and feedforward is laterally string stable irrespective of the chosen look-ahead distance. However, additional oscillations are observed at the start and end of the lane change caused by conflicting signs of the feedback and feedforward input. These conflicting signs are due to the two different control objectives. The feedforward controller wants to follow the *cm* of the preceding vehicle, while the feedback controller wants to follow the rear bumper of the preceding vehicle. As a result, the chosen feedforward input is not suited to improve the performance of the system, although it results in string stable behavior, the oscillations would be very uncomfortable for the driver. Next, the controller is implemented in the experimental setup and the performance of the system will be evaluated.

Chapter 5

Experimental results

The last step in the evaluation of the performance of the controller, is by implementing it in the experimental setup. In this chapter, experimental results are presented using the steering controller developed in Chapter 3 and Chapter 4. The controller is implemented into the Toyota Prius III used by TNO for the development of ITS applications. The experiments are conducted at the Aldenhoven Testing Center (ATC) of RWTH Aachen University GmbH in Germany. This chapter is organized as follows. In Section 5.1, the experimental setup is presented, in Section 5.2, implementation aspects are addressed and Section 5.3 contains the experimental results. Finally, in Section 5.4, the conclusion of this chapter is presented.

5.1 Experimental setup

TNO uses a Toyota Prius III as an experimental platform for the development of ITS applications. A photograph of the two vehicles used for conducting the experiments is presented in Figure 5.1a. The test vehicles are factory standard Toyota Prius III modified with additional sensors and hardware such as a camera behind the windshield, a wireless communication module and GPS sensor. Furthermore, as presented in Figure 5.1b, in the trunk of the vehicle several additional hardware components are positioned. The Real-Time Platform is a small computer equipped with a real-time operating system. The Real-Time Platform is connected through the Vehicle Gateway, which is positioned in the passenger compartment, to the Controller Area Network (CAN) bus of the vehicle. This provides the possibility to communicate with the vehicle's sensors and actuators and control, for example, the steering, accelerating and breaking of the vehicle. In the trunk, also an ethernet switch, which provides the communication between the Real-Time Platform and the HMI, is placed. Further, an ITS G5 Gateway enables the wireless communication between the two vehicles in the platoon and, as already mentioned previously, a GPS sensor. A more detailed description of the experimental setup can be found in Tzempetzis (2015).

Test scenario

When designing a test scenario for obtaining experimental results, elements as safety and the objective of the experiments have to be carefully considered. The test scenario for the experiments

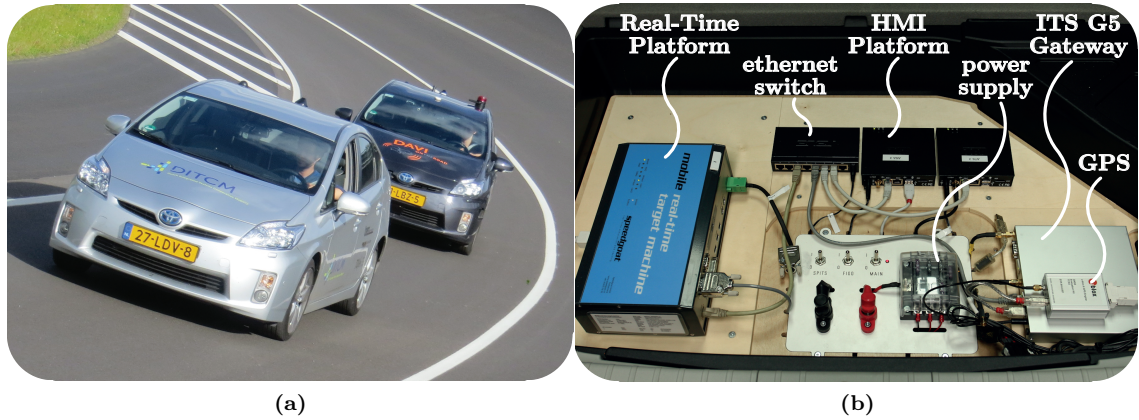


Figure 5.1: (a) Two vehicle platoon used for the experiments. (b) A close-up of the hardware in the trunk of the Prius.

is based on the same lane change manoeuvre which is used for the time-domain simulations in Chapter 4. A benefit of performing a lane change manoeuvre is that the needed lateral displacement of the vehicle can be determined *a priori*. As a result, it can be guaranteed that the platoon stays within the limited space available for lateral manoeuvring. However, there is also a drawback when choosing this manoeuvre. For proper evaluation of the controller it is desired to have an input which excites the platoon dynamics over the frequency range of interest for the assessment of lateral string stability. When a lane change manoeuvre is performed only one specific frequency can be chosen to excite the platoon dynamics. Excitation signals which are rich in frequency content, e.g. white noise or a multi sine signal, are desired from a validation point of view, however, it is not possible to determine what the lateral displacement of a platoon will be *a priori*. As the available lateral displacement on the test track is limited, a signal which is rich in frequency content, without being able to determine *a priori* the needed lateral displacement cannot be used.

The lane change manoeuvre used in the experiments has the same parameters as the lane change manoeuvre used in Chapter 4. This results in a lane change manoeuvre with duration of 4s and a lateral displacement of 3.5m. A lane change manoeuvre with a longer duration, which results in a lower frequency input, could not be realized by the first vehicle in the platoon. This is caused by issues presented in the next section.

5.2 Implementation challenges

During the implementation of the controller on the test vehicles, several issues were encountered. In this section, these issues are discussed in further details and the consequences for performance of the controller is investigated:

- Due to time limitations, the choice was made, not to model the actuator dynamics, actuator delay and sensing delay. Although this is common approach in literature (Lu and Tomizuka, 2003; Rajamani, 2011; Solyom et al., 2013), this means that the error dynamics model and vehicle model used for controller design and simulations, allows for a higher bandwidth than possible in practice.

- Determining accurately the rotational heading angle of a vehicle, by only using a standard GPS sensor is very unreliable. The global position based on GPS can have a large error. The orientation angle of a vehicle is based on this signal and therefore may also have a large error. This provides significant challenges in obtaining a measured signal of good quality of the rotational error between two vehicles. Therefore, a practical solution to this, is to assume that the orientation error between vehicle i and vehicle $i - 1$ ($\dot{\psi}_{e_i}$), is equal to the measured angle between the center line of the vehicle and the rear bumper of the preceding vehicle. The assumption is then made that the orientation of vehicle $i - 1$ is equal to the measured angle, as is shown in Figure 5.2.

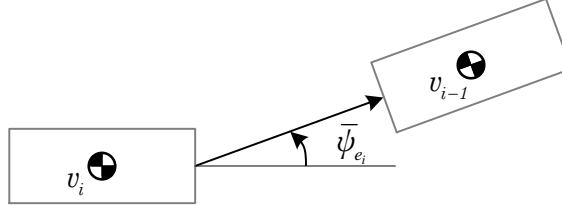


Figure 5.2: Proposal practical solution to obtain the orientation angle between two vehicles.

- The signals \dot{y}_{e_i} and $\dot{\psi}_{e_i}$ are, in practice, significantly influenced by noise which results in signals of lower quality.

Additionally, although not a significant issue, is that the sensor used for measuring the steering wheel angle is positioned at the top of the steering column. The steering column, for safety reasons, is not a rigid construction. This, in combination with the compliance of the bushes and rubbers used to mount the steering column and steering rack, results in a small offset of the steering angle, of which the direction is depending on the banking of the road surface. This small difference between the reference angle of the steering wheel and the actual angle of the wheels, also results in a zero steering angle not corresponding to a zero heading angle of the vehicle.

A common approach in compensating for the modelling inaccuracies and the fact that measured signals are significantly influenced by noise, is to reduce the bandwidth of the controller based on practical results. For a LQR design approach this can be achieved by lowering the weighting gains in the matrix Q . In Table 5.1, the old and new weighting gains for matrix Q are presented (where the new weighting gains are obtained by manually tuning the controller based on experimental results, while still fulfilling the requirements for LQR controller synthesis). As can be seen in Table

Weighting gains		Weighting gains	
q_1	0.25	q_1	0.00225
q_2	0.01	q_2	0
q_3	1	q_3	0.05
q_4	0	q_4	0

(a)

(b)

Table 5.1: (a) Old weighting gains. (b) New weighting gains, obtained based on manual tuning.

5.1, the influence of the issues mentioned above is significant and results in a considerable loss of

performance of the closed-loop system. Especially, the weighting which penalizes the rotational error had to be considerably reduced before the vehicle would follow without having nervous steering behavior. This also causes a significant loss in damping of the system. As is shown in Appendix C, where increasing the weighting gain related to the rotational error (q_3) results in the addition of damping to the system.

In Figure 5.3, the string stability complementary sensitivity is presented for different look-ahead distances when using the old and new weighting gains and the platoon model in (4.16). The new system fulfills the requirements for strict \mathcal{L}_2 string stability when the look-ahead distance is increased to 26m. It has to be noted that the interconnect string model in (4.16) does not include the mentioned steering dynamics and delay and sensing delay. However, it provides already an indication in the amount of performance loss in the system.

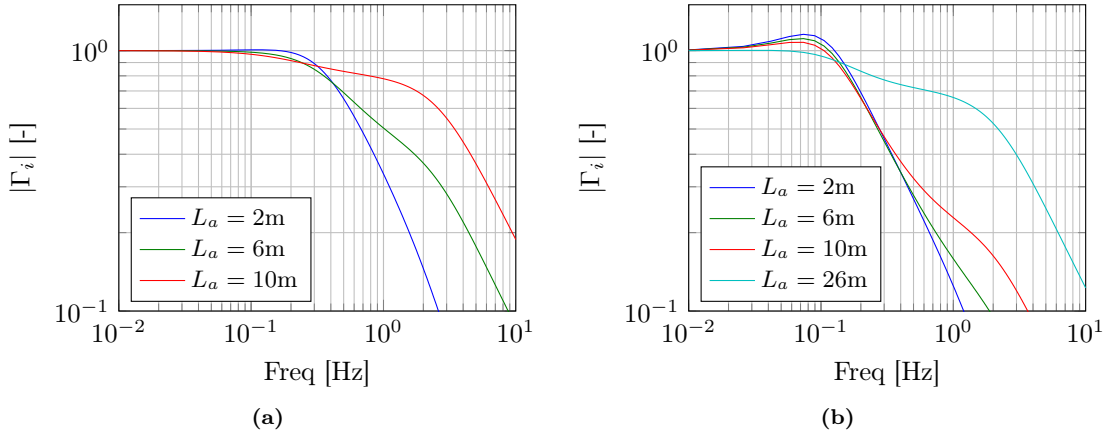


Figure 5.3: (a) Model based result of the magnitude of the string stability complementary sensitivity $|\Gamma_i|$ with $i \in \mathcal{K}_n$, for the interconnected string which only uses feedback (4.16), and the weighting gains of Table 5.1a. (b) Model based result of the magnitude of the string stability complementary sensitivity $|\Gamma_i|$ with $i \in \mathcal{K}_n$, for the interconnected string which only uses feedback (4.16), and the weighting gains of Table 5.1b.

5.3 Experimental results

In this section, the experimental results are presented. The first experiment is conducted with $\bar{V}_x = 15\text{m/s}$ and the look-ahead distance is based on the longitudinal spacing policy. The longitudinal spacing policy is defined according to a constant time gap spacing policy and can be written as follows, $d_{r_i}(t) = r + h\bar{V}_x(t)$, $i \in \mathcal{K}_n$, where h is the desired time gap and r is the standstill distance which for all experiments is $r = 2.5\text{m}$. Although the longitudinal spacing policy is velocity depending, as mentioned in Chapter 2, for the lateral vehicle model to be valid, the velocity \bar{V}_x has to be constant, which results in d_{r_i} also being constant.

For the first experiment $h = 1\text{s}$ is used, which results in a look-ahead distance of 17.5m . Since this is smaller than the required 26m , the system is assessed as string unstable based on the model. This can also be observed in the experimental results presented in Figure 5.4, where the corresponding steer inputs and yaw-rates of the vehicles in the platoon during a lane change are presented. As the system is string unstable, vehicle 2 has a larger steer input and yaw rate compared to vehicle

1. For the next experiment $h = 0.6\text{s}$, which results in a look-ahead distance of 11.5m. In Figure

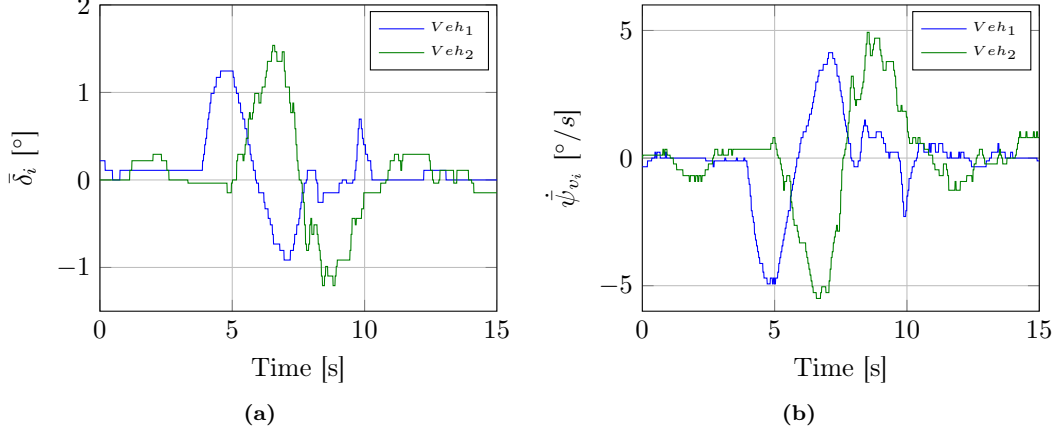


Figure 5.4: Test 1.1: $\bar{V}_x = 15\text{m/s}$, $L_a = 17.5\text{m}$, only feedback. (a) Steer input of the two vehicle platoon during the lane change. (b) Yaw-rate response of the two vehicle platoon during the lane change.

5.5, the experimental results are presented when a lane change is performed with $\bar{V}_x = 15\text{m/s}$ and $h = 0.6\text{s}$. As shown in this figure, there is a significant increase of the steer input and yaw-rate response of vehicle 2 compared to vehicle 1. Furthermore, due to a lack of damping, which is caused by considerably less weighting on the rotational error, there are additional oscillations compared to time-domain simulation results in the previous chapter until a steady-state situation is achieved.

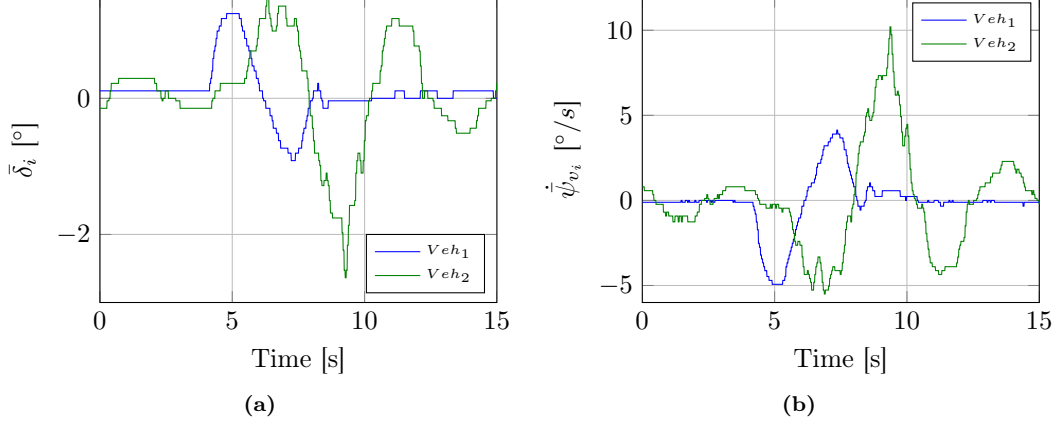


Figure 5.5: Test 1.2: $\bar{V}_x = 15\text{m/s}$, $L_a = 11.5\text{m}$, only feedback. (a) Steer input of the two vehicle platoon during the lane change. (b) Yaw-rate response of the two vehicle platoon during the lane change.

The addition of a feedforward steer input did not improve the responds of the system. Adding the feedforward caused very nervous steering behavior of the vehicle and resulted often in a loss of

target, which thereby resulted in an interrupted experiment. In Figure 5.6, the steer inputs and yaw-rate responses are presented when a lane change is performed with $\bar{V}_x = 15\text{m/s}$ and $h = 0.6\text{s}$ when using feedback and feedforward steer input. As can be seen, vehicle 2 responds faster to the steer input of vehicle 1, compared to the other two experiments. However, there are significantly more oscillations compared to, for example, the results in Figure 5.4. This behavior could already be observed in the time-domain simulation results of the system with feedback and feedforward presented in Section 4.4. However, in practice, the amplitude of the oscillations and the amount of oscillations are significantly larger.

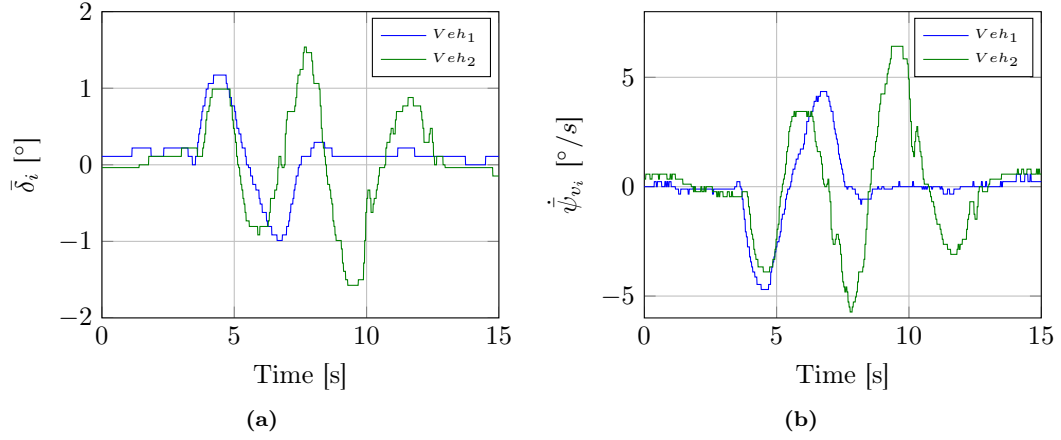


Figure 5.6: Test 1.4: $\bar{V}_x = 15\text{m/s}$, $L_a = 11.5\text{m}$, feedback and feedforward. (a) Steer input of the two vehicle platoon during the lane change. (b) Yaw-rate response of the two vehicle platoon during the lane change.

5.4 Conclusion

In this chapter, the steering controller is implemented in an experimental platoon of Toyota Prius vehicles and the performance is evaluated. Due to a combination of unmodeled steering dynamics and delay, sensor delay, low quality measurement signals and problems in accurately obtaining the rotational error between two vehicles, the bandwidth of the controller had to be significantly reduced, by manually tuning the controller. Using LQR controller synthesis, this can be achieved by reducing the weighting gains in matrix Q . Especially, the weighting gain q_3 , which penalizes the rotational error $\bar{\psi}_{e_i}$ had to be reduced significantly. As mentioned in Section 3.3, penalizing $\bar{\psi}_{e_i}$ results in adding damping to the system. Decreasing the weighting gain for $\bar{\psi}_{e_i}$, results in a significant loss of damping in the system. The system can still fulfill the requirements for strict \mathcal{L}_2 string stability by increasing the look-ahead distance. However, a large look-ahead distance is conflicting with the control objective for longitudinal control, which is to achieve strict \mathcal{L}_2 string stability while maintaining short inter-vehicle distances. Choosing a velocity of 15m/s and a time gap of 1s, results in an inter-vehicle distance of 17.5m, while at this velocity a minimum look-ahead distance of 26m is necessary to achieve strict \mathcal{L}_2 string stability in lateral direction. Furthermore, adding a feedforward steer input does not increase the performance of the system. Adding feedforward results, initially, in a faster response of the platoon. However, it also results in additional oscillations in the vehicle response due to the conflicting signs of the feedback and

feedforward, as is shown in Section 4.4. If the longitudinal spacing policy is used to determine the look-ahead distance, lateral string stability can not be achieved with the new set of practically tuned weighting gains.

Chapter 6

Conclusions & Recommendations

In this chapter, the main conclusions regarding the work conducted in this thesis are presented. Furthermore, based on the obtained results, recommendations are given for future research.

6.1 Conclusions

The goal of this master thesis is to develop a steering controller for vehicles in a platoon, which guarantees stable vehicle following behavior in the lateral direction and lateral string stability for a platoon of infinite length. This steering controller should be, in a wide operating region, robust against changing velocity and changing look-ahead distances, while respecting actuator bandwidth limitations and have a velocity-depending steer input such that large steer inputs at high velocity are prevent from occurring.

For this purpose, a non-linear model is derived in Chapter 2 which describes the lateral and rotational dynamics of a vehicle, whereafter this model is linearized using the origin as linearization point. In the origin all vehicle states and input are equal to zero. Next, a linearized model of the error-dynamics between a reference point in front of the vehicle and the *cm* of the vehicle is used to synthesize a feedback controller based on an LQR-design approach. An LQR-design approach is chosen, because it is robust in a wide operating region of the different velocities and look-ahead distances. Furthermore, it is desired, for safety reasons, that the steer input decreases with increasing velocity. Using an LQR-based controller design approach, this can be integrated into the controller design, as is evidenced in Chapter 3.

A homogeneous interconnected string model of n vehicles is obtained in Chapter 4 by substituting the proposed controller in the lateral vehicle dynamics model. Next, lateral string stability of this system is assessed. The string stability complementary sensitivity of the system is evaluated to determine if the system is strict \mathcal{L}_2 string stable (in terms of the lateral dynamics). In the case of feedback control, the requirements for being strictly \mathcal{L}_2 string stable are met if the look-ahead distance is chosen sufficiently large. To improve the performance of the system, such that it is possible to achieve string stability irrespective of the look-ahead distance, a feedforward steer input is added. However, the ideal feedforward, based on the error dynamics between two vehicles, is depending on vehicle states with respect to a global frame (the ideal feedforward results in

perfect tracking behavior when all errors converged to zero). As it is difficult to obtain accurate global vehicle state information in practice by, for example, using GPS, the choice is made to investigate if using the steer input of the preceding vehicle as a feedforward input results in the desired performance increase, while being aware that this is not the ideal feedforward input. The addition of such feedforward results in the system meeting the requirements for being strict \mathcal{L}_2 string stable independent of the look-ahead distance. Next, time-domain simulations are conducted with the interconnected string model by considering a lane change scenario. It is shown that, by using the feedback controller and the look-ahead sufficiently large, string stability can be achieved in lateral direction. Due to the choice of the state vector and neglecting communication delay, the interconnected string model with feedback and feedforward input changes into a directed feed-through system. This means that each vehicle in the platoon directly obtains information about the disturbance introduced by the virtual reference vehicle and the errors of all preceding vehicles in the platoon. In the time-domain simulations results, it is shown that the addition of the feedforward input results in string stable behavior for small look-ahead distances. However, oscillations are introduced due to the conflicting signs of the feedback and feedforward input, these oscillations are caused by the different control objectives of both inputs.

Finally, the controller is implemented in a platoon consisting out of two experimental vehicles in Chapter 5. The bandwidth of the controller had to be significantly reduced to be able to compensate for the unmodeled actuator dynamics and delay, sensing delay and the low quality of the measurements of the lateral velocity error and rotational velocity error. This resulted in a substantial loss of damping in the closed-loop system dynamics. Damping can be added to the system by increasing the look-ahead distance. However, to achieve strict \mathcal{L}_2 string stability, the look-ahead distance has to be increased to such a large extent, that it becomes conflicting with requirements on the longitudinal spacing policy. During the experiments, it is shown that lateral string stability can not be achieved with the manually tuned controller, when using the longitudinal spacing policy to determine the maximum look-ahead distance. Furthermore, the addition of using a feedforward steer input results in, initially, a faster response. However, it causes a significant increase in oscillations of transient behavior of the vehicle. Unfortunately, this means that, although lateral string stability can be achieved, it cannot be achieved within the maximum inter-vehicle distance set by the longitudinal spacing policy.

6.2 Recommendations

The proposed control method results in stable vehicle following behavior in lateral direction and lateral string stability if the look-ahead distance is chosen sufficiently large. However, there are limitations to its applicability and challenges related to the implementation in the experimental vehicles, which provides opportunities for further research.

It is shown that, although common in literature, neglecting the model actuator dynamics and delay and sensing delay has a significant influence on the performance of the system. Therefore, these should be incorporated into the error dynamics model and vehicle dynamics model to provide a more accurate model as basis for controller design and lateral string-stability analysis.

For the derivation of the error dynamics derivation, the look-ahead distance was positioned on the centerline of the vehicle. However, a human driver, while driving, in general, looks into the direction he or she steers. Positioning the look-ahead distance on the centerline of the front wheel would mimic this behavior and could potentially lead to a better response of the system.

Implementing the control law with feedback and feedforward steer input into the interconnected string model resulted in direct feed-through system. In this system each vehicle in the platoon

receives information about the input of the virtual reference vehicle and the errors of all preceding vehicles. However, in practice, a vehicle, in general, only obtains information of the preceding vehicle. The direct feed-through system is a result of a combination of the choice of states of the vehicle, error states and feedforward input. A different choice of vehicle states could prevent this from occurring, where the state vector used in longitudinal control could be used as a template for the new state vector.

In the current control objective used for lateral control, a vehicle responds at the same moment in time to a disturbance of a preceding vehicle. A consequence of this is that the following vehicle will cut the corner compared to the preceding vehicle. Although, this is not an issue when driving in a straight line on the highway, in an urban setting this causes significant challenges. A solution to this problem could be to change the control objective to a trajectory following control objective, such that the following vehicle will steer at the same position rather than at the same time.

In practice, it is very challenging to accurately determine the rotational error between two vehicles. The calculation of the rotational error could be improved using state information of the preceding vehicle which can be obtained via wireless communication already available. This communicated state information of the preceding vehicle could also be used to improve the quality of the signals of the lateral error velocity and rotational error velocity.

Another approach to improve the lateral performance could be tune the controller such that to bandwidth of the controller does more comply with the expected frequency input related to a certain velocity. In the current controller, the bandwidth of the controller is a result of the chosen values of the weighting gains in the state weighting matrix and control weighting matrix, without tuning the bandwidth of the system to an expected frequency input related to certain velocity.

Due to the challenges encountered during the experimental tests, it is recommended to investigate which requirements of the experimental vehicles are needed for lateral vehicle following and lateral string stability. Based on these requirement, evaluate if the current setup of the Toyota Prius fulfills these requirements or improvement of the setup is necessary.

Finally, it is recommended to further investigate what the control objective in lateral direction should be if it is decided to follow path of the preceding vehicle, for example, if the path of the *cm* of the preceding vehicle or the path of the front axle of the preceding vehicle should be followed. Furthermore, it is recommended to investigated what the influence of this new control objective is on the closed-loop platoon dynamics and the lateral string stability of the platoon.

Bibliography

- Arem, B. van, Driel, C. van, and Visser, R. (2006). The impact of cooperative adaptive cruise control on traffic-flow characteristics. *IEEE Transactions on Intelligent Transportation Systems*, 7(4), p. 429–436.
- Bergenhem, C., Shladover, S., Coelingh, E., Englund, C., and Tsugawa, S. (2012). Overview of platooning systems. In *Proceedings of the 19th ITS World Congress*, 2012.
- Friedland, B. (2012). *Control system design: an introduction to state-space methods*. Courier Corporation.
- Guldner, J., Sienel, W., Tan, H., Ackermann, J., Patwardhan, S., and Bunte, T. (1999). Robust automatic steering control for look-down reference systems with front and rear sensors. *IEEE Transactions on Control Systems Technology*, 7(1), p. 2–11.
- He, C. and Mehrmann, V. (1994). Stabilization of large linear systems.
- Hingwe, P. and Tomizuka, M. (1997). Experimental evaluation of a chatter free sliding mode control for lateral control in AHS. In *Proceedings of the American Control Conference*, 1997, 5, p. 3365–3369, IEEE.
- Hingwe, P., Wang, J., Tai, M., and Tomizuka, M. (2000). Lateral control of heavy duty vehicles for automated highway system: Experimental study on a tractor semi-trailer. *California Partners for Advanced Transit and Highways (PATH)*.
- Khatir, M. and Davison, E. (2005). Decentralized control of a large platoon of vehicles operating on a plane with steering dynamics. In *Proceedings of the American Control Conference*, 2005. p. 2159–2165, IEEE.
- Lu, G. and Tomizuka, M. (2003). A laser scanning radar based autonomous lateral vehicle following control scheme for automated highways. In *Proceedings of the 2003 American Control Conference*, 2003, 1, p. 30–35, IEEE.
- Naus, G., Vugts, R., Ploeg, J., van de Molengraft, M., and Steinbuch, M. (2010). String-stable CACC design and experimental validation: A frequency-domain approach. *IEEE Transactions on Vehicular Technology*, 59(9), p. 4268–4279.
- Öncü, S. (2013). *String Stability of Interconnected Vehicles: Network-aware Modelling, Analysis & Experiments*. Ph.D. thesis, Technical University Eindhoven.
- Pacejka, H. (2005). *Tyre and vehicle dynamics*. Elsevier.

- Pant, A., Seiler, P., Koo, T., and Hedrick, K. (2001). Mesh stability of unmanned aerial vehicle clusters. In *Proceedings of the American Control Conference, 2001*, **1**, p. 62–68, IEEE.
- Papadimitriou, I. and Tomizuka, M. (2004). Lateral control of platoons of vehicles on highways: the autonomous following based approach. *International journal of vehicle design*, **36**(1), p. 24–37.
- Papadimitriou, I., Lu, G., and Tomizuka, M (2003). Autonomous lateral following consideration for vehicle platoons. In *Proceedings IEEE/ASME International Conference on Advanced Intelligent Mechatronics, 2003*, **1**, p. 401–406, IEEE.
- Peppard, L. (1974). String stability of relative-motion PID vehicle control systems. *IEEE Transactions on Automatic Control*, **19**(5), p. 579–581.
- Ploeg, J. (2014). *Analysis And Design Of Controllers For Cooperative And Automated Driving*. Ph.D. thesis, Technical University Eindhoven.
- Ploeg, J., van de Wouw, N., and Nijmeijer, H. (2014). \mathcal{L}_p string stability of cascaded systems: Application to vehicle platooning. *IEEE Transactions on Control Systems Technology*, **22**(2), p. 786–793.
- Rajamani, R. (2011). *Vehicle dynamics and control*. Springer.
- Seiler, P., Pant, A., and Hedrick, J. (2003). A systems interpretation for observations of bird V-formations. *Journal of theoretical biology*, **221**(2), p. 279–287.
- Shladover, S., Desoer, C., Hedrick, J., Tomizuka, M., Walrand, J., Zhang, W., McMahon, D., Peng, H., Sheikholeslam, S., and McKeown, N. (1991). Automated vehicle control developments in the PATH program. *IEEE Transactions on Vehicular Technology*, **40**(1), p. 114–130.
- Snider, J. (2009). Automatic steering methods for autonomous automobile path tracking. *Robotics Institute, Pittsburgh, PA, Tech. Rep. CMU-RITR-09-08*.
- Solyom, S. and Coelingh, E. (2013). Performance limitations in vehicle platoon control. *Intelligent Transportation Systems Magazine, IEEE*, **5**(4), p. 112–120.
- Solyom, S., Idelchi, A., and Salamah, B. (2013). Lateral Control of Vehicle Platoons. In *IEEE International Conference on Systems, Man, and Cybernetics (SMC), 2013*. p. 4561–4565, IEEE.
- Swaroop, D. (1997). String stability of interconnected systems: An application to platooning in automated highway systems. *California Partners for Advanced Transit and Highways (PATH)*.
- Swaroop, D. and Hedrick, J. (1996). String stability of interconnected systems. *IEEE Transactions on Automatic Control*, **41**(3), p. 349–357.
- Tzempetzi, D. (2015). Towards a safety concept for cooperative automated driving. Technical Report, Eindhoven University of Technology, Stan Ackerman Institute.
- White, R. and Tomizuka, M. (2001). Autonomous following lateral control of heavy vehicles using laser scanning radar. In *Proceedings of the American Control Conference, 2001*, **3**, p. 2333–2338, IEEE.
- van de Wouw, N. (2010). *Lecture Notes, 4J400 - Multibody Dynamics*. TU/e.

Appendix A

Single-track vehicle model

In Figure A.1, a single-track vehicle model is presented. A single-track vehicle model, is a simplified vehicle where the tires of the front and rear axle are lumped together into an 'equivalent' tire. Furthermore, is it assumed that the height of the center of mass (from hereon abbreviated with *cm*) of the vehicle is zero. The single-track vehicle model is used to obtain the lateral and rotational dynamics of the vehicle. For the derivation of the lateral and rotational dynamics of the vehicle, a global right-handed frame is defined, with the orientation of a set $\underline{\vec{e}}^0 := [\ \vec{e}_1^0 \ \vec{e}_2^0 \ \vec{e}_3^0 \]^T$ of three mutually orthogonal unit vectors \vec{e}_1^0 , \vec{e}_2^0 and \vec{e}_3^0 . The *cm* of the vehicle is positioned in the origin of frame $\underline{\vec{e}}^1$ and this frame is fixed to the vehicle body. Furthermore, frame $\underline{\vec{e}}^1$ consist, likewise to frame $\underline{\vec{e}}^0$, out of a set of three mutually orthogonal unit vectors \vec{e}_1^1 , \vec{e}_2^1 and \vec{e}_3^1 , where vector \vec{e}_1^1 is oriented in the forward direction along the center axis of the vehicle. The front tire is positioned in the origin of frame $\underline{\vec{e}}^2$ which consists, as well as frame $\underline{\vec{e}}^0$ and frame $\underline{\vec{e}}^1$, out of a set of three mutually orthogonal unit vectors \vec{e}_1^2 , \vec{e}_2^2 and \vec{e}_3^2 , where vector \vec{e}_1^2 is oriented in forward direction of the front tire. F_{yf} , F_{yr} and F_d are the lateral front tire force, the lateral rear tire force and the drive force acting upon the *cm* of the vehicle. \vec{V}_v , \vec{V}_f and \vec{V}_r are the velocity vectors of the *cm* of the vehicle and the front and rear tyres, while V_x and V_y are the longitudinal and lateral velocity of the *cm* with respect to body-fixed frame $\underline{\vec{e}}^1$. ψ_v is the rotational velocity of the *cm* and V_{xf} and V_{yf} are the longitudinal and lateral velocity of the front tire with respect to frame $\underline{\vec{e}}^2$, while V_{xr} and V_{yr} are the longitudinal and lateral velocity of the rear tire with respect to frame $\underline{\vec{e}}^1$. Furthermore, α_f , α_r and β are the side-slip angles of front and rear tyres and the side-slip angle of the *cm*, while l_f and l_r are the distances between the *cm* and the front and rear axle, respectively. $\vec{r}_{f/v}$ is the distance vector between the *cm* and the front tire, and $\vec{r}_{r/v}$ is the distance vector between the *cm* and the rear tire.

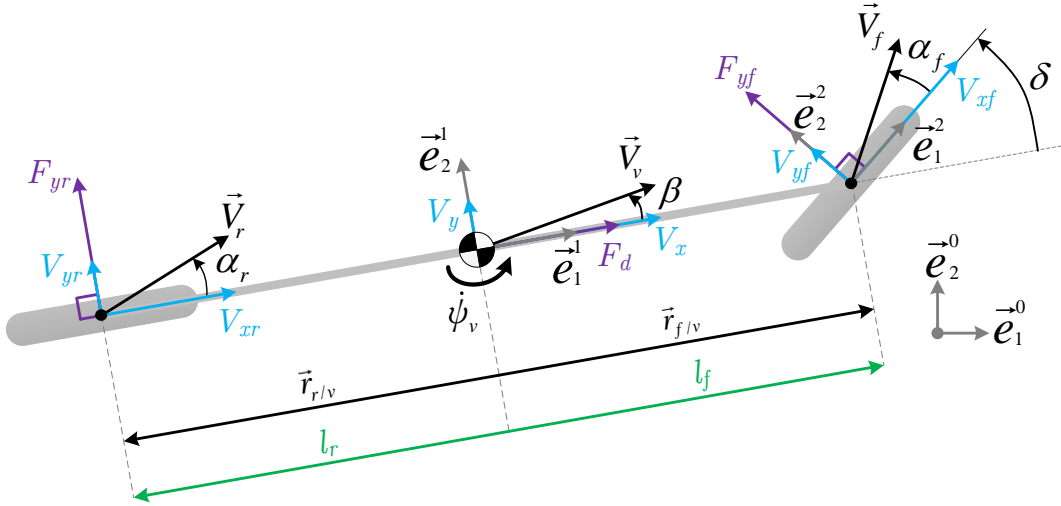


Figure A.1: Schematic representation of a single-track vehicle model.

In the derivation of the direction cosine matrices between the different frames $\cos(\delta)$ is denoted as $C\delta$ and $\sin(\delta)$ is denoted as $S\delta$. The direction cosine matrix \underline{A}^{21} from frame \underline{e}^2 to frame \underline{e}^1 is defined as:

$$\begin{aligned}\underline{e}^2 &= \underline{A}^{21}\underline{e}^1, \\ &= \begin{bmatrix} C\delta & S\delta & 0 \\ -S\delta & C\delta & 0 \\ 0 & 0 & 1 \end{bmatrix} \underline{e}^1,\end{aligned}\quad (\text{A.1})$$

where δ is the steering angle of the front wheel. The direction cosine matrix \underline{A}^{12} from frame \underline{e}^1 to frame \underline{e}^2 is defined as:

$$\begin{aligned}\underline{e}^1 &= \underline{A}^{12}\underline{e}^2, \\ &= (\underline{A}^{21})^{-1}\underline{e}^2, \\ &= \begin{bmatrix} C\delta & -S\delta & 0 \\ S\delta & C\delta & 0 \\ 0 & 0 & 1 \end{bmatrix} \underline{e}^2.\end{aligned}\quad (\text{A.2})$$

The velocity vector of the *cm* of the vehicle is defined as follows:

$$\vec{V}_v = \underline{V}_v{}^{1T} \underline{e}^1 = [V_x \ V_y \ 0] \underline{e}^1. \quad (\text{A.3})$$

The acceleration vector of the *cm* of the vehicle is calculated by taking the time derivative of (A.3):

$$\begin{aligned}
\dot{\vec{V}}_v &= \dot{\underline{V}}_v^{1T} \underline{\vec{e}}^1 + \underline{V}_v^{1T} \dot{\underline{\vec{e}}}^1, \\
&= \dot{\underline{V}}_v^{1T} - \underline{V}_v^{1T} {}^{10}\tilde{\omega}^1 \underline{\vec{e}}^1, \\
&= [\dot{V}_x \quad \dot{V}_y \quad 0] \underline{\vec{e}}^1 - [V_x \quad V_y \quad 0] \begin{bmatrix} 0 & -\dot{\psi}_v & 0 \\ \dot{\psi}_v & 0 & 0 \\ 0 & 0 & 0 \end{bmatrix} \underline{\vec{e}}^1, \\
&= [\dot{V}_x - V_y \dot{\psi}_v \quad \dot{V}_y + V_x \dot{\psi}_v \quad 0]^T \underline{\vec{e}}^1,
\end{aligned} \tag{A.4}$$

where $\dot{\vec{e}}^1$ can be expressed as $-{}^{10}\tilde{\omega}^1 \underline{\vec{e}}^1$ by applying the Poisson equations presented in van de Wouw (2010). Matrix ${}^{10}\tilde{\omega}^1$ is a skew-symmetric matrix related to the angular velocity of frame $\underline{\vec{e}}^1$ with respect to frame $\underline{\vec{e}}^0$ expressed in coordinates with respect to frame $\underline{\vec{e}}^1$. The translational equation of motion of the *cm* of the vehicle can be described as follows:

$$\begin{aligned}
m\dot{\vec{V}}_v &= \sum \vec{F} = \vec{F}_{yf} + \vec{F}_{yr} + \vec{F}_d, \\
&= \underline{F}_{yf}^{2T} \underline{A}^{21} \underline{\vec{e}}^1 + \underline{F}_{yr}^{1T} \underline{\vec{e}}^1 + \underline{F}_d^{1T} \underline{\vec{e}}^1, \\
&= \begin{bmatrix} 0 \\ F_{yf} \\ 0 \end{bmatrix}^T \begin{bmatrix} C\delta & S\delta & 0 \\ -S\delta & C\delta & 0 \\ 0 & 0 & 1 \end{bmatrix} \underline{\vec{e}}^1 + \begin{bmatrix} 0 \\ F_{yr} \\ 0 \end{bmatrix}^T \underline{\vec{e}}^1 + \begin{bmatrix} F_d \\ 0 \\ 0 \end{bmatrix}^T \underline{\vec{e}}^1, \\
&= \begin{bmatrix} -F_{yf}S\delta + F_d \\ F_{yf}C\delta + F_{yr} \\ 0 \end{bmatrix}^T \underline{\vec{e}}^1.
\end{aligned} \tag{A.5}$$

The rotational equation of motion of the *cm* of the vehicle can be described as follows (the rotation is only around \vec{e}_3^1):

$$\begin{aligned}
\sum \vec{M} &= \mathbf{J} \cdot \dot{\vec{\omega}} + \vec{\omega} \times (\mathbf{J} \cdot \vec{\omega}), \\
[\sum M_x \quad \sum M_y \quad \sum M_z]^T \underline{\vec{e}}^1 &= I_z \vec{e}_3^1 \vec{e}_3^1 \cdot \ddot{\psi}_v \vec{e}_3^1 + \dot{\psi}_v \vec{e}_3^1 \times (I_z \vec{e}_3^1 \vec{e}_3^1 \cdot \dot{\psi}_v \vec{e}_3^1), \\
[0 \quad 0 \quad \sum M_z]^T \underline{\vec{e}}^1 &= [0 \quad 0 \quad I_z \ddot{\psi}_v]^T \underline{\vec{e}}^1, \\
\sum M_z \vec{e}_3^1 &= I_z \ddot{\psi}_v \vec{e}_3^1,
\end{aligned} \tag{A.6}$$

where

$$\begin{aligned}
\mathbf{J} &= \underline{\vec{e}}^{1T} J \underline{\vec{e}}^1, \\
&= \underline{\vec{e}}^{1T} \begin{bmatrix} I_x & 0 & 0 \\ 0 & I_y & 0 \\ 0 & 0 & I_z \end{bmatrix} \underline{\vec{e}}^1,
\end{aligned} \tag{A.7}$$

and

$$\begin{aligned}
\vec{\omega} &= \underline{\omega}^1 \underline{\vec{e}}^1, \\
&= [0 \quad 0 \quad \dot{\psi}_v]^T \underline{\vec{e}}^1.
\end{aligned} \tag{A.8}$$

Herein,

$$\begin{aligned}
M_z \underline{\vec{e}}_3^1 &= \vec{r}_{f/v} \times \vec{F}_{yf} + \vec{r}_{r/v} \times \vec{F}_{yr}, \\
&= \begin{bmatrix} l_f \\ 0 \\ 0 \end{bmatrix}^T \underline{\vec{e}}^1 \times \begin{bmatrix} -F_{yf}S\delta \\ F_{yf}C\delta \\ 0 \end{bmatrix}^T \underline{\vec{e}}^1 + \begin{bmatrix} -l_r \\ 0 \\ 0 \end{bmatrix}^T \underline{\vec{e}}^1 \times \begin{bmatrix} 0 \\ F_{yr} \\ 0 \end{bmatrix}^T \underline{\vec{e}}^1, \\
&= [0 \ 0 \ l_f F_{yf} C \delta] \underline{\vec{e}}^1 + [0 \ 0 \ -l_r F_y r] \underline{\vec{e}}^1, \\
&= (l_f F_{yf} C \delta - l_r F_{yr}) \underline{\vec{e}}_3^1.
\end{aligned} \tag{A.9}$$

When (A.9) is substituted in (A.6), the equation is obtained for the rotational dynamics of the vehicle:

$$(l_f F_{yf} C \delta - l_r F_{yr}) = I_z \ddot{\psi}_v. \tag{A.10}$$

The equations of motion of the vehicle are then given by:

$$\begin{aligned}
\begin{bmatrix} \sum F_x \\ \sum F_y \\ \sum M_z \end{bmatrix}^T \underline{\vec{e}}^1 &= \begin{bmatrix} m \ddot{x}_v \\ m \ddot{y}_v \\ I_z \ddot{\psi}_v \end{bmatrix}^T \underline{\vec{e}}^1, \\
&= \begin{bmatrix} m (\dot{V}_x - V_y \dot{\psi}_v) \\ m (\dot{V}_y + V_x \dot{\psi}_v) \\ I_z \ddot{\psi}_v \end{bmatrix}^T \underline{\vec{e}}^1.
\end{aligned} \tag{A.11}$$

When (A.5) and (A.10) is substituted in (A.11), the translational and rotational dynamics of the vehicle can be described as follows:

$$\begin{bmatrix} m (\dot{V}_x - V_y \dot{\psi}_v) \\ m (\dot{V}_y + V_x \dot{\psi}_v) \\ I_z \ddot{\psi}_v \end{bmatrix}^T \underline{\vec{e}}^1 = \begin{bmatrix} -F_{yf}S\delta + F_d \\ F_{yf}C\delta + F_{yr} \\ l_f F_{yf} C \delta - l_r F_{yr} \end{bmatrix}^T \underline{\vec{e}}^1. \tag{A.12}$$

Tyre models

The developed lateral tire forces F_{yf} and F_{yr} are depending on the size of the side-slip angle of the tire, the lateral stiffness of the tire, the friction between the road surface and the tire and the nominal force at on the tire. The tire forces can be calculated by using a non-linear tire model, for example the Magic Formula developed by Pacejka (2005). The Magic Formula is non-linear mathematical model that describes tire behaviour based on empirical data. Figure A.2 contains an example of a non-linear tire force characteristic calculated by the Magic Formula.

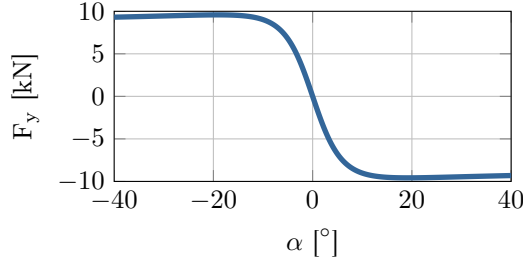


Figure A.2: An example of a non-linear tire characteristic calculated by the Magic Formula.

The tire characteristics of the test vehicle used by TNO is measured and a tire model is derived using the Tyre estimator¹ and Magic Formula. Around the origin the tire forces can be approximated using the following relation:

$$F_{yi} = -C_i \alpha_i, \quad i \in \{f, r\}, \quad (\text{A.13})$$

where C_i is the lateral stiffness of the front or rear tire and α_i the side slip angle of the front and rear tire, respectively. However, approximating the tire model also imposes limitations on the size of the side-slip angles for which the model is still representative for the actual developed lateral tire forces. The approximation is only valid when the side-slip angles are within $\pm 0.5^\circ$. The side-slip angle ($\alpha_i, i \in \{f, r\}$) of the tire is calculated by taking the arctangent of the lateral velocity (V_{yi}) and the longitudinal velocity (V_{xi}) of the tire, where i indicates the front or rear tire, respectively:

$$\alpha_i = \text{atan} \left(\frac{V_{yi}}{V_{xi}} \right), \quad i \in \{f, r\}. \quad (\text{A.14})$$

The velocity of the front tire can be calculated as follows:

$$\begin{aligned} \vec{V}_f &= \vec{V}_v + \dot{\vec{r}}_{f/v}, \\ &= \underline{V}_v {}^T \underline{A}^{12} \vec{e}^2 - r_{f/v} {}^T \underline{\omega} {}^1 \underline{A}^{12} \vec{e}^2 \\ &= \begin{bmatrix} V_x & V_y & 0 \end{bmatrix} \begin{bmatrix} C\delta & -S\delta & 0 \\ S\delta & C\delta & 0 \\ 0 & 0 & 1 \end{bmatrix} \vec{e}^2 - \\ &\quad \begin{bmatrix} l_f \\ 0 \\ 0 \end{bmatrix} {}^T \begin{bmatrix} 0 & -\dot{\psi}_v & 0 \\ \dot{\psi}_v & 0 & 0 \\ 0 & 0 & 0 \end{bmatrix} \begin{bmatrix} C\delta & -S\delta & 0 \\ S\delta & C\delta & 0 \\ 0 & 0 & 1 \end{bmatrix} \vec{e}^2, \\ &= \begin{bmatrix} V_x C\delta + (V_y + l_f \dot{\psi}_v) S\delta \\ -V_x S\delta + (V_y + l_f \dot{\psi}_v) C\delta \\ 0 \end{bmatrix} \vec{e}^2. \end{aligned} \quad (\text{A.15})$$

¹https://www.tno.nl/content.cfm?context=thema&content=prop_case&laag1=894&laag2=914&laag3=104&item_id=1790&taal=2

Velocity of the rear tire is derived as follows:

$$\begin{aligned}
\vec{V}_r &= \vec{V}_v + \dot{\vec{r}}_{r/v}, \\
&= \underline{V}_v^T \vec{e}^1 - \underline{r}_{r/v}^T \underline{\omega}^T \underline{\tilde{\omega}}^1 \vec{e}^1, \\
&= \begin{bmatrix} V_x \\ V_y \\ 0 \end{bmatrix}^T \vec{e}^1 - \begin{bmatrix} -l_r \\ 0 \\ 0 \end{bmatrix}^T \begin{bmatrix} 0 & -\dot{\psi}_v & 0 \\ \dot{\psi}_v & 0 & 0 \\ 0 & 0 & 0 \end{bmatrix} \vec{e}^1, \\
&= [V_x \quad V_y - l_r \dot{\psi}_v \quad 0] \vec{e}^1.
\end{aligned} \tag{A.16}$$

When equation (A.14), (A.15) and are substituted in (A.13), the following equation for the front tire force is obtained:

$$\begin{aligned}
F_{yf} &= -C_f \operatorname{atan} \left(\frac{\vec{V}_f \cdot \vec{e}_2^2}{\vec{V}_f \cdot \vec{e}_1^2} \right), \\
&= -C_f \operatorname{atan} \left(\frac{-V_x S \delta + (V_y + l_f \dot{\psi}_v) C \delta}{V_x C \delta + (V_y + l_f \dot{\psi}_v) S \delta} \right).
\end{aligned} \tag{A.17}$$

The rear lateral tire force can be calculated by substituting (A.14) and (A.16) into (A.13), this results in the following equation:

$$\begin{aligned}
F_{yr} &= -C_r \operatorname{atan} \left(\frac{\vec{V}_r \cdot \vec{e}_2^1}{\vec{V}_r \cdot \vec{e}_1^1} \right), \\
&= -C_r \operatorname{atan} \left(\frac{V_y - l_r \dot{\psi}_v}{V_x} \right).
\end{aligned} \tag{A.18}$$

Non-linear single track vehicle model

When it is assumed that the driving force F_d in equation (A.12) is available such that $\dot{V}_x = 0$, the following non-linear dynamic model is obtained, which describes the lateral and rotational dynamics of the cm of the vehicle:

$$\begin{bmatrix} \dot{V}_y \\ \ddot{\psi}_v \end{bmatrix}^T \vec{e}^1 = \begin{bmatrix} \frac{1}{m} (F_{yf} C \delta + F_{yr}) - V_x \dot{\psi}_v \\ \frac{1}{I_z} (l_f F_{yf} C \delta - l_r F_{yr}) \end{bmatrix}^T \vec{e}^1. \tag{A.19}$$

Equation (A.17) and (A.18) can be substituted in (A.19), resulting in the following non-linear model:

$$\begin{bmatrix} \dot{V}_y \\ \ddot{\psi}_v \end{bmatrix}^T \vec{e}^1 = \begin{bmatrix} -\frac{1}{m} \left(C \delta C_f \operatorname{atan} \left(\frac{-V_x S \delta + (V_y + l_f \dot{\psi}_v) C \delta}{V_x C \delta + (V_y + l_f \dot{\psi}_v) S \delta} \right) + C_r \operatorname{atan} \left(\frac{V_y - l_r \dot{\psi}_v}{V_x} \right) \right) - V_x \dot{\psi}_v \\ -\frac{1}{I_z} \left(l_f C \delta C_f \operatorname{atan} \left(\frac{-V_x S \delta + (V_y + l_f \dot{\psi}_v) C \delta}{V_x C \delta + (V_y + l_f \dot{\psi}_v) S \delta} \right) - l_r C_r \operatorname{atan} \left(\frac{V_y - l_r \dot{\psi}_v}{V_x} \right) \right) \end{bmatrix}^T \vec{e}^1. \tag{A.20}$$

Linearized single-track vehicle model

One of the drawbacks of the non-linear model is that linear control theory and linear stability analysis is not applicable anymore. Equation (A.20) can be linearized around the origin by using a first order Taylor series expansion, where $f(x, u)$ is equal to equation (A.20), $x = [V_y \ \dot{\psi}_v]^T$, $u = \delta$ and \bar{V}_x for which $\dot{V}_x = 0$. The resulting model can be used for controller development in combination linear control theory and linear stability analysis.

$$\begin{aligned} \dot{x} &= f(x, u) \Big|_{\substack{x=0 \\ u=0}} + \frac{\partial f(x, u)}{\partial x} \Big|_{\substack{x=0 \\ u=0}} (x - 0) + \frac{\partial f(x, u)}{\partial u} \Big|_{\substack{x=0 \\ u=0}} (u), \\ \begin{bmatrix} \dot{\bar{V}}_y \\ \ddot{\psi}_v \end{bmatrix} &= \begin{bmatrix} -\frac{C_f + C_r}{m\bar{V}_x} & -\frac{C_f l_f - C_r l_r}{m\bar{V}_x} - \bar{V}_x \\ -\frac{C_f l_f - C_r l_r}{I_z \bar{V}_x} & -\frac{C_f l_f^2 + C_r l_r^2}{I_z \bar{V}_x} \end{bmatrix} \begin{bmatrix} \bar{V}_y \\ \dot{\psi}_v \end{bmatrix} + \begin{bmatrix} \frac{C_f}{C_f l_f} \\ \frac{C_f m}{I_z} \end{bmatrix} \bar{\delta}, \end{aligned} \quad (\text{A.21})$$

The chosen definition of x and u results in a linearized vehicle model in state-space according to the following formulation:

$$\dot{x} = Ax + Bu, \quad (\text{A.22})$$

with

$$A = \begin{bmatrix} -\frac{C_f + C_r}{m\bar{V}_x} & -\frac{C_f l_f - C_r l_r}{m\bar{V}_x} - \bar{V}_x \\ -\frac{C_f l_f - C_r l_r}{I_z \bar{V}_x} & -\frac{C_f l_f^2 + C_r l_r^2}{I_z \bar{V}_x} \end{bmatrix}, \quad B = \begin{bmatrix} \frac{C_f}{C_f l_f} \\ \frac{C_f m}{I_z} \end{bmatrix}, \quad x = \begin{bmatrix} \bar{V}_y \\ \dot{\psi}_v \end{bmatrix} \quad \text{and} \quad u = \bar{\delta}.$$

Open-loop pole locations of (A.22) for $\bar{V} \in \mathcal{S}$, where $\mathcal{S} = \{ \bar{V}_x \in \mathbb{N} \mid 1 \leq \bar{V}_x \leq 40 \}$

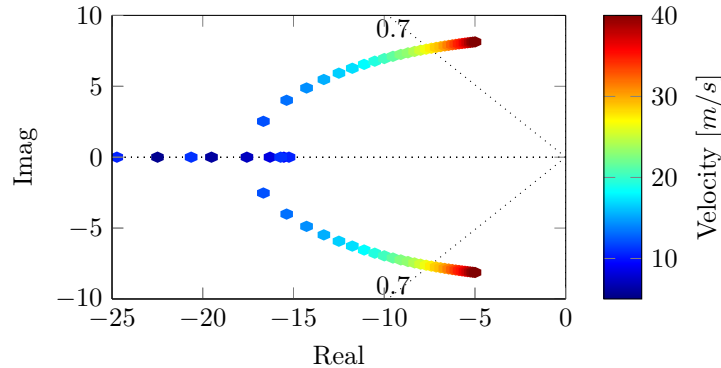


Figure A.3: Open-loop poles of (A.22).

Interval linear tire response

As stated in subsection A the non-linear and linearized model have a small interval on which both models have approximately the same response. In Figure A.4a and A.4b the front and rear tire characteristics of the non-linear and linearized model are presented.

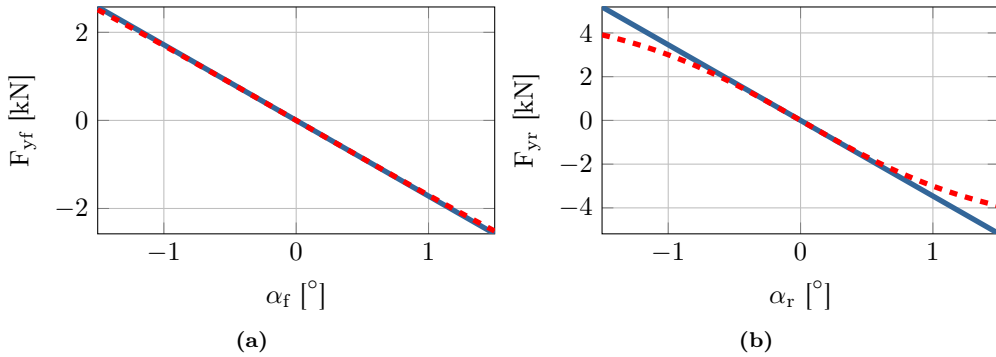


Figure A.4: (a) The front lateral forces as function of the side-slip angles of the non-linear and linearized model. (b) The rear lateral forces as function of the side-slip angles of the non-linear and linearized model.

As can be observed, both tire models develop almost same lateral forces when the side-slip angle of the tyres stay within the interval of $-0.5^\circ < \alpha < 0.5^\circ$. This means that the results of the linearized vehicle model with linear tyres are only valid when the tire side-slip angles are within $\pm 0.5^\circ$. If the side-slip angles are outside of this interval, the lateral forces calculated by the linearized model will be larger than actually possible. On the interval of $-0.5^\circ < \alpha < 0.5^\circ$, the Root Mean Square Error (RMSE) between the non-linear and linearized model for the front tire is $0.52N$ and for the rear tire $23.9N$. Although the RMSE of the rear tire model is larger, it is still acceptable. The large difference in RMSE is due to the weight distribution of the vehicle and the under steer dynamics of the vehicle. The largest error occurs at -0.5° or 0.5° , at these slip angles the relative error are only 0.06% for the front tire and 1.44% for the rear tire. Furthermore, the RMSE for the front tire on interval $-1^\circ < \alpha < 1^\circ$ is only $6.85N$, which is 0.39% .

Appendix B

Error dynamics derivation with look-ahead distance

In Chapter 2, the error dynamics between a reference point and a look-ahead point in front of the vehicle are derived by applying a state transformation. An alternative approach in deriving these error dynamics is to used the multi body method of Section 2.2. In this chapter the error dynamics between the reference point r_l and the look-ahead point v_l are derived. In addition to the variables already presented in Section 2.2, Figure B.1 contains vectors $\vec{r}_{v_l/v}$ and $\vec{r}_{r_l/r}$, which are the vectors between the *cm* of the vehicle and the look-ahead point v_l and the reference point r and the look-ahead point r_l , respectively, which have length $l_f + L_{fb} + L_a$ and $(l_f + L_{fb} + L_a) C(\psi_v - \psi_r)$, where l_{fb} is the distance between the front axle and the front bumper. Now, let us assume that the lateral error between the reference point r_l and the look-ahead point v_l is the difference between vectors \vec{r}_{v_l} and \vec{r}_{r_l} . Vectors \vec{r}_{v_l} and \vec{r}_{r_l} than can be written as a function of the vectors $\vec{r}_v + \vec{r}_{v_l/v}$ and the vectors $\vec{r}_r + \vec{r}_{r_l/r}$, respectively. This results in the following lateral error:

$$\begin{aligned} y_{el} &= (\vec{r}_{v_l} - \vec{r}_{r_l}) \cdot \vec{e}_2^2, \\ &= (\vec{r}_v + \vec{r}_{v_l/v} - \vec{r}_r - \vec{r}_{r_l/r}) \cdot \vec{e}_2^2, \end{aligned} \quad (\text{B.1})$$

Equal to Section 2.2, it is assumed that any disturbance caused by the lateral movement on the longitudinal dynamics is compensated for by a longitudinal controller, such that longitudinal position and velocity errors remain unaffected, i.e:

$$(\vec{r}_v + \vec{r}_{v_l/v} - \vec{r}_r - \vec{r}_{r_l/r}) \cdot \vec{e}_1^2 = 0. \quad (\text{B.2})$$

and

$$(\vec{V}_v + \dot{\vec{r}}_{v_l/v} - \vec{V}_r - \dot{\vec{r}}_{r_l/r}) \cdot \vec{e}_1^2 = 0, \quad (\text{B.3})$$

where $\vec{V}_v = \dot{\vec{r}}_v$ and $\vec{V}_r = \dot{\vec{r}}_r$. The velocity of point r_l can be written as follows:

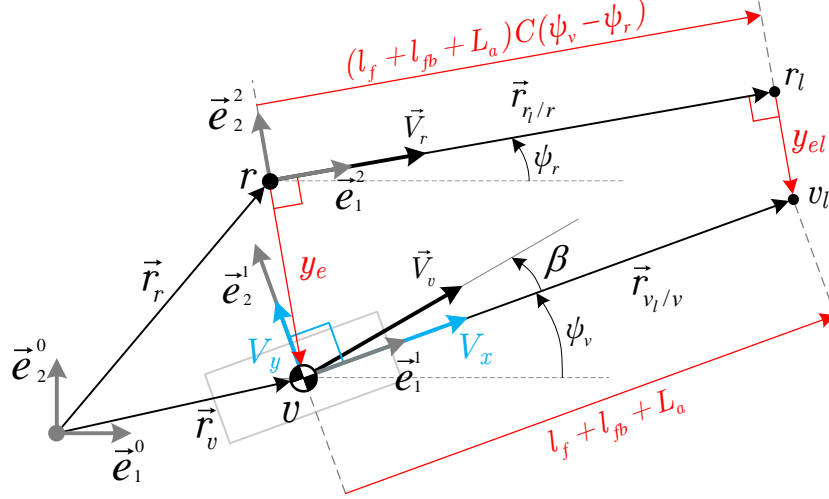


Figure B.1: Schematic representation of the lateral and rotational errors between the reference point r_l and the look-ahead point v_l .

$$\begin{aligned}
\vec{V}_{r_l} &= \vec{V}_r + \dot{\vec{r}}_{r_l/r}, \\
&= \vec{V}_r - \underline{r}_{r_l/r} {}^{2T} 20 \underline{\omega}^2 \underline{\vec{e}}^2, \\
&= [V_r \ 0 \ 0] \underline{\vec{e}}^2 - [(l_f + l_{fb} + L_a) C(\psi_v - \psi_r) \ 0 \ 0] \begin{bmatrix} 0 & -\dot{\psi}_r & 0 \\ \dot{\psi}_r & 0 & 0 \\ 0 & 0 & 0 \end{bmatrix} \underline{\vec{e}}^2, \\
&= [V_r \ (l_f + l_{fb} + L_a) C(\psi_v - \psi_r) \dot{\psi}_r \ 0] \underline{\vec{e}}^2,
\end{aligned} \tag{B.4}$$

where \vec{V}_r is substituted from (2.7). The acceleration of point r_l can be determined by taking the time derivative of (B.4), this results in the following:

$$\begin{aligned}
\dot{\vec{V}}_{r_l} &= \dot{\vec{V}}_r + \ddot{\vec{r}}_{r_l/r}, \\
&= \dot{\vec{V}}_r - \underline{r}_{r_l/r} {}^{2T} 20 \dot{\underline{\omega}}^2 \underline{\vec{e}}^2 - \underline{r}_{r_l/r} {}^{2T} 20 \underline{\omega}^2 \dot{\underline{\vec{e}}}^2, \\
&= \dot{\vec{V}}_r - \underline{r}_{r_l/r} {}^{2T} 20 \dot{\underline{\omega}}^2 \underline{\vec{e}}^2 + \underline{r}_{r_l/r} {}^{2T} ({}^{20} \underline{\omega}^2)^2 \underline{\vec{e}}^2, \\
&= \begin{bmatrix} \dot{V}_r \\ V_r \dot{\psi}_r \\ 0 \end{bmatrix} {}^T \underline{\vec{e}}^2 - \begin{bmatrix} (l_f + l_{fb} + L_a) C(\psi_v - \psi_r) \\ 0 \\ 0 \end{bmatrix} {}^T \begin{bmatrix} 0 & -\ddot{\psi}_r & 0 \\ \ddot{\psi}_r & 0 & 0 \\ 0 & 0 & 0 \end{bmatrix} \underline{\vec{e}}^2 \\
&\quad + \begin{bmatrix} (l_f + l_{fb} + L_a) C(\psi_v - \psi_r) \\ 0 \\ 0 \end{bmatrix} {}^T \left(\begin{bmatrix} 0 & -\dot{\psi}_r & 0 \\ \dot{\psi}_r & 0 & 0 \\ 0 & 0 & 0 \end{bmatrix} \right)^2 \underline{\vec{e}}^2, \\
&= \begin{bmatrix} \dot{V}_r - (l_f + l_{fb} + L_a) C(\psi_v - \psi_r) \dot{\psi}_r^2 \\ V_r \dot{\psi}_r + (l_f + l_{fb} + L_a) C(\psi_v - \psi_r) \dot{\psi}_r \\ 0 \end{bmatrix} {}^T \underline{\vec{e}}^2,
\end{aligned} \tag{B.5}$$

where $\dot{\vec{V}}_r$ is obtained from (2.13). The velocity of the look-ahead point v_l can be formulated as follows:

$$\begin{aligned}
\dot{\vec{V}}_{v_l} &= \dot{\vec{V}}_v + \dot{\vec{r}}_{v_l/v}, \\
&= \dot{\vec{V}}_v - \underline{r}_{v_l/v}^{1T} \underline{\omega}^1 \underline{A}^{12} \vec{e}^2, \\
&= \begin{bmatrix} V_x C(\psi_r - \psi_v) + V_y S(\psi_r - \psi_v) \\ V_y C(\psi_r - \psi_v) - V_x S(\psi_r - \psi_v) \\ 0 \end{bmatrix}^T \vec{e}^2 \\
&\quad - \begin{bmatrix} l_f + l_{fb} + L_a \\ 0 \\ 0 \end{bmatrix}^T \begin{bmatrix} 0 & -\dot{\psi}_v & 0 \\ \dot{\psi}_v & 0 & 0 \\ 0 & 0 & 0 \end{bmatrix} \begin{bmatrix} C(\psi_r - \psi_v) & -S(\psi_r - \psi_v) & 0 \\ S(\psi_r - \psi_v) & C(\psi_r - \psi_v) & 0 \\ 0 & 0 & 1 \end{bmatrix} \vec{e}^2, \\
&= \begin{bmatrix} V_x C(\psi_r - \psi_v) + V_y S(\psi_r - \psi_v) + (l_f + l_{fb} + L_a) \dot{\psi}_v S(\psi_r - \psi_v) \\ V_y C(\psi_r - \psi_v) - V_x S(\psi_r - \psi_v) + (l_f + l_{fb} + L_a) \dot{\psi}_v C(\psi_r - \psi_v) \\ 0 \end{bmatrix}^T \vec{e}^2, \tag{B.6}
\end{aligned}$$

where $\dot{\vec{V}}_v$ is substituted from (2.16). The acceleration of point v_l can be obtained by taking the time derivative of (B.6) and is written as follows:

$$\begin{aligned}
\dot{\vec{V}}_{v_l} &= \dot{\vec{V}}_v + \ddot{\vec{r}}_{v_l/v}, \\
&= \dot{\vec{V}}_v - \underline{r}_{v_l/v}^{1T} \underline{\omega}^1 \underline{A}^{12} \vec{e}^2 - \underline{r}_{v_l/v}^{1T} \underline{\omega}^1 \underline{A}^{12} \dot{\vec{e}}^2 - \underline{r}_{v_l/v}^{1T} \underline{\omega}^1 \underline{A}^{12} \ddot{\vec{e}}^2, \\
&= \dot{\vec{V}}_v - \underline{r}_{v_l/v}^{1T} \underline{\omega}^1 \underline{A}^{12} \vec{e}^2 - \underline{r}_{v_l/v}^{1T} \underline{\omega}^1 \underline{A}^{12} \dot{\vec{e}}^2 + \underline{r}_{v_l/v}^{1T} \underline{\omega}^1 \underline{A}^{1220} \underline{\omega}^2 \vec{e}^2, \\
&= \begin{bmatrix} \dot{V}_x C(\psi_r - \psi_v) + \dot{V}_y S(\psi_r - \psi_v) - V_y \dot{\psi}_v C(\psi_r - \psi_v) + V_x \dot{\psi}_v S(\psi_r - \psi_v) \\ \dot{V}_y C(\psi_r - \psi_v) - \dot{V}_x S(\psi_r - \psi_v) + V_x \dot{\psi}_v C(\psi_r - \psi_v) + V_y \dot{\psi}_v S(\psi_r - \psi_v) \\ 0 \end{bmatrix}^T \vec{e}^2 \\
&\quad - \begin{bmatrix} l_f + l_{fb} + L_a \\ 0 \\ 0 \end{bmatrix}^T \begin{bmatrix} 0 & -\ddot{\psi}_v & 0 \\ \ddot{\psi}_v & 0 & 0 \\ 0 & 0 & 0 \end{bmatrix} \begin{bmatrix} C(\psi_r - \psi_v) & -S(\psi_r - \psi_v) & 0 \\ S(\psi_r - \psi_v) & C(\psi_r - \psi_v) & 0 \\ 0 & 0 & 1 \end{bmatrix} \vec{e}^2 \\
&\quad - \begin{bmatrix} l_f + l_{fb} + L_a \\ 0 \\ 0 \end{bmatrix}^T \begin{bmatrix} 0 & -\dot{\psi}_v & 0 \\ \dot{\psi}_v & 0 & 0 \\ 0 & 0 & 0 \end{bmatrix} (\dot{\psi}_r - \dot{\psi}_v) \begin{bmatrix} -S(\psi_r - \psi_v) & -C(\psi_r - \psi_v) & 0 \\ C(\psi_r - \psi_v) & -S(\psi_r - \psi_v) & 0 \\ 0 & 0 & 0 \end{bmatrix} \vec{e}^2 \\
&\quad + \begin{bmatrix} l_f + l_{fb} + L_a \\ 0 \\ 0 \end{bmatrix}^T \begin{bmatrix} 0 & -\dot{\psi}_v & 0 \\ \dot{\psi}_v & 0 & 0 \\ 0 & 0 & 0 \end{bmatrix} \begin{bmatrix} C(\psi_r - \psi_v) & -S(\psi_r - \psi_v) & 0 \\ S(\psi_r - \psi_v) & C(\psi_r - \psi_v) & 0 \\ 0 & 0 & 1 \end{bmatrix} \\
&\quad \begin{bmatrix} 0 & -\dot{\psi}_r & 0 \\ \dot{\psi}_r & 0 & 0 \\ 0 & 0 & 0 \end{bmatrix} \vec{e}^2, \\
&= \begin{bmatrix} \dot{V}_x C(\psi_r - \psi_v) + \dot{V}_y S(\psi_r - \psi_v) - V_y \dot{\psi}_v C(\psi_r - \psi_v) + V_x \dot{\psi}_v S(\psi_r - \psi_v) \\ \quad + (l_f + l_{fb} + L_a) \ddot{\psi}_v S(\psi_r - \psi_v) + (l_f + l_{fb} + L_a) \dot{\psi}_v^2 C(\psi_r - \psi_v) \\ \dot{V}_y C(\psi_r - \psi_v) - \dot{V}_x S(\psi_r - \psi_v) + V_y \dot{\psi}_v S(\psi_r - \psi_v) + V_x \dot{\psi}_v C(\psi_r - \psi_v) \\ \quad + (l_f + l_{fb} + L_a) \ddot{\psi}_v C(\psi_r - \psi_v) + (l_f + l_{fb} + L_a) \dot{\psi}_v^2 S(\psi_r - \psi_v) \\ 0 \end{bmatrix}^T \vec{e}^2, \tag{B.7}
\end{aligned}$$

where $\dot{\vec{V}}_v$ is obtained from (2.17). As presented in (B.1), the lateral error y_{el} is defined as the difference between vectors $\vec{r}_v + \vec{r}_{v_l/v}$ and vectors $\vec{r}_r + \vec{r}_{r_l/r}$ in the \vec{e}_2^2 -direction. The first- and second-order time derivatives of (B.1) can be obtained as follows:

$$\begin{aligned}\dot{y}_{el} &= \left(\dot{\vec{r}}_v + \dot{\vec{r}}_{v_l/v} - \dot{\vec{r}}_r - \dot{\vec{r}}_{r_l/r} \right) \cdot \vec{e}_2^2 + (\vec{r}_v + \vec{r}_{v_l/v} - \vec{r}_r - \vec{r}_{r_l/r}) \cdot \dot{\vec{e}}_2^2, \\ &= \left(\vec{V}_v + \dot{\vec{r}}_{v_l/v} - \vec{V}_r - \dot{\vec{r}}_{r_l/r} \right) \cdot \vec{e}_2^2 - (\vec{r}_v + \vec{r}_{v_l/v} - \vec{r}_r - \vec{r}_{r_l/r}) \cdot \dot{\psi}_r \vec{e}_1^2, \\ &= \left(\vec{V}_{v_l} - \vec{V}_{r_l} \right) \cdot \vec{e}_2^2 - (\vec{r}_v + \vec{r}_{v_l/v} - \vec{r}_r - \vec{r}_{r_l/r}) \cdot \dot{\psi}_r \vec{e}_1^2,\end{aligned}\quad (\text{B.8})$$

and

$$\begin{aligned}\ddot{y}_{el} &= \left(\dot{\vec{V}}_{v_l} - \dot{\vec{V}}_{r_l} \right) \cdot \vec{e}_2^2 + \left(\vec{V}_{v_l} - \vec{V}_{r_l} \right) \cdot \dot{\vec{e}}_2^2 - \left(\vec{V}_v + \dot{\vec{r}}_{v_l/v} - \vec{V}_r - \dot{\vec{r}}_{r_l/r} \right) \cdot \dot{\psi}_r \vec{e}_1^2 \\ &\quad - (\vec{r}_v + \vec{r}_{v_l/v} - \vec{r}_r - \vec{r}_{r_l/r}) \cdot \ddot{\psi}_r \vec{e}_1^2 - (\vec{r}_v + \vec{r}_{v_l/v} - \vec{r}_r - \vec{r}_{r_l/r}) \cdot \dot{\psi}_r \dot{\vec{e}}_1^2, \\ &= \left(\dot{\vec{V}}_{v_l} - \dot{\vec{V}}_{r_l} \right) \cdot \vec{e}_2^2 - \left(\vec{V}_{v_l} - \vec{V}_r \right) \cdot \dot{\psi}_r \vec{e}_1^2 - \left(\vec{V}_{v_l} - \vec{V}_{r_l} \right) \cdot \dot{\psi}_r \vec{e}_1^2 \\ &\quad - (\vec{r}_v + \vec{r}_{v_l/v} - \vec{r}_r - \vec{r}_{r_l/r}) \cdot \ddot{\psi}_r \vec{e}_1^2 - (\vec{r}_v + \vec{r}_{v_l/v} - \vec{r}_r - \vec{r}_{r_l/r}) \cdot \dot{\psi}_r^2 \vec{e}_2^2.\end{aligned}\quad (\text{B.9})$$

As mentioned in Section 2.2 and in the beginning of this chapter, it is assumed that all disturbances caused by the lateral movement of the vehicle onto the longitudinal dynamics are compensated by a longitudinal controller, such that the dynamics in the \vec{e}_1^2 -direction remain unaffected. This assumption results in all errors in the \vec{e}_2^2 -directions being equal to zero, i.e. $(\vec{r}_v + \vec{r}_{v_l/v} - \vec{r}_r - \vec{r}_{r_l/r}) \cdot \vec{e}_1^2 = 0$ and $(\vec{V}_v + \dot{\vec{r}}_{v_l/v} - \vec{V}_r - \dot{\vec{r}}_{r_l/r}) \cdot \vec{e}_2^2 = 0$. When this assumption is applied to (B.8) and (B.9) the following equations are obtained for the first- and second-order time derivatives of (B.1):

$$\dot{y}_{el} = \left(\vec{V}_{v_l} - \vec{V}_{r_l} \right) \cdot \vec{e}_2^2, \quad (\text{B.10})$$

$$\ddot{y}_{el} = \left(\dot{\vec{V}}_{v_l} - \dot{\vec{V}}_{r_l} \right) \cdot \vec{e}_2^2 - (\vec{r}_v + \vec{r}_{v_l/v} - \vec{r}_r - \vec{r}_{r_l/r}) \cdot \dot{\psi}_r^2 \vec{e}_2^2. \quad (\text{B.11})$$

Substituting (B.4) and (B.6) into (B.10) and (B.1), (B.5) and, (B.7) into (B.11), the following non-linear lateral error dynamics are obtained:

$$\begin{aligned}\dot{y}_{el} &= V_y C(\psi_r - \psi_v) - V_x S(\psi_r - \psi_v) + (l_f + l_{fb} + L_a) \dot{\psi}_v C(\psi_r - \psi_v) \\ &\quad - (l_f + l_{fb} + L_a) C(\psi_v - \psi_r) \dot{\psi}_r\end{aligned}\quad (\text{B.12})$$

$$\begin{aligned}\ddot{y}_{el} &= \dot{V}_y C(\psi_r - \psi_v) - \dot{V}_x S(\psi_r - \psi_v) + V_y \dot{\psi}_v S(\psi_r - \psi_v) + V_x \dot{\psi}_v C(\psi_r - \psi_v) - V_r \dot{\psi}_r \\ &\quad + L_a (l_f + l_{fb} + L_a) \ddot{\psi}_v C(\psi_r - \psi_v) + (l_f + l_{fb} + L_a) \dot{\psi}_v^2 S(\psi_r - \psi_v) \\ &\quad - (l_f + l_{fb} + L_a) C(\psi_v - \psi_r) \ddot{\psi}_r - y_{el} \dot{\psi}_r^2.\end{aligned}\quad (\text{B.13})$$

The control problem is formulated in the \mathbb{R}^2 space, which implies that all rotations occur around the z -axis of each frame and that the z -axis of all frames are orientated in the same direction. The rotational error and its first- and second-order time derivatives can therefore be written as follows:

$$\psi_{el} = \psi_v - \psi_r, \quad (\text{B.14})$$

$$\dot{\psi}_{el} = \dot{\psi}_v - \dot{\psi}_r, \quad (\text{B.15})$$

$$\ddot{\psi}_{el} = \ddot{\psi}_v - \ddot{\psi}_r. \quad (\text{B.16})$$

Now, equation (B.14) can be substituted into (B.12) and (B.13), which results in:

$$\dot{y}_{el} = V_y C \psi_{el} + V_x S \psi_{el} + (l_f + l_{fb} + L_a) \dot{\psi}_v C \psi_{el} - (l_f + l_{fb} + L_a) C \psi_{el} \dot{\psi}_r, \quad (\text{B.17})$$

$$\begin{aligned}\ddot{y}_{el} &= \dot{V}_y C \psi_{el} + \dot{V}_x S \psi_{el} - V_y \dot{\psi}_v S \psi_{el} + V_x \dot{\psi}_v C \psi_{el} - V_r \dot{\psi}_r + (l_f + l_{fb} + L_a) \ddot{\psi}_v C \psi_{el} \\ &\quad - (l_f + l_{fb} + L_a) \dot{\psi}_v^2 S \psi_{el} - (l_f + l_{fb} + L_a) C \psi_{el} \ddot{\psi}_r - y_{el} \dot{\psi}_r^2.\end{aligned}\quad (\text{B.18})$$

Furthermore, (B.17) can be used to formulate an expression for V_y :

$$V_y = \frac{\dot{y}_{el} - V_x S \psi_{el} - (l_f + l_{fb} + L_a) \dot{\psi}_v C \psi_{el} + (l_f + l_{fb} + L_a) C \psi_{el} \dot{\psi}_r}{C \psi_{el}}, \quad (\text{B.19})$$

and (B.15) is used to derive an expression for $\dot{\psi}_v$:

$$\dot{\psi}_v = \dot{\psi}_{el} + \dot{\psi}_r. \quad (\text{B.20})$$

When the lateral vehicle dynamics of (2.31), (B.19) and (B.20) are substituted in (B.18) and based on (B.3), the velocity error in \vec{e}_1^2 -direction is equal to zero which results in $V_r = V_x$, the following equation for the second-order time derivative of the non-linear lateral error dynamics is obtained:

$$\begin{aligned} \ddot{y}_{el} &= \\ &\left(\frac{C \delta C_f \text{atan} \left(\frac{-V_x S \delta + \left(\frac{\dot{y}_{el} - V_x S \psi_{el} - (l_f + l_{fb} + L_a) C \psi_{el} (\dot{\psi}_{el} + \dot{\psi}_r) + (l_f + l_{fb} + L_a) C \psi_{el} \dot{\psi}_r + l_f (\dot{\psi}_{el} + \dot{\psi}_r)}{C \psi_{el}} \right) C \delta}{V_x C \delta + \left(\frac{\dot{y}_{el} - V_x S \psi_{el} - (l_f + l_{fb} + L_a) C \psi_{el} (\dot{\psi}_{el} + \dot{\psi}_r) + L_a C \psi_{el} \dot{\psi}_r + l_f (\dot{\psi}_{el} + \dot{\psi}_r)}{C \psi_{el}} \right) S \delta} \right)}{m} \right. \\ &\left. - \frac{C_r \text{atan} \left(\frac{\frac{\dot{y}_{el} - V_x S \psi_{el} - (l_f + l_{fb} + L_a) C \psi_{el} (\dot{\psi}_{el} + \dot{\psi}_r) + (l_f + l_{fb} + L_a) C \psi_{el} \dot{\psi}_r - l_r (\dot{\psi}_{el} + \dot{\psi}_r)}{C \psi_{el}}}{V_x} \right)}{m} - V_x (\dot{\psi}_{el} + \dot{\psi}_r) \right) C \psi_{el} \\ &+ \dot{V}_x S \psi_{el} + V_x (\dot{\psi}_{el} + \dot{\psi}_r) C \psi_{el} - V_x \dot{\psi}_r \\ &- \frac{\dot{y}_{el} - V_x S \psi_{el} - (l_f + l_{fb} + L_a) C \psi_{el} (\dot{\psi}_{el} + \dot{\psi}_r) + (l_f + l_{fb} + L_a) C \psi_{el} \dot{\psi}_r (\dot{\psi}_{el} + \dot{\psi}_r) S \psi_{el}}{C \psi_{el}} \\ &- \frac{C \delta C_f l_f \text{atan} \left(\frac{-V_x S \delta + \left(\frac{\dot{y}_{el} - V_x S \psi_{el} - (l_f + l_{fb} + L_a) C \psi_{el} (\dot{\psi}_{el} + \dot{\psi}_r) + (l_f + l_{fb} + L_a) C \psi_{el} \dot{\psi}_r + l_f (\dot{\psi}_{el} + \dot{\psi}_r)}{C \psi_{el}} \right) C \delta}{V_x C \delta + \left(\frac{\dot{y}_{el} - V_x S \psi_{el} - (l_f + l_{fb} + L_a) C \psi_{el} (\dot{\psi}_{el} + \dot{\psi}_r) + (l_f + l_{fb} + L_a) C \psi_{el} \dot{\psi}_r + l_f (\dot{\psi}_{el} + \dot{\psi}_r)}{C \psi_{el}} \right) S \delta} \right)}{I_z} \\ &- \frac{C_r l_r \text{atan} \left(\frac{\frac{\dot{y}_{el} - V_x S \psi_{el} - (l_f + l_{fb} + L_a) C \psi_{el} (\dot{\psi}_{el} + \dot{\psi}_r) + (l_f + l_{fb} + L_a) C \psi_{el} \dot{\psi}_r - l_r (\dot{\psi}_{el} + \dot{\psi}_r)}{C \psi_{el}}}{V_x} \right)}{I_z} (l_f + l_{fb} + L_a) C \psi_{el} \\ &- (l_f + l_{fb} + L_a) (\dot{\psi}_{el} + \dot{\psi}_r)^2 S \psi_{el} - (l_f + l_{fb} + L_a) C \psi_{el} \ddot{\psi}_r - y_{el} \dot{\psi}_r^2. \end{aligned} \quad (\text{B.21})$$

Furthermore, when the rotational vehicle dynamics in (2.32), (B.19) and (B.20) are substituted in (B.16), the following equation for the second-order time derivative of the non-linear rotational

error dynamics is obtained:

$$\begin{aligned} \ddot{\psi}_{el} &= \\ &\frac{C\delta C_f l_f \tan \left(\frac{-V_x S \delta + \left(\frac{\dot{y}_{el} - V_x S \psi_{el} - (l_f + l_{fb} + L_a) \dot{\psi}_{el} C \psi_{el} + (l_f + l_{fb} + L_a) C \psi_{el} \dot{\psi}_r}{C \psi_{el}} + l_f (\dot{\psi}_r + \dot{\psi}_{el}) \right) C \delta}{V_x C \delta + \left(\frac{\dot{y}_{el} - V_x S \psi_{el} - (l_f + l_{fb} + L_a) \dot{\psi}_{el} C \psi_{el} + (l_f + l_{fb} + L_a) C \psi_{el} \dot{\psi}_r}{C \psi_{el}} + l_f (\dot{\psi}_r + \dot{\psi}_{el}) \right) S \delta} \right)}{I_z} \\ &+ \frac{C_r l_r \tan \left(\frac{\frac{\dot{y}_{el} - V_x S \psi_{el} - (l_f + l_{fb} + L_a) \dot{\psi}_{el} C \psi_{el} + (l_f + l_{fb} + L_a) C \psi_{el} \dot{\psi}_r}{C \psi_{el}} - l_r (\dot{\psi}_r + \dot{\psi}_{el})}{V_x} \right)}{I_z} - \ddot{\psi}_r. \quad (B.22) \end{aligned}$$

Now, a state vector and input vector are chosen as $\zeta_2 = [y_{el} \quad \dot{y}_{el} \quad \psi_{el} \quad \dot{\psi}_{el}]^T$ and $\gamma_2 = [\delta \quad \dot{\psi}_r \quad \ddot{\psi}_r]^T$. For analysis purposes it is desired to obtain the linear model of the lateral and rotational error dynamics. An equilibrium for (B.21) and (B.22) can be found by setting all time derivatives in (B.21) and (B.22) to zero. Equation (B.21) and (B.22) are than equal to zero when also $\psi_{el} = 0$ and $\delta = 0$, i.e. the origin is an equilibrium for (B.21) and (B.22). Furthermore, linearization also relies on the assumption that all inputs will be small ($< 10^\circ$). As already stated in Section 2.2, the linearized vehicle model is a LPV model, with V_x as varying parameter. Therefore, the longitudinal velocity V_x has to be constant, i.e. $\dot{V}_x = 0$, for the vehicle model and thereby the error dynamics model to be valid. Linearizing (B.21) results in the following:

$$\begin{aligned} \ddot{y}_{el}(\zeta_2, \gamma_2) &= \frac{\partial \ddot{y}_{el}}{\partial y_{el}} \Big|_{\zeta_2 = \underline{0}, \gamma_2 = \underline{0}} (\bar{y}_{el} - 0) + \frac{\partial \ddot{y}_{el}}{\partial \dot{y}_{el}} \Big|_{\zeta_2 = \underline{0}, \gamma_2 = \underline{0}} (\dot{\bar{y}}_{el} - 0) + \frac{\partial \ddot{y}_{el}}{\partial \psi_{el}} \Big|_{\zeta_2 = \underline{0}, \gamma_2 = \underline{0}} (\bar{\psi}_{el} - 0) \\ &\quad + \frac{\partial \ddot{y}_{el}}{\partial \dot{\psi}_{el}} \Big|_{\zeta_2 = \underline{0}, \gamma_2 = \underline{0}} (\dot{\bar{\psi}}_{el} - 0) + \frac{\partial \ddot{y}_{el}}{\partial \delta} \Big|_{\zeta_2 = \underline{0}, \gamma_2 = \underline{0}} \bar{\delta} + \frac{\partial \ddot{y}_{el}}{\partial \dot{\psi}_r} \Big|_{\zeta_2 = \underline{0}, \gamma_2 = \underline{0}} \dot{\bar{\psi}}_r + \frac{\partial \ddot{y}_{el}}{\partial \ddot{\psi}_r} \Big|_{\zeta_2 = \underline{0}, \gamma_2 = \underline{0}} \ddot{\bar{\psi}}_r, \\ &= - \left(\frac{C_f + C_r}{m \bar{V}_x} + \frac{(l_f + l_{fb} + L_a) (C_f l_f - C_r l_r)}{I_z \bar{V}_x} \right) \dot{\bar{y}}_{el} \\ &\quad + \left(\frac{C_f + C_r}{m} + \frac{(l_f + l_{fb} + L_a) (C_f l_f - C_r l_r)}{I_z} \right) \bar{\psi}_{el} \\ &\quad + \left(\frac{C_f (l_{fb} + L_a) + C_r (l_f + l_{fb} + L_a + l_r)}{m V_x} \right. \\ &\quad \left. + \frac{(l_f + l_{fb} + L_a) (C_f l_f (l_{fb} + L_a) - C_r l_r (l_f + l_{fb} + L_a + l_r))}{I_z \bar{V}_x} \right) \dot{\bar{\psi}}_{el} \\ &\quad + \left(\frac{C_f}{m} + \frac{C_f l_f (l_f + l_{fb} + L_a)}{I_z} \right) \bar{\delta} + \left(\frac{C_f (l_{fb} + L_a) + C_r (l_f + l_{fb} + L_a + l_r)}{m \bar{V}_x} \right. \\ &\quad \left. + \frac{L_a (C_f l_f (l_{fb} + L_a) + C_r l_r (l_f + l_{fb} + L_a + l_r))}{I_z \bar{V}_x} - \bar{V}_x \right) \dot{\bar{\psi}}_r \\ &\quad - (l_f + l_{fb} + L_a) \ddot{\bar{\psi}}_r. \quad (B.23) \end{aligned}$$

where \bar{V}_x is the longitudinal velocity for which $\dot{V}_x = 0$ and \bar{y}_{el} , $\dot{\bar{y}}_{el}$ and so forth are the linearized states and inputs. When (B.22) is linearized the following equation is obtained:

$$\begin{aligned}\ddot{\psi}_{el}(\zeta_2, \gamma_2) &= \frac{\partial \ddot{\psi}_{el}}{\partial y_{el}} \Big|_{\substack{\zeta_2 = \underline{0} \\ \gamma_2 = \underline{0}}} (\bar{y}_{el} - 0) + \frac{\partial \ddot{\psi}_{el}}{\partial \dot{y}_{el}} \Big|_{\substack{\zeta_2 = \underline{0} \\ \gamma_2 = \underline{0}}} (\dot{\bar{y}}_{el} - 0) + \frac{\partial \ddot{\psi}_{el}}{\partial \psi_{el}} \Big|_{\substack{\zeta_2 = \underline{0} \\ \gamma_2 = \underline{0}}} (\bar{\psi}_{el} - 0) \\ &\quad + \frac{\partial \ddot{\psi}_{el}}{\partial \psi_{el}} \Big|_{\substack{\zeta_2 = \underline{0} \\ \gamma_2 = \underline{0}}} (\dot{\bar{\psi}}_{el} - 0) + \frac{\partial \ddot{\psi}_{el}}{\partial \delta} \Big|_{\substack{\zeta_2 = \underline{0} \\ \gamma_2 = \underline{0}}} \bar{\delta} + \frac{\partial \ddot{\psi}_{el}}{\partial \dot{\psi}_r} \Big|_{\substack{\zeta_2 = \underline{0} \\ \gamma_2 = \underline{0}}} \dot{\bar{\psi}}_r + \frac{\partial \ddot{\psi}_{el}}{\partial \ddot{\psi}_r} \Big|_{\substack{\zeta_2 = \underline{0} \\ \gamma_2 = \underline{0}}} \ddot{\bar{\psi}}_r \\ &= -\frac{C_f l_f - C_r l_r}{I_z \bar{V}_x} \dot{\bar{y}}_{el} + \frac{C_f l_f - C_r l_r}{I_z} \bar{\psi}_{el} + \frac{C_f l_f (l_{fb} + L_a) - C_r l_r (l_f + l_{fb} + L_a + l_r)}{I_z \bar{V}_x} \dot{\bar{\psi}}_{el} \\ &\quad + \frac{C_f l_f^2 - C_r l_r^2}{I_z} \dot{\bar{\psi}}_r - \ddot{\bar{\psi}}_r.\end{aligned}\tag{B.24}$$

When choosing a state vector as $x_{el} = \begin{bmatrix} \bar{y}_{el} & \dot{\bar{y}}_{el} & \bar{\psi}_{el} & \dot{\bar{\psi}}_{el} \end{bmatrix}^T$, the following state-space representation of the error dynamics can be derived:

$$\begin{aligned}\dot{x}_{el} &= A_{el} x_{el} + B_{el_1} \bar{\delta} + B_{el_2} \dot{\bar{\psi}}_r + B_{el_3} \ddot{\bar{\psi}}_r, \\ \begin{bmatrix} \dot{\bar{y}}_{el} \\ \ddot{\bar{y}}_{el} \\ \dot{\bar{\psi}}_{el} \\ \ddot{\bar{\psi}}_{el} \end{bmatrix} &= \begin{bmatrix} 0 & 1 & 0 & 0 \\ 0 & -\frac{\kappa_1 + \kappa_2}{\bar{V}_x} & \kappa_1 + \kappa_2 & \frac{\kappa_1(l_{fb} + L_a) + \kappa_2(l_f + l_{fb} + L_a + l_r)}{\bar{V}_x} \\ 0 & 0 & 1 & 0 \\ 0 & -\frac{C_f l_f - C_r l_r}{I_z \bar{V}_x} & \frac{C_f l_f - C_r l_r}{I_z} & \frac{C_f l_f (l_{fb} + L_a) - C_r l_r (l_f + l_{fb} + L_a + l_r)}{I_z \bar{V}_x} \end{bmatrix} \begin{bmatrix} \bar{y}_{el} \\ \dot{\bar{y}}_{el} \\ \bar{\psi}_{el} \\ \dot{\bar{\psi}}_{el} \end{bmatrix} + \\ &\quad \begin{bmatrix} 0 \\ \kappa_1 \\ 0 \\ \frac{C_f l_f}{I_z} \end{bmatrix} \bar{\delta} + \begin{bmatrix} 0 \\ -\frac{\kappa_1 l_f - \kappa_2 l_r}{\bar{V}_x} - \bar{V}_x \\ 0 \\ -\frac{C_f l_f^2 - C_r l_r^2}{I_z \bar{V}_x} \end{bmatrix} \dot{\bar{\psi}}_r + \begin{bmatrix} 0 \\ -(l_f + l_{fb} + L_a) \\ 0 \\ -1 \end{bmatrix} \ddot{\bar{\psi}}_r,\end{aligned}\tag{B.25}$$

where,

$$\begin{aligned}\kappa_1 &= C_f \left(\frac{1}{m} + \frac{l_f (l_f + l_{fb} + L_a)}{I_z} \right), \\ \kappa_2 &= C_r \left(\frac{1}{m} - \frac{l_r (l_f + l_{fb} + L_a)}{I_z} \right),\end{aligned}$$

and $\bar{\delta}$ is the control input and $\dot{\bar{\psi}}_r$ and $\ddot{\bar{\psi}}_r$ are considered as exogenous disturbances to the system.

Appendix C

Tuning LQR weighting gains

In Figure C.1 the open-loop poles of (2.37) are presented. The objective for controller synthesis is to shift the poles in the origin into the LHP without affected the large poles which are related to the dynamic response of the vehicle to a steer input. The controller gains calculated using

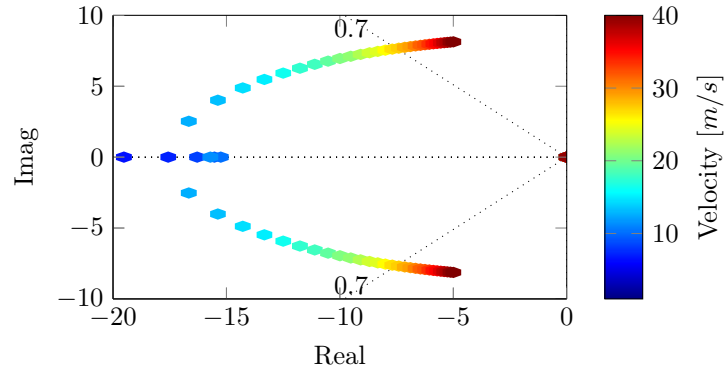


Figure C.1: Open-loop poles of (2.37).

LQR controller synthesis and are based, as already presented in (3.6), on using the following cost function:

$$\mathcal{J} = \int_t^\infty [x'_{el}(\tau)Qx_{el}(\tau) + \bar{\delta}'(\tau)R\bar{\delta}(\tau)] d\tau, \quad (\text{C.1})$$

where x_{el} is the state vector, $\bar{\delta}$ the input vector and Q and R are the weighting matrices for state vector x_{el} and input vector $\bar{\delta}$, respectively. Weighting matrices Q and R can be used to penalize a certain state or input and can therefore be considered as design parameters. One of the design requirements is to have a decreasing steer input with increasing velocity. Therefore, matrix R is designed as follows:

$$R = 2V_x \quad (\text{C.2})$$

The state vector is formulated as follows:

$$x_{el} = \begin{bmatrix} \bar{y}_{el} & \dot{\bar{y}}_{el} & \bar{\psi}_{el} & \dot{\bar{\psi}}_{el} \end{bmatrix}^T \quad (\text{C.3})$$

and weighting matrix Q as:

$$Q = \begin{bmatrix} q_1 & 0 & 0 & 0 \\ 0 & q_2 & 0 & 0 \\ 0 & 0 & q_3 & 0 \\ 0 & 0 & 0 & q_4 \end{bmatrix}. \quad (\text{C.4})$$

This means that q_1 can penalize \bar{y}_{el} , q_2 can penalize $\dot{\bar{y}}_{el}$, etcetera. Before randomly assigning values to the weighting gains it is desired to first obtain more insight in how each weighting gain individually can influence the response of the system. Applying the LQR controller synthesis results in the following feedback law:

$$\delta_{fb} = -K_{el}x_{el}, \quad (\text{C.5})$$

By using the state transformation of (2.41) and open-loop system in (2.37), the following closed-loop system can be obtained:

$$\dot{x}_e = (A_e - B_{e1}K_{el}C_{L_a})x_e + B_{e2}\dot{\bar{\psi}}_r + B_{e3}\ddot{\bar{\psi}}_r. \quad (\text{C.6})$$

For the investigation of the influence of Q on the closed-loop pole location of (C.6) it is assumed that $\bar{V}_x \in \mathcal{S}$ and $L_a = 0$. Furthermore, three sets of weighting gains are defined as follows:

- $\mathcal{Z}_1 = \{ 0.1 \ 0.25 \ 0.5 \ 1 \}$
- $\mathcal{Z}_2 = \{ 0.01 \ 0.1 \ 0.25 \ 0.5 \}$
- $\mathcal{Z}_3 = \{ 0.5 \ 1 \ 5 \ 10 \}$

Equation (C.6) is used to determine the closed-loop pole locations with $\dot{\bar{\psi}}_r = \ddot{\bar{\psi}}_r = 0$.

Weighting gain q_1

First, the influence of q_1 to the system is investigated. For the analysis different values for $q_1 \in \mathcal{Z}_1$ are compared, while $q_2 = q_3 = q_4 = 0$. In Figure C.2a the closed-loop pole locations for (C.6) with $\bar{V}_x \in \mathcal{S}$ and $L_a = 0$ are presented. As is shown, increasing q_1 only has a minor effect on the locations of the poles related to the dynamic behavior of the vehicle. While increasing q_1 , results in a significant shift of the poles in the origin into the LHP. However, this also results in the changing the poles near the origin into a complex conjugated pole pair. In Figure C.2b, the magnitude plot of the string stability complementary sensitivity is presented. It is shown that increasing q_1 results in a performance increase of the system.

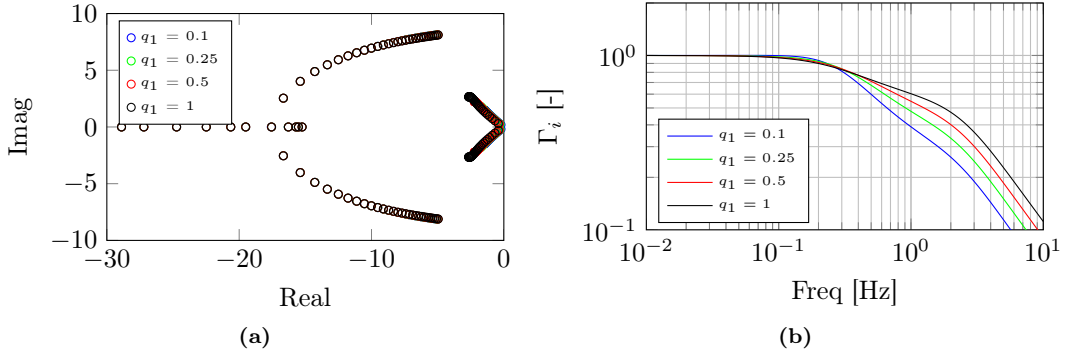


Figure C.2: (a) Closed-loop pole locations of (C.6) for $q_1 \in \mathcal{Z}_1$, $q_2 = q_3 = q_4 = 0$, $\dot{\bar{\psi}}_r = \ddot{\bar{\psi}}_r = 0$, $\bar{V}_x \in \mathcal{S}$ and $L_a = 0$. (b) Magnitude plot of the string stability complementary sensitivity for $q_1 \in \mathcal{Z}_1$, $q_2 = q_3 = q_4 = 0$, $\bar{V}_x = 15\text{m/s}$ and $L_a = 6\text{m}$.

In Figure C.3, the time responses of the errors to a step input are presented for $q_1 \in \mathcal{Z}_1$ and $q_2 = q_3 = q_4 = 0$. Increasing q_1 results in a smaller steady state errors, while it results in a faster response of the system with less overshoot.

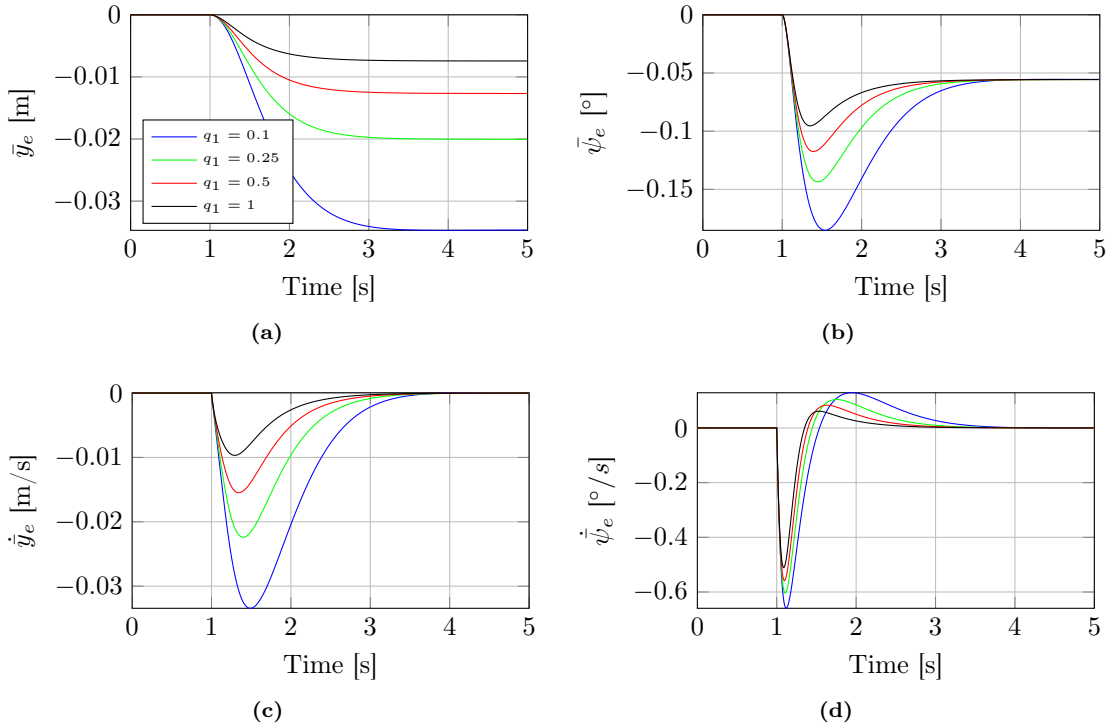


Figure C.3: Time responses of the errors to a step input for $q_1 \in \mathcal{Z}_1$, $q_2 = q_3 = q_4 = 0$, $\bar{V}_x = 15\text{m/s}$ and $L_a = 6\text{m}$.

Figure C.4 contains the control input to the system to a the step input, for $q_1 \in \mathcal{Z}_1$ and $q_2 = q_3 = q_4 = 0$. It can be observed that a larger value for q_1 results in a faster response of the system and results in having less overshoot compared to the steady state steer input of the system.

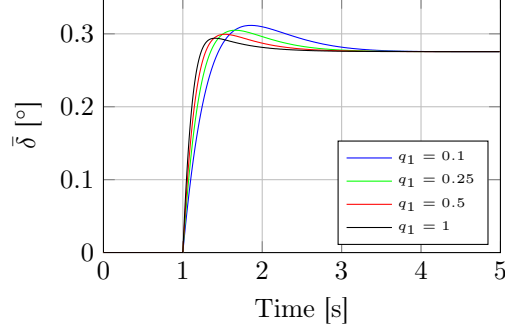


Figure C.4: Control input to a step input for $q_1 \in \mathcal{Z}_1$, $q_2 = q_3 = q_4 = 0$, $\bar{V}_x = 15\text{m/s}$ and $L_a = 6\text{m}$.

Based on the results presented, it can be concluded that weighting gain q_1 has a positive influence on the response of the system. Without having a significant influence on the closed-loop pole locations of the system, even for larger values of q_1 . However, larger values of q_1 increasing the complex part of the poles near the origin. This will result in a faster responds of the system, at the expense of having more oscillations in the time-domain responses at higher velocities.

Weighting gain q_2

Next, the influence of q_2 is analyzed. In Figure C.5a, the closed-loop pole locations of (C.6) are presented for $q_2 \in \mathcal{Z}_2$ and $q_1 = q_3 = q_4 = 0$. Increasing q_2 shifts the poles in the origin into the LHP without changing them into a complex conjugated pair. However, the location of the poles related to the dynamics of the vehicle are also significantly influenced. Thereby, the requirement of not influencing the locations of the poles related to the dynamics response of the vehicle is not fulfilled. Figure C.5b presents the magnitude plot of the string stability complementary sensitivity for $q_2 \in \mathcal{Z}_2$ and $q_1 = q_3 = q_4 = 0$. Increasing q_2 , results in a higher magnitude of $|\Gamma_i|$ and thereby results in a better performance of the system. However, as mentioned before, the dynamic response of the vehicle to a steer input is also altered.

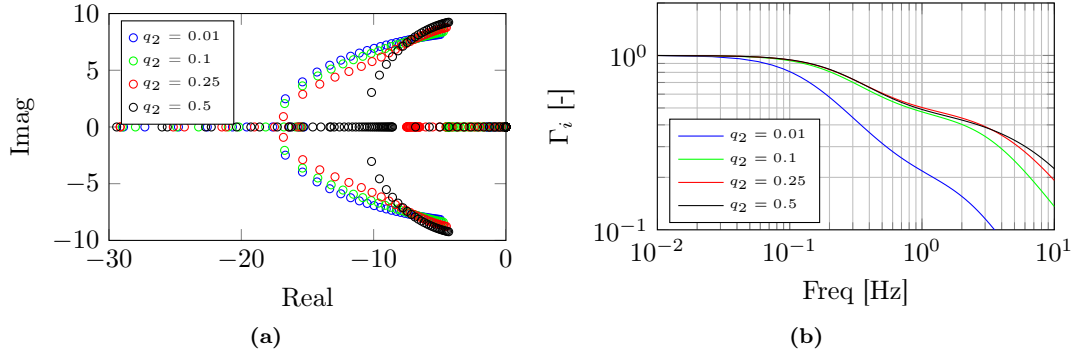


Figure C.5: (a) Closed-loop pole locations of (C.6) for $q_2 \in \mathcal{Z}_2$, $q_2 = q_3 = q_4 = 0$, $\dot{\bar{\psi}}_r = \ddot{\bar{\psi}}_r = 0$, $\bar{V}_x \in \mathcal{S}$ and $L_a = 0$. (b) Magnitude plot of the string stability complementary sensitivity for $q_2 \in \mathcal{Z}_1$, $q_1 = q_3 = q_4 = 0$, $\bar{V}_x = 15\text{m/s}$ and $L_a = 6\text{m}$.

In Figure C.6, the time responses of the errors to a step input are presented for $q_2 \in \mathcal{Z}_2$ and $q_1 = q_3 = q_4 = 0$. As is shown, only using q_2 results in a very slow convergence of \bar{y}_e to its steady state value. Furthermore, $\dot{\bar{y}}_e$ converges to a steady error, rather than to zero as is the case in Figure C.3c. However, increasing q_2 does not result in overshoot of the rotational error, as is the case with q_1 .

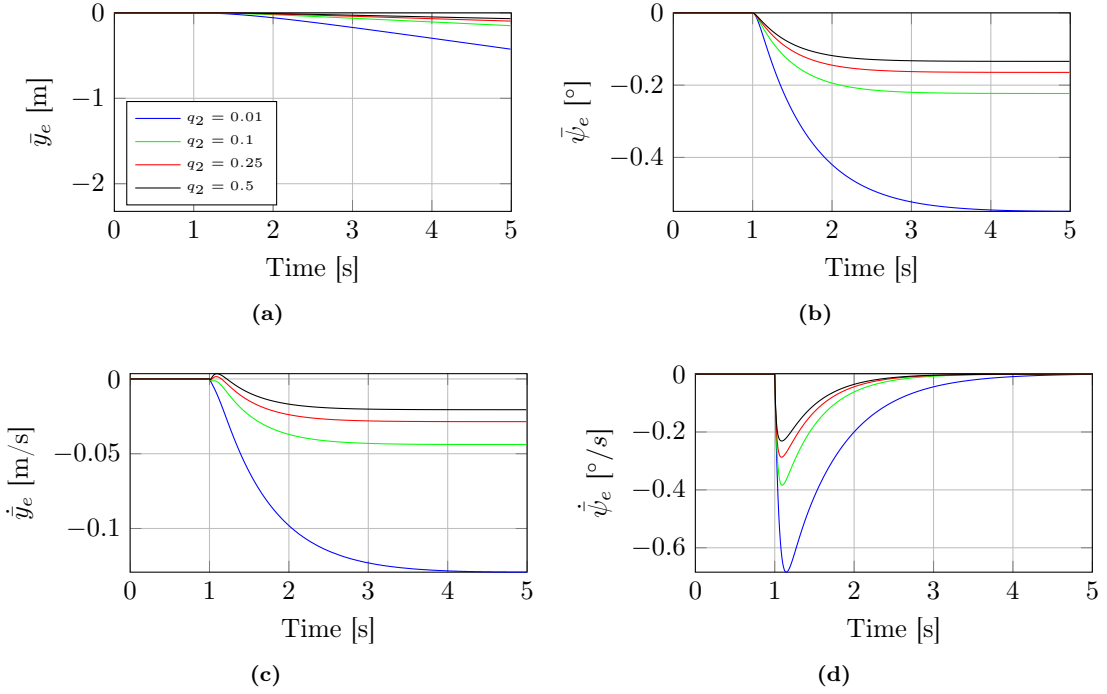


Figure C.6: Time responses of the errors to a step input for $q_2 \in \mathcal{Z}_2$, $q_1 = q_3 = q_4 = 0$, $\bar{V}_x = 15\text{m/s}$ and $L_a = 6\text{m}$.

In Figure C.7, the control input for the system to a the step input is presented for $q_2 \in \mathcal{Z}_2$ and $q_2 = q_3 = q_4 = 0$. Increasing q_2 results in a faster responds of the system. However, as mentioned before, this is caused by changing the vehicle responds.

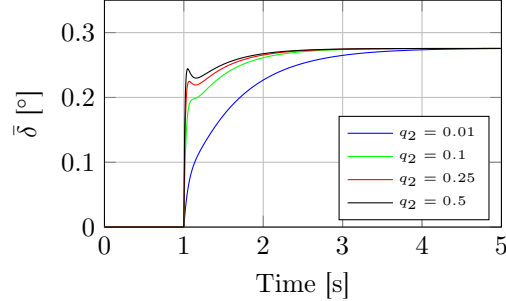


Figure C.7: Control input to a step input for $q_2 \in \mathcal{Z}_2$, $q_1 = q_3 = q_4 = 0$, $\bar{V}_x = 15\text{m/s}$ and $L_a = 6\text{m}$.

Based on the presented results, the use of large values for q_2 have to be avoided. Small values ($0.01 <$) for q_2 can be used to compensate for certain unwanted influence of the other weighting gains. However, caution is advised when doing this.

Weighting gain q_3

Next, the influence of q_3 on the closed-loop system in (C.6) is investigated. In Figure C.8a, the closed-loop pole locations of (C.6) are presented for $q_3 \in \mathcal{Z}_3$ and $q_1 = q_2 = q_4 = 0$. As is shown, q_3 has a small influence on the location of the poles related to the dynamic behavior of the vehicle, only for larger values (> 1) of q_3 , the poles locations related to the dynamic behavior of the vehicle are influenced. However, increasing q_3 results only in shifting one pole in the origin into the left half plane, while the other pole remains in the origin. In Figure C.8b, the magnitude plot of the string stability complementary sensitivity for $q_3 \in \mathcal{Z}_3$ and $q_1 = q_2 = q_4 = 0$ is presented. As is shown in Figure C.8b, increasing q_3 results in a higher bandwidth of the system, which results in a better tracking performance.

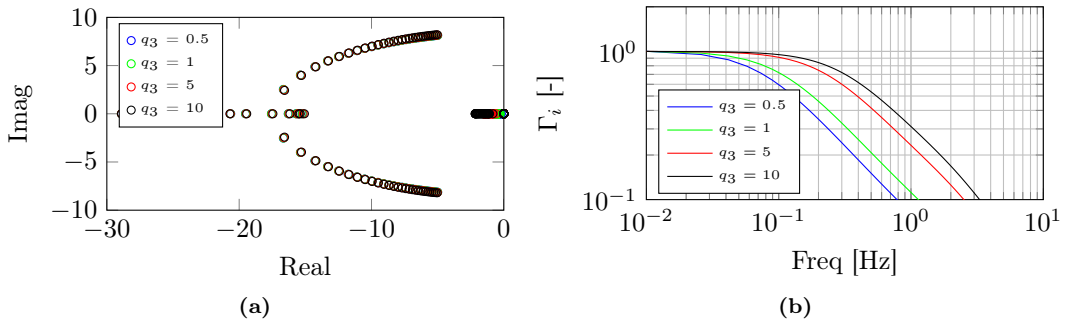


Figure C.8: (a) Closed-loop pole locations of (C.6) for $q_3 \in \mathcal{Z}_3$, $q_1 = q_2 = q_4 = 0$, $\dot{\psi}_r = \ddot{\psi}_r = 0$, $\bar{V}_x \in \mathcal{S}$ and $L_a = 0$. (b) Magnitude plot of the string stability complementary sensitivity for $q_3 \in \mathcal{Z}_1$, $q_1 = q_2 = q_4 = 0$, $\bar{V}_x = 15\text{m/s}$ and $L_a = 6\text{m}$.

In Figure C.9, the time responses of the errors to a step input are presented for $q_3 \in \mathcal{Z}_3$ and $q_1 = q_2 = q_4 = 0$. A larger value for q_3 results in a smaller steady state rotational error, while $\dot{\psi}_e$ converges asymptotically to zero.

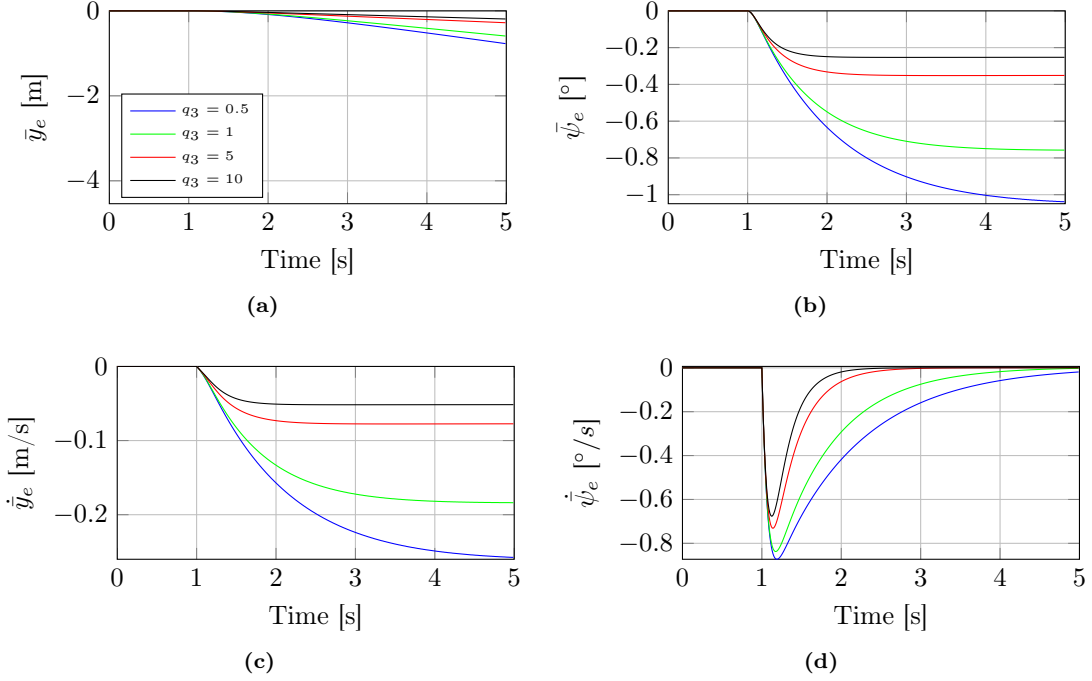


Figure C.9: Time responses of the errors to a step input for $q_3 \in \mathcal{Z}_3$, $q_1 = q_2 = q_4 = 0$, $\bar{V}_x = 15\text{m/s}$ and $L_a = 6\text{m}$.

However, the lateral error \bar{y}_e converges only very slowly to its steady state value. Furthermore, \dot{y}_e does not converge to zero as is the case in Figure C.3c. In Figure C.10, the control input for the system to a the step input is presented for $q_3 \in \mathcal{Z}_3$ and $q_1 = q_2 = q_4 = 0$. The control input converges asymptotically to the steady state steer input. However, the system has a very slow response as is shown in Figure C.9, especially the convergence of the lateral error \bar{y}_e to the steady state error.

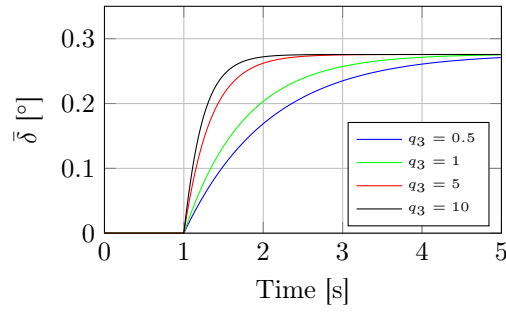


Figure C.10: Control input to a step input for $q_3 \in \mathcal{Z}_3$, $q_1 = q_2 = q_4 = 0$, $\bar{V}_x = 15\text{m/s}$ and $L_a = 6\text{m}$.

Based on the obtained results, q_3 can be used to improve the reduction of the rotational errors, without affecting the location of the poles related to the dynamic behavior of the vehicle. However, q_3 does not influence the lateral position or velocity error. This results in a very slow convergence of these errors.

Weighting gain q_4

Finally, the influence of q_4 on the closed-loop system in (C.6) is investigated. In Figure C.11a, the closed-loop pole locations of (C.6) are presented for $q_4 \in \mathcal{Z}_1$ and $q_1 = q_2 = q_3 = 0$. As can be observed, q_4 only influences the location of the poles related to the dynamic behavior of the vehicle. While the poles located in the origin, remain in the origin. In Figure C.11b, the magnitude plot of the string stability complementary sensitivity is presented. Increasing the value q_4 , does not significantly improve the performance of the system.

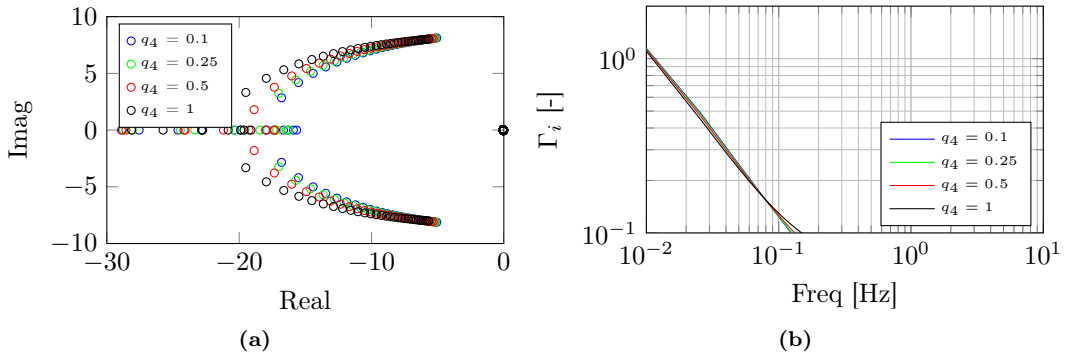


Figure C.11: (a) Closed-loop pole locations of (C.6) for $q_4 \in \mathcal{Z}_1$, $q_1 = q_2 = q_3 = 0$, $\dot{\psi}_r = \ddot{\psi}_r = 0$, $\bar{V}_x \in \mathcal{S}$ and $L_a = 0$. (b) Magnitude plot of the string stability complementary sensitivity for $q_4 \in \mathcal{Z}_1$, $q_1 = q_2 = q_3 = 0$, $\bar{V}_x = 15\text{m/s}$ and $L_a = 6\text{m}$.

In Figure C.6, the time responses of the errors to a step input are presented for $q_4 \in \mathcal{Z}_2$ and $q_1 = q_2 = q_3 = 0$. As is shown, only using q_4 results in a very slow convergence of all error states. Which means that state q_4 does not have a significant influence on the performance of the system.

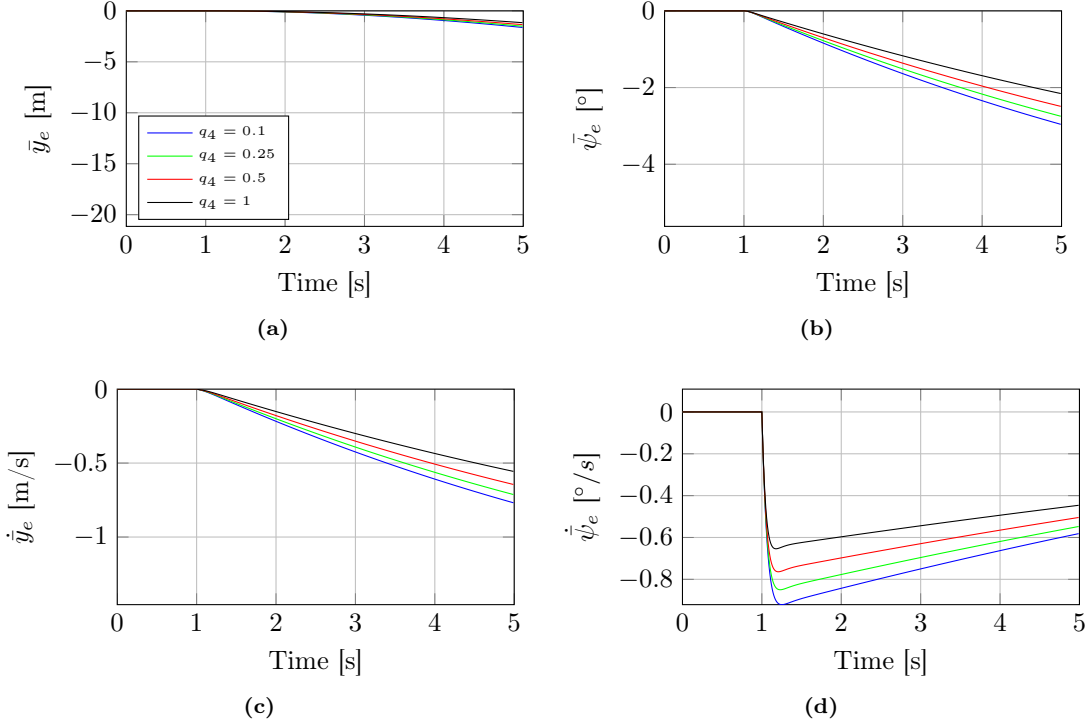


Figure C.12: Time responses of the errors to a step input for $q_4 \in \mathcal{Z}_1$, $q_1 = q_2 = q_3 = 0$, $\bar{V}_x = 15\text{m/s}$ and $L_a = 6\text{m}$.

In Figure C.10, the control input for the system to a the step input is presented for $q_3 \in \mathcal{Z}_3$ and $q_1 = q_2 = q_4 = 0$. As can be observed, the system only responses very slowly to the step input.

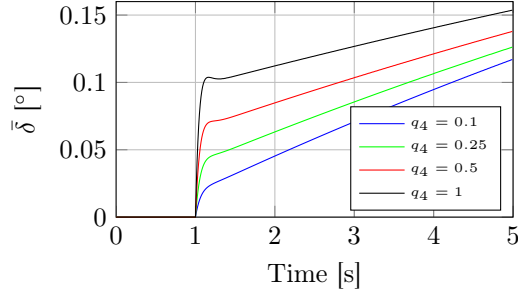


Figure C.13: Control input to a step input for $q_4 \in \mathcal{Z}_1$, $q_1 = q_2 = q_3 = 0$, $\bar{V}_x = 15\text{m/s}$ and $L_a = 6\text{m}$.

As can be observed from the results presented in this section, q_4 has no positive influence on the response of the system. Therefore, it is advised not add a value to weighting gain q_4 .

Different configuration of Q

In this section, the influence of matrix Q onto the closed-loop poles for different settings of Q is investigated. Different settings for Q are chosen based on the results presented on the influence of q_1, q_2, q_3 and q_4 . Furthermore, for the pole location analysis it is assumed that exogenous inputs $\dot{\psi}_r = \ddot{\psi}_r = 0$. For the first setting, the weighting gains of matrix Q have the following values:

Set 1	
q_1	0.2
q_2	0.001
q_3	2
q_4	0

Table C.1: Values for weighting gains of setting 1.

In Figure 3.3a, the open-loop of pole positions of (2.37) for $\bar{V}_x \in \mathcal{S}$ are presented and Figure C.14b contains the closed-loop poles of (C.6) for $\bar{V}_x \in \mathcal{S}$ and $L_a = 0$. As can be observed, the position of the poles related to dynamics of the vehicle remain unaffected, while in the closed-loop system the poles near the origin are shifted into the LHP. In Figure C.14c and Figure C.14d the closed-loop poles of (C.6) for $\bar{V}_x \in \mathcal{S}$ and $L_a \in \mathcal{T}$ are presented, where the magenta colored arrow indicates the influence of \bar{V}_x on the closed-loop pole locations and the cyan colored arrow shows the influence of L_a onto the closed-loop pole locations.

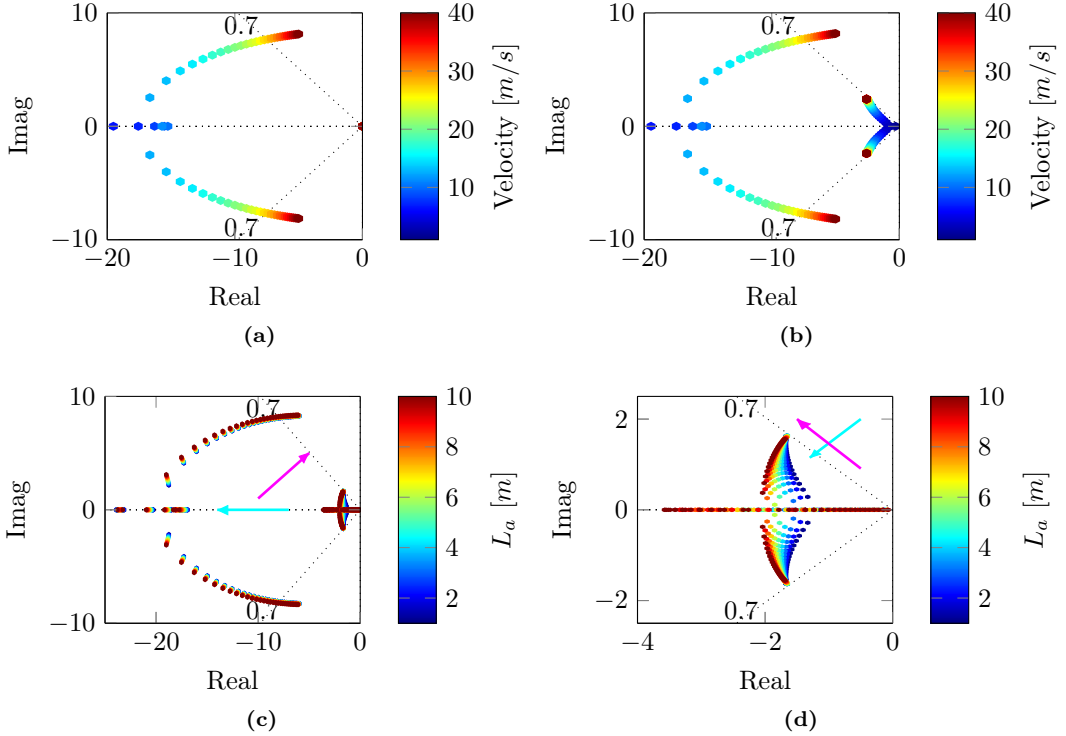


Figure C.14: (a) Open-loop poles of (2.37) for $\bar{V}_x \in \mathcal{S}$. (b) Closed-loop poles of (C.6) for $\bar{V}_x \in \mathcal{S}$ and $L_a = 0$. (c) Closed-loop poles of (C.6) for $\bar{V}_x \in \mathcal{S}$ and $L_a \in \mathcal{T}$. (d) Closed-loop poles of (C.6) close to the origin for $\bar{V}_x \in \mathcal{S}$ and $L_a \in \mathcal{T}$.

The next set of weighting gains have the following values:

Set 2	
q_1	0.25
q_2	0.01
q_3	1
q_4	0

Table C.2: Values for weighting gains of setting 2.

In Figure C.15a the open-loop of pole positions of (2.37) for $\bar{V}_x \in \mathcal{S}$ are presented and in Figure C.15b the closed-loop poles of (C.6) for $\bar{V}_x \in \mathcal{S}$ and $L_a = 0$. As can be observed, the position of the poles related to dynamics of the vehicle remain unaffected, while in the closed-loop system the poles near the origin are shifted into the LHP. In Figure C.15c and Figure C.15d the closed-loop poles of (C.6) for $\bar{V}_x \in \mathcal{S}$ and $L_a \in \mathcal{T}$ are presented, where the magenta colored arrow indicates the influence of \bar{V}_x on the closed-loop pole locations and the cyan colored arrow shows the influence of L_a onto the closed-loop pole locations.

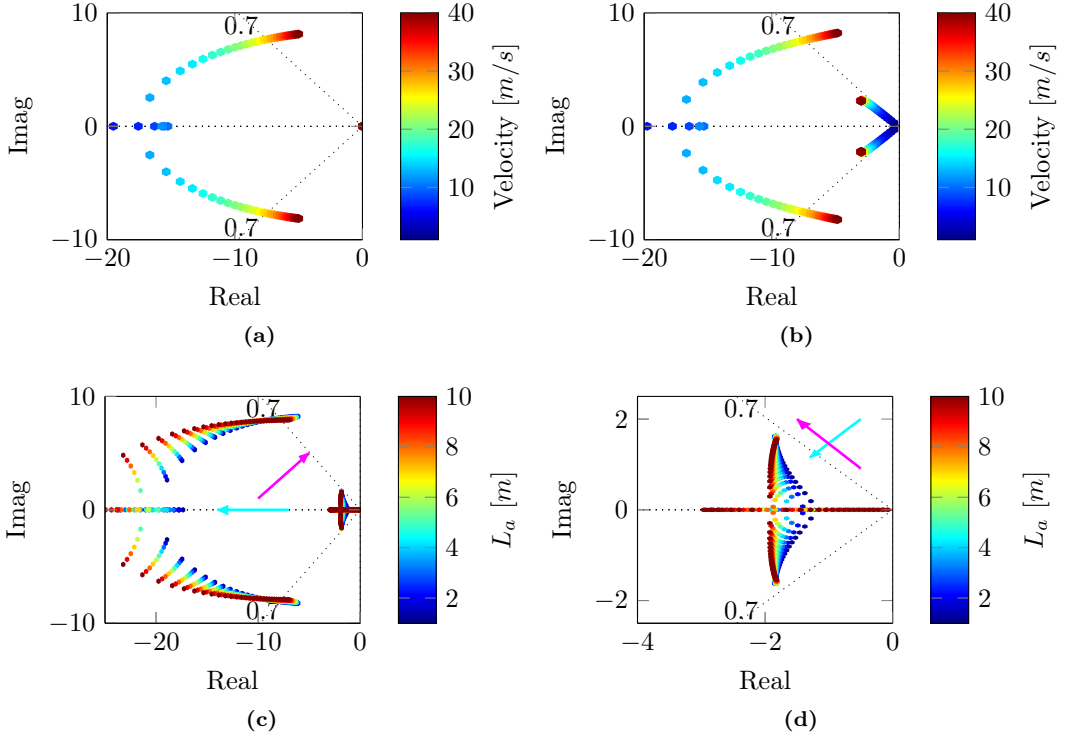


Figure C.15: (a) Open-loop poles of (2.37) for $\bar{V}_x \in \mathcal{S}$. (b) Closed-loop poles of (C.6) for $\bar{V}_x \in \mathcal{S}$ and $L_a = 0$. (c) Closed-loop poles of (C.6) for $\bar{V}_x \in \mathcal{S}$ and $L_a \in \mathcal{T}$. (d) Closed-loop poles of (C.6) close to the origin for $\bar{V}_x \in \mathcal{S}$ and $L_a \in \mathcal{T}$.

The third set of weighting gains are chosen as follows:

Set 3	
q_1	0.1
q_2	0.005
q_3	2
q_4	0

Table C.3: Values for weighting gains of setting 3.

In Figure C.16a, the open-loop of pole positions of (2.37) for $\bar{V}_x \in \mathcal{S}$ are presented and in Figure C.16b the closed-loop poles of (C.6) for $\bar{V}_x \in \mathcal{S}$ and $L_a = 0$. As can be observed, the position of the poles related to dynamics of the vehicle remain unaffected, while in the closed-loop system the poles near the origin are shifted into the LHP. In Figure C.16c and Figure C.16d the closed-loop poles of (C.6) for $\bar{V}_x \in \mathcal{S}$ and $L_a \in \mathcal{T}$ are presented, where the magenta colored arrow indicates the influence of \bar{V}_x on the closed-loop pole locations and the cyan colored arrow shows the influence of L_a onto the closed-loop pole locations.

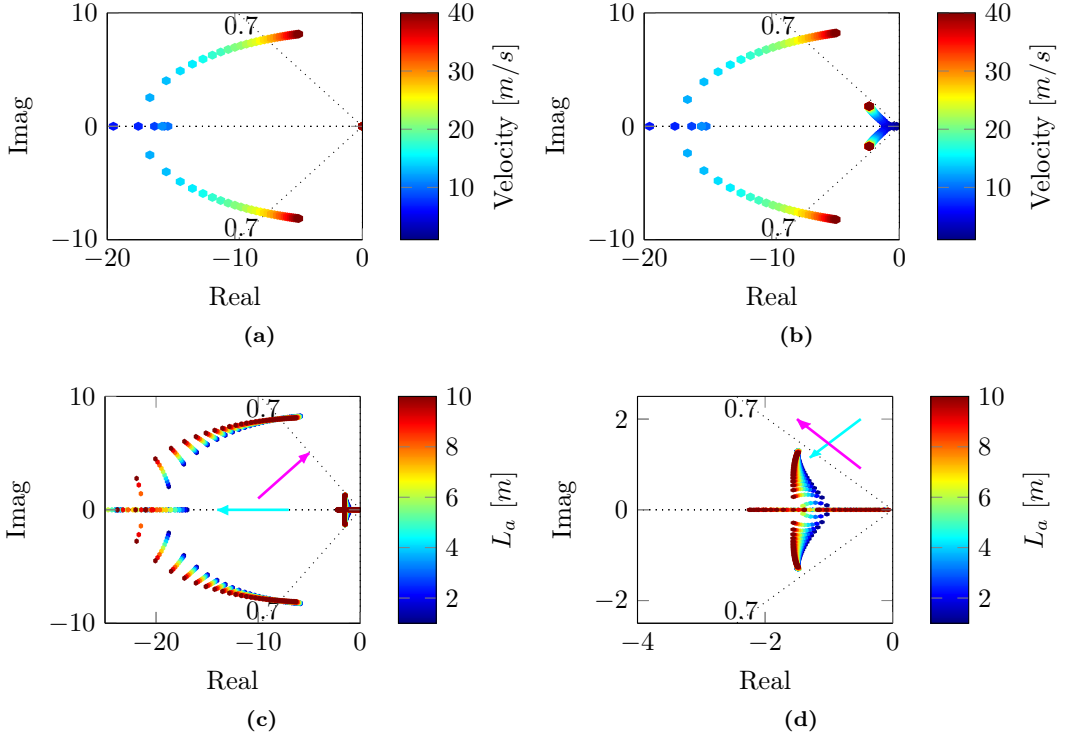


Figure C.16: (a) Open-loop poles of (2.37) for $\bar{V}_x \in \mathcal{S}$. (b) Closed-loop poles of (C.6) for $\bar{V}_x \in \mathcal{S}$ and $L_a = 0$. (c) Closed-loop poles of (C.6) for $\bar{V}_x \in \mathcal{S}$ and $L_a \in \mathcal{T}$. (d) Closed-loop poles of (C.6) close to the origin for $\bar{V}_x \in \mathcal{S}$ and $L_a \in \mathcal{T}$.

The last set of weighting gains have the following values:

Set 4	
q_1	0.1
q_2	0.00
q_3	0.2
q_4	0

Table C.4: Values for weighting gains of setting 4.

In Figure C.17a the open-loop of pole positions of (2.37) for $\bar{V}_x \in \mathcal{S}$ are presented and in Figure C.17b the closed-loop poles of (C.6) for $\bar{V}_x \in \mathcal{S}$ and $L_a = 0$. As can be observed, the position of the poles related to dynamics of the vehicle remain unaffected, while in the closed-loop system the poles near the origin are shifted into the LHP. In Figure C.17c and Figure C.17d the closed-loop poles of (C.6) for $\bar{V}_x \in \mathcal{S}$ and $L_a \in \mathcal{T}$ are presented, where the magenta colored arrow indicates the influence of \bar{V}_x on the closed-loop pole locations and the cyan colored arrow shows the influence of L_a onto the closed-loop pole locations.

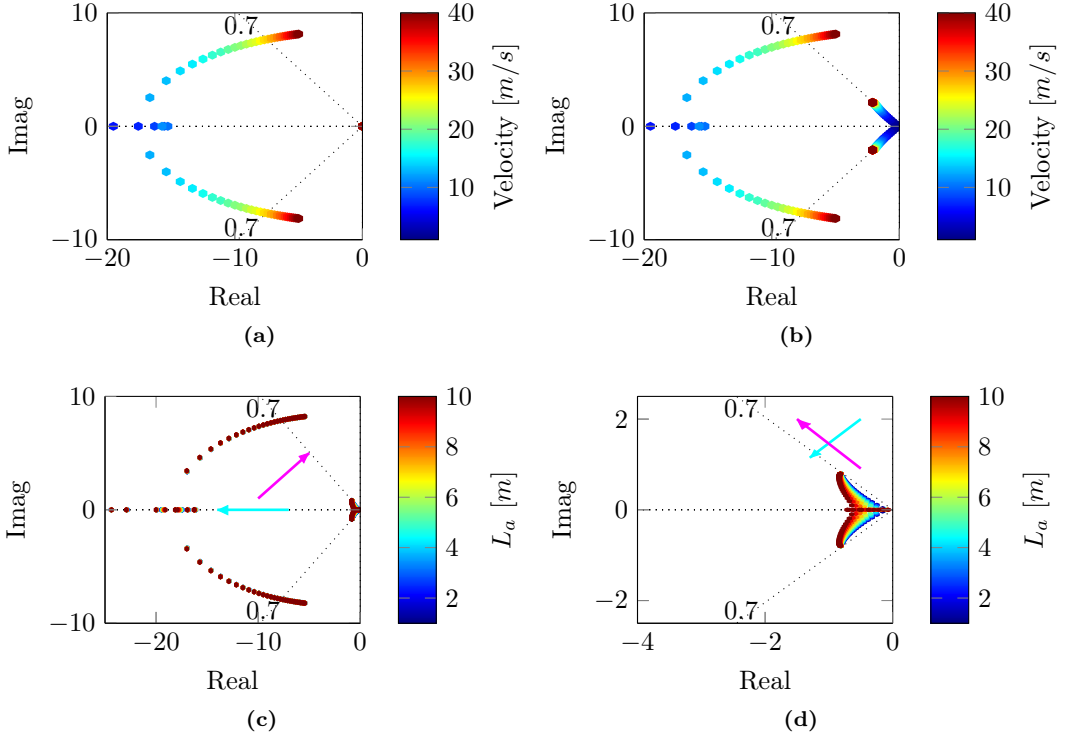


Figure C.17: (a) Open-loop poles of (2.37) for $\bar{V}_x \in \mathcal{S}$. (b) Closed-loop poles of (C.6) for $\bar{V}_x \in \mathcal{S}$ and $L_a = 0$. (c) Closed-loop poles of (C.6) for $\bar{V}_x \in \mathcal{S}$ and $L_a \in \mathcal{T}$. (d) Closed-loop poles of (C.6) close to the origin for $\bar{V}_x \in \mathcal{S}$ and $L_a \in \mathcal{T}$.

All four sets of weighting gains influence the locations of the closed-loop poles near the origin, without affecting the location of the poles related to the dynamic behavior of the vehicle.

In Figure C.18, the string stability complementary sensitivity is presented for the different settings of Q . Setting 1 results in the highest bandwidth, while setting 2 results in the smallest magnitude, setting 3 has the lowest cross over frequency and setting 4 results in the largest magnitude of $|\Gamma_i|$.

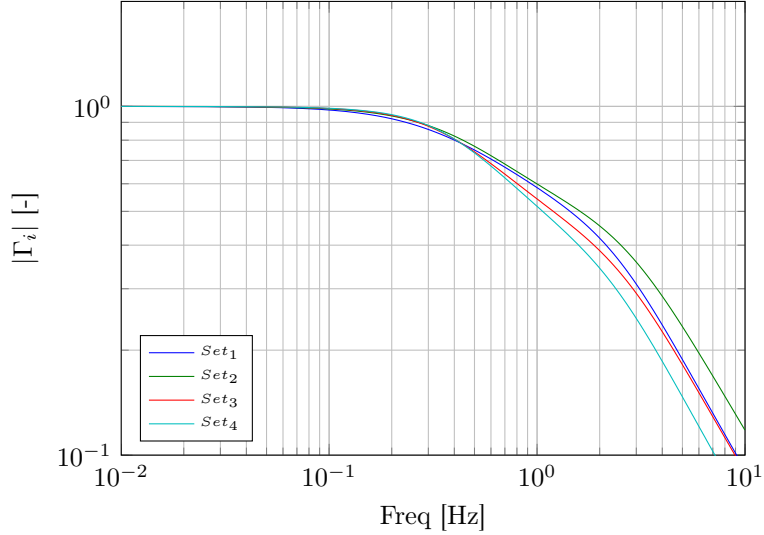


Figure C.18: String stability complementary sensitivity function for different settings of Q .

In the next section, the time response of the system with the different sets of weighting gains will be analyzed to investigate which set of weighting gains results in the smallest errors and the lowest amount of steer input.

Time-domain simulations results step response

For the time-domain simulations the closed-loop system as formulated in (C.6) is used, where it is assumed that $\ddot{\psi}_r = 0$ and $\dot{\psi}_r$ is used as input to disturb the system with a step in, which is shown in Figure 3.6a. The simulations are conducted with $\bar{V}_x = 15\text{m/sm/s}$ and $L_a = 6\text{m}$, and the influence of the different configuration of matrix Q is investigated. In Figure C.19 the error states of (C.6) for the different configurations of Q to the step input of Figure 3.6a are presented.

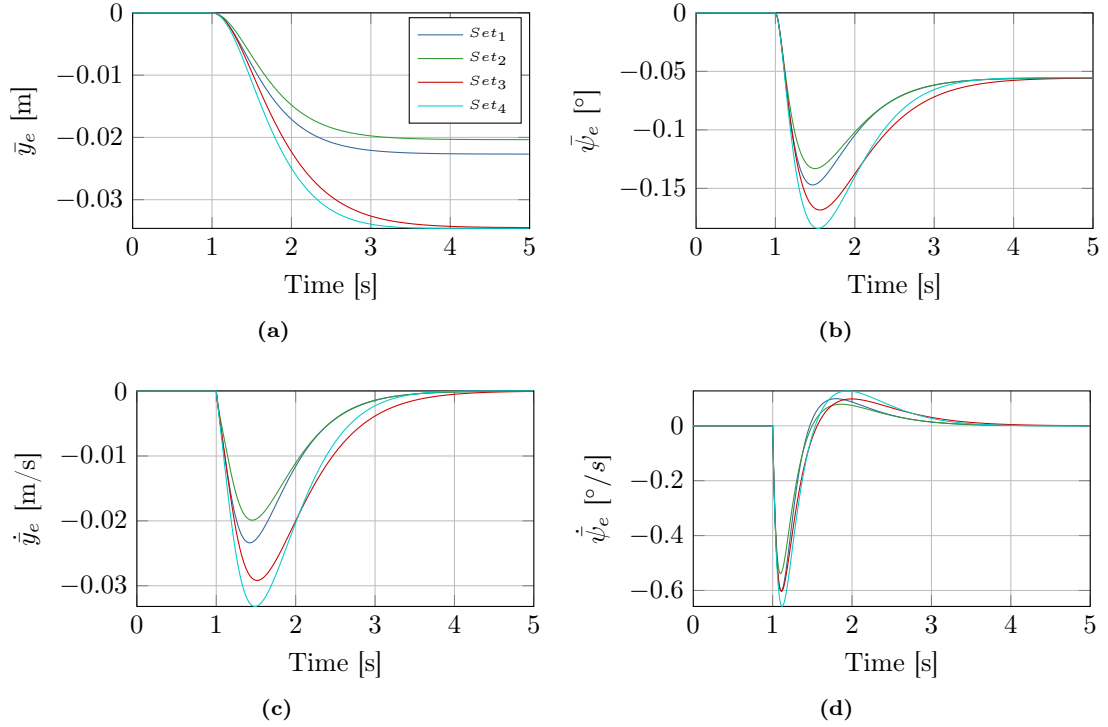


Figure C.19: Error states of (C.6) for the different configurations of Q to a step input as shown in Figure 3.6a for $\bar{V}_x = 15\text{m/s}$ and $L_a = 6\text{m}$.

As can be seen, setting 2 results in the smallest steady-state error of \bar{y}_e and causes the smallest errors for $\dot{\bar{y}}_e$, $\bar{\psi}_e$ and $\dot{\bar{\psi}}_e$. Furthermore, setting 2 also results in smallest amount of overshoot of state $\dot{\bar{\psi}}_e$. In Figure C.20a the control input for the different settings for matrix Q is presented. Although the differences are small, as can be seen in Figure C.20b, setting 2 results in lowest maximum control input to the system.

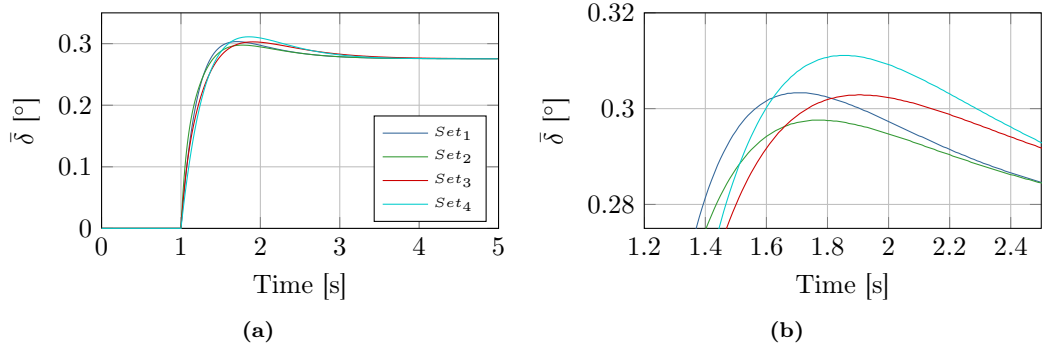


Figure C.20: (a) Control input for the different settings of Q , $\bar{V}_x = 15\text{m/s}$ and $L_a = 6\text{m}$. (b) Zoom of the control input for the different settings of Q , between Time is 1.2s and 2.5s .

Conclusion

In this appendix, the influence of weighting matrix Q onto the closed-loop pole locations and time responses of the error states to a step input is investigated. The goal is to find values for the weighting gains in matrix Q which results in the smallest errors, minimum of overshoot and the lowest control input. First, the influence of each individual gain onto the closed-loop pole positions is investigated, whereafter four different configurations of matrix Q are formulated and analyzed based on the resulting closed-loop pole location and time simulations of a step input. The second configuration of matrix Q yielded the smallest steady-state error of state \bar{y}_e and $\bar{\psi}_e$, the smallest errors for states $\dot{\bar{y}}_e$ and $\dot{\bar{\psi}}_e$ and the smallest control input to the system.

Appendix D

Error dynamics between two vehicles

In this appendix the error dynamics are derived between two vehicles when a vehicle is positioned at point r_l in Figure 2.3. These error dynamics can then be used to obtain the feedforward input in Section 4.3. For the derivation of the error dynamics three reference frames are introduced, a global and two others, attached to vehicle $i-1$ and vehicle i , respectively. The global right-handed frame is defined, with the orientation of a set $\bar{e}^0 := [\bar{e}_1^0 \bar{e}_2^0 \bar{e}_3^0]^T$ of three mutually orthogonal unit vectors \bar{e}_1^0, \bar{e}_2^0 and \bar{e}_3^0 . The *cm* of vehicle $i-1$ is positioned in the origin of frame \bar{e}^{i-1} , which is fixed to the vehicle body. Furthermore, frame \bar{e}^{i-1} consists, likewise to frame \bar{e}^0 , of a set of three mutually orthogonal unit vectors $\bar{e}_1^{i-1}, \bar{e}_2^{i-1}$ and \bar{e}_3^{i-1} , where vector \bar{e}_1^{i-1} is oriented in the forward direction along the center axis of vehicle $i-1$. The *cm* of vehicle i is positioned in the origin of frame \bar{e}^i and consists, likewise to frame \bar{e}^0 and \bar{e}^{i-1} , of a set of three mutually orthogonal unit vectors \bar{e}_1^i, \bar{e}_2^i and \bar{e}_3^i , where vector \bar{e}_1^i is oriented in forward direction of vehicle i . The error dynamics, between the *cm* of vehicle $i-1$ and the *cm* of vehicle i are derived with respect to frame \bar{e}^{i-1} . In Figure D.1, vectors $\vec{r}_{v_{i-1}}$ and \vec{r}_{v_i} are, respectively, the distance vectors between the origin of the global frame \bar{e}^0 and the *cm* of vehicle $i-1$ and the origin of global frame \bar{e}^0 and the *cm* of the vehicle $i-1$, these vectors are omitted for clarity reasons. However, both vectors are defined as the position vector of the vehicle in Figure 2.2. Vector $\vec{r}_{r_l/v_{i-1}}$ is the distance of the *cm* of vehicle $i-1$ to the rear bumper, with length $l_r + l_{rb}$, where l_r is the distance between the *cm* and the rear axle and l_{rb} the distance between the rear axle and the rear bumper, respectively. \vec{r}_{v_l/v_i} is the vector of the *cm* of vehicle i to the look-ahead point v_l , with length $l_f + l_{fb} + L_a$, where l_f is the distance between the *cm* and the front axle, l_{fb} the distance between the front axle and front bumper, and L_a the look-ahead distance, respectively. The vectors $\vec{V}_{v_{i-1}}$ and \vec{V}_{v_i} are the absolute velocity vectors of the center of masses of vehicle $i-1$ and i , respectively. $V_{x_{i-1}}$ and $V_{y_{i-1}}$ are the longitudinal and lateral velocity of *cm* of vehicle $i-1$ with respect to body-fixed frame \bar{e}^{i-1} and V_{x_i} and V_{y_i} are the longitudinal and lateral velocity of *cm* of vehicle i with respect to body-fixed frame \bar{e}^i . $\psi_{v_{i-1}}$ is the angle from frame \bar{e}^0 to frame \bar{e}^{i-1} , ψ_{v_i} is the angle from frame \bar{e}^0 to frame \bar{e}^i and β_{i-1} and β_i are the side-slip angles of vehicle $i-1$ and i , respectively. y_{el_i} is the lateral error between the look-ahead point v_l of vehicle i and the rear bumper of vehicle $i-1$, with respect to frame \bar{e}^{i-1} , which can be written as:

$$y_{el_i} = (\vec{r}_{v_l} - \vec{r}_{r_l}) \cdot \bar{e}_2^{i-1}. \quad (\text{D.1})$$

The velocity vector of point r_l can now be written as follows:

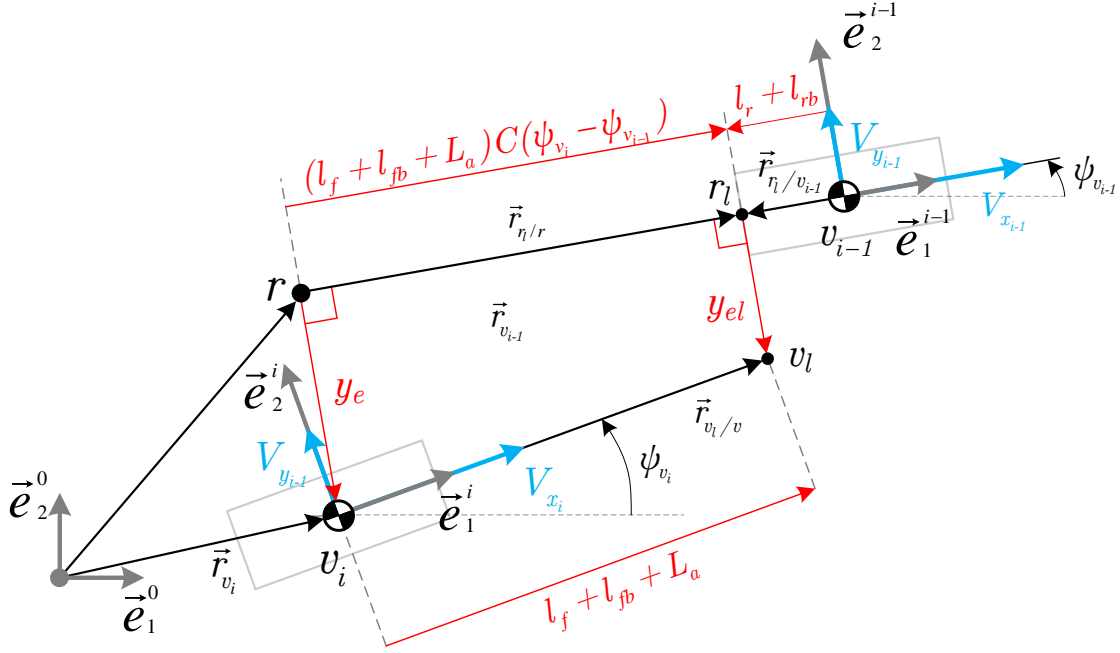


Figure D.1: A schematic representation of the lateral control problem used to derive the lateral and rotational error dynamics between the *cm* of two vehicles.

$$\begin{aligned}
 \vec{V}_{r_l} &= \vec{V}_r + \dot{\vec{r}}_{r_l/r} - \dot{\vec{r}}_{r_l/v_{i-1}}, \\
 &= \vec{V}_r - r_{r_l/r}^{i-1T} i^{-1,0} \tilde{\underline{\omega}}^{i-1} \vec{e}^{i-1} + r_{r_l/v_{i-1}}^{i-1T} i^{-1,0} \tilde{\underline{\omega}}^{i-1} \vec{e}^{i-1}, \\
 &= \begin{bmatrix} V_{x_{i-1}} \\ V_{y_{i-1}} \\ 0 \end{bmatrix}^T \vec{e}^{i-1} - \begin{bmatrix} (l_f + l_{fb} + L_a)C(\psi_{v_i} - \psi_{v_{i-1}}) \\ 0 \\ 0 \end{bmatrix}^T \begin{bmatrix} 0 & -\dot{\psi}_{v_{i-1}} & 0 \\ \dot{\psi}_{v_{i-1}} & 0 & 0 \\ 0 & 0 & 0 \end{bmatrix} \vec{e}^{i-1} \\
 &\quad + \begin{bmatrix} -(l_r + l_{rb}) \\ 0 \\ 0 \end{bmatrix}^T \begin{bmatrix} 0 & -\dot{\psi}_{v_{i-1}} & 0 \\ \dot{\psi}_{v_{i-1}} & 0 & 0 \\ 0 & 0 & 0 \end{bmatrix} \vec{e}^{i-1}, \\
 &= [V_{x_{i-1}} \quad V_{y_{i-1}} + (l_f + l_{fb} + L_a)C(\psi_{v_i} - \psi_{v_{i-1}})\dot{\psi}_{v_{i-1}} + (l_r + l_{rb})\dot{\psi}_{v_{i-1}} \quad 0] \vec{e}^{i-1}.
 \end{aligned} \tag{D.2}$$

The acceleration vector of point r_l can now be obtained by taking the time derivative of (D.2) and using the previously presented Poisson equations to obtain the time derivative of \vec{e}^{i-1} . This

results in the following:

$$\begin{aligned}
\dot{\vec{V}}_{r_l} &= \dot{\vec{V}}_r - r_{r_l/r}^{i-1T} \underline{\dot{\omega}}^{i-1} \underline{\vec{e}}^{i-1} + r_{r_l/r}^{i-1T} (\underline{\dot{\omega}}^{i-1})^2 \underline{\vec{e}}^{i-1} + r_{r_l/v_{i-1}}^{i-1T} \underline{\dot{\omega}}^{i-1} \underline{\vec{e}}^{i-1} \\
&\quad - r_{r_l/v_{i-1}}^{i-1T} (\underline{\dot{\omega}}^{i-1})^2 \underline{\vec{e}}^{i-1}, \\
&= \left[\begin{array}{c} \dot{V}_{x_{i-1}} - V_{y_{i-1}} \dot{\psi}_{v_{i-1}} \\ \dot{V}_{y_{i-1}} + V_{x_{i-1}} \dot{\psi}_{v_{i-1}} \\ 0 \end{array} \right]^T \underline{\vec{e}}^{i-1} - \left[\begin{array}{c} (l_f + l_{fb} + L_a)C(\psi_{v_i} - \psi_{v_{i-1}}) \\ 0 \\ 0 \end{array} \right]^T \left[\begin{array}{ccc} 0 & -\ddot{\psi}_{v_{i-1}} & 0 \\ \ddot{\psi}_{v_{i-1}} & 0 & 0 \\ 0 & 0 & 0 \end{array} \right] \underline{\vec{e}}^{i-1} \\
&\quad + \left[\begin{array}{c} (l_f + l_{fb} + L_a)C(\psi_{v_i} - \psi_{v_{i-1}}) \\ 0 \\ 0 \end{array} \right]^T \left(\left[\begin{array}{ccc} 0 & -\dot{\psi}_{v_{i-1}} & 0 \\ \dot{\psi}_{v_{i-1}} & 0 & 0 \\ 0 & 0 & 0 \end{array} \right] \right)^2 \underline{\vec{e}}^{i-1} \\
&\quad + \left[\begin{array}{c} -(l_r + l_{rb}) \\ 0 \\ 0 \end{array} \right]^T \left[\begin{array}{ccc} 0 & -\ddot{\psi}_{v_{i-1}} & 0 \\ \ddot{\psi}_{v_{i-1}} & 0 & 0 \\ 0 & 0 & 0 \end{array} \right] \underline{\vec{e}}^{i-1} \\
&\quad - \left[\begin{array}{c} -(l_r + l_{rb}) \\ 0 \\ 0 \end{array} \right]^T \left(\left[\begin{array}{ccc} 0 & -\dot{\psi}_{v_{i-1}} & 0 \\ \dot{\psi}_{v_{i-1}} & 0 & 0 \\ 0 & 0 & 0 \end{array} \right] \right)^2 \underline{\vec{e}}^{i-1}, \\
&= \left[\begin{array}{c} \dot{V}_{x_{i-1}} - V_{y_{i-1}} \dot{\psi}_{v_{i-1}} - (l_f + l_{fb} + L_a)C(\psi_{v_i} - \psi_{v_{i-1}})\dot{\psi}_{v_{i-1}}^2 - (l_r + l_{rb})\dot{\psi}_{v_{i-1}}^2 \\ \dot{V}_{y_{i-1}} + V_{x_{i-1}} \dot{\psi}_{v_{i-1}} + (l_f + l_{fb} + L_a)C(\psi_{v_i} - \psi_{v_{i-1}})\ddot{\psi}_{v_{i-1}} + (l_r + l_{rb})\ddot{\psi}_{v_{i-1}} \\ 0 \end{array} \right]^T \underline{\vec{e}}^{i-1}.
\end{aligned} \tag{D.3}$$

The velocity vector of point v_l can be written as follows:

$$\begin{aligned}
\vec{V}_{v_l} &= \vec{V}_i + \dot{\vec{r}}_{v_l/v_i} \\
&= \vec{V}_i - r_{v_l/v_i}^{iT} \underline{\dot{\omega}}^i \underline{A}^{i,i-1} \underline{\vec{e}}^{i-1}, \\
&= \left[\begin{array}{c} V_{x_i} C(\psi_{v_{i-1}} - \psi_{v_i}) + V_{y_i} S(\psi_{v_{i-1}} - \psi_{v_i}) \\ V_{y_i} C(\psi_{v_{i-1}} - \psi_{v_i}) + V_{x_i} S(\psi_{v_{i-1}} - \psi_{v_i}) \\ 0 \end{array} \right]^T \underline{\vec{e}}^{i-1} \\
&\quad - \left[\begin{array}{c} l_f + l_{fb} + L_a \\ 0 \\ 0 \end{array} \right]^T \left[\begin{array}{ccc} 0 & -\dot{\psi}_{v_i} & 0 \\ \dot{\psi}_{v_i} & 0 & 0 \\ 0 & 0 & 0 \end{array} \right] \left[\begin{array}{ccc} C(\psi_{v_{i-1}} - \psi_{v_i}) & -S(\psi_{v_{i-1}} - \psi_{v_i}) & 0 \\ S(\psi_{v_{i-1}} - \psi_{v_i}) & C(\psi_{v_{i-1}} - \psi_{v_i}) & 0 \\ 0 & 0 & 1 \end{array} \right] \underline{\vec{e}}^{i-1}, \\
&= \left[\begin{array}{c} V_{x_i} C(\psi_{v_{i-1}} - \psi_{v_i}) + V_{y_i} S(\psi_{v_{i-1}} - \psi_{v_i}) + (l_f + l_{fb} + L_a)\dot{\psi}_{v_i} S(\psi_{v_{i-1}} - \psi_{v_i}) \\ V_{y_i} C(\psi_{v_{i-1}} - \psi_{v_i}) - V_{x_i} S(\psi_{v_{i-1}} - \psi_{v_i}) + (l_f + l_{fb} + L_a)\dot{\psi}_{v_i} C(\psi_{v_{i-1}} - \psi_{v_i}) \\ 0 \end{array} \right]^T \underline{\vec{e}}^{i-1}.
\end{aligned} \tag{D.4}$$

The time derivative of direction cosine matrix $\underline{A}^{i,i-1}$ is written in the following way:

$$\dot{\underline{A}}^{i,i-1} = \left(\dot{\psi}_{v_{i-1}} - \dot{\psi}_{v_i} \right) \left[\begin{array}{ccc} -S(\psi_{v_{i-1}} - \psi_{v_i}) & -C(\psi_{v_{i-1}} - \psi_{v_i}) & 0 \\ C(\psi_{v_{i-1}} - \psi_{v_i}) & -S(\psi_{v_{i-1}} - \psi_{v_i}) & 0 \\ 0 & 0 & 0 \end{array} \right]. \tag{D.5}$$

The acceleration vector of point r_l can be determined as follows, where (D.5) is substituted for $\dot{\underline{A}}^{i,i-1}$:

$$\begin{aligned}
\dot{\vec{V}}_{v_l} &= \dot{\vec{V}}_{v_l} - \ddot{\vec{r}}_{v_l/v_i} \\
&= \dot{\vec{V}}_{v_l} - r_{v_l/v_i} {}^{iT}{}^i \dot{\underline{\omega}}^i \underline{A}^{i,i-1} \underline{\vec{e}}^{i-1} - r_{v_l/v_i} {}^{iT}{}^i \underline{\omega}^i \dot{\underline{A}}^{i,i-1} \underline{\vec{e}}^{i-1} + r_{v_l/v_i} {}^{iT}{}^i \underline{\omega}^i \underline{A}^{i,i-1} {}^{i-1} \underline{\vec{e}}^{i-1}, \\
&= \begin{bmatrix} \dot{V}_{x_i} C(\psi_{v_{i-1}} - \psi_{v_i}) + \dot{V}_{y_i} S(\psi_{v_{i-1}} - \psi_{v_i}) + V_{x_i} \dot{\psi}_v S(\psi_{v_{i-1}} - \psi_{v_i}) - V_{y_i} \dot{\psi}_v C(\psi_{v_{i-1}} - \psi_{v_i}) \\ \dot{V}_{y_i} C(\psi_{v_{i-1}} - \psi_{v_i}) - \dot{V}_{x_i} S(\psi_{v_{i-1}} - \psi_{v_i}) + V_{x_i} \dot{\psi}_v C(\psi_{v_{i-1}} - \psi_{v_i}) + V_{y_i} \dot{\psi}_v S(\psi_{v_{i-1}} - \psi_{v_i}) \\ 0 \end{bmatrix}^T \underline{\vec{e}}^{i-1} \\
&\quad - \begin{bmatrix} l_f + l_{fb} + L_a \\ 0 \\ 0 \end{bmatrix}^T \begin{bmatrix} 0 & -\ddot{\psi}_{v_i} & 0 \\ \ddot{\psi}_{v_i} & 0 & 0 \\ 0 & 0 & 0 \end{bmatrix} \begin{bmatrix} C(\psi_{v_{i-1}} - \psi_{v_i}) & -S(\psi_{v_{i-1}} - \psi_{v_i}) & 0 \\ S(\psi_{v_{i-1}} - \psi_{v_i}) & C(\psi_{v_{i-1}} - \psi_{v_i}) & 0 \\ 0 & 0 & 1 \end{bmatrix} \underline{\vec{e}}^{i-1} \\
&\quad - \begin{bmatrix} l_f + l_{fb} + L_a \\ 0 \\ 0 \end{bmatrix}^T \begin{bmatrix} 0 & -\dot{\psi}_{v_i} & 0 \\ \dot{\psi}_{v_i} & 0 & 0 \\ 0 & 0 & 0 \end{bmatrix} (\dot{\psi}_{v_{i-1}} - \dot{\psi}_{v_i}) \\
&\quad \begin{bmatrix} -S(\psi_{v_{i-1}} - \psi_{v_i}) & -C(\psi_{v_{i-1}} - \psi_{v_i}) & 0 \\ C(\psi_{v_{i-1}} - \psi_{v_i}) & -S(\psi_{v_{i-1}} - \psi_{v_i}) & 0 \\ 0 & 0 & 0 \end{bmatrix} \underline{\vec{e}}^{i-1} \\
&\quad + \begin{bmatrix} l_f + l_{fb} + L_a \\ 0 \\ 0 \end{bmatrix}^T \begin{bmatrix} 0 & -\dot{\psi}_{v_i} & 0 \\ \dot{\psi}_{v_i} & 0 & 0 \\ 0 & 0 & 0 \end{bmatrix} \begin{bmatrix} C(\psi_{v_{i-1}} - \psi_{v_i}) & -S(\psi_{v_{i-1}} - \psi_{v_i}) & 0 \\ S(\psi_{v_{i-1}} - \psi_{v_i}) & C(\psi_{v_{i-1}} - \psi_{v_i}) & 0 \\ 0 & 0 & 1 \end{bmatrix} \\
&\quad \begin{bmatrix} 0 & -\dot{\psi}_{v_{i-1}} & 0 \\ \dot{\psi}_{v_{i-1}} & 0 & 0 \\ 0 & 0 & 0 \end{bmatrix} \underline{\vec{e}}^{i-1}, \\
&= \begin{bmatrix} \dot{V}_{x_i} C(\psi_{v_{i-1}} - \psi_{v_i}) + \dot{V}_{y_i} S(\psi_{v_{i-1}} - \psi_{v_i}) + V_{x_i} \dot{\psi}_v S(\psi_{v_{i-1}} - \psi_{v_i}) - V_{y_i} \dot{\psi}_v C(\psi_{v_{i-1}} - \psi_{v_i}) \\ + (l_f + l_{fb} + L_a) \ddot{\psi}_v S(\psi_{v_{i-1}} - \psi_{v_i}) - (l_f + l_{fb} + L_a) \dot{\psi}_v^2 C(\psi_{v_{i-1}} - \psi_{v_i}) \\ \dot{V}_{y_i} C(\psi_{v_{i-1}} - \psi_{v_{i-1}}) - \dot{V}_{x_i} S(\psi_{v_{i-1}} - \psi_{v_i}) + V_{x_i} \dot{\psi}_v C(\psi_{v_{i-1}} - \psi_{v_i}) + V_{y_i} \dot{\psi}_v S(\psi_{v_{i-1}} - \psi_{v_i}) \\ + (l_f + l_{fb} + L_a) \ddot{\psi}_v C(\psi_{v_{i-1}} - \psi_{v_i}) + (l_f + l_{fb} + L_a) \dot{\psi}_v^2 S(\psi_{v_{i-1}} - \psi_{v_i}) \\ 0 \end{bmatrix}^T \underline{\vec{e}}^{i-1}. \tag{D.6}
\end{aligned}$$

As presented in equation (B.10), the lateral velocity error between two points can be written as follows:

$$\dot{y}_{el_i} = (\vec{V}_{v_l} - \vec{V}_{r_l}) \cdot \vec{e}_2^{i-1}. \tag{D.7}$$

Equation (D.2) and (D.4), can now be substituted into (D.7), this results in:

$$\begin{aligned}
\dot{y}_{el_i} &= V_{y_i} C(\psi_{v_{i-1}} - \psi_{v_i}) - V_{x_i} S(\psi_{v_{i-1}} - \psi_{v_i}) + (l_f + l_{fb} + L_a) \dot{\psi}_v C(\psi_{v_{i-1}} - \psi_{v_i}) \\
&\quad - \dot{\psi}_{v_{i-1}} (l_f + l_{fb} + L_a) C(\psi_{v_i} - \psi_{v_{i-1}}) - \dot{\psi}_{v_{i-1}} (l_r + l_{rb}) - V_{y_{i-1}}. \tag{D.8}
\end{aligned}$$

Based on (2.21), the lateral acceleration error can be obtained as follows:

$$\ddot{y}_{el_i} = (\dot{\vec{V}}_{v_l} - \dot{\vec{V}}_{r_l}) \cdot \vec{e}_2^{i-1} - (\vec{r}_{v_l} - \vec{r}_{r_l}) \cdot \dot{\psi}_{v_{i-1}}^2 \vec{e}_2^{i-1}. \tag{D.9}$$

Now, by substituting (D.3) and (D.6) into (D.9), the lateral acceleration error can be written as follows:

$$\begin{aligned}\ddot{y}_{el_i} &= \dot{V}_{y_i} C(\psi_{v_{i-1}} - \psi_{v_i}) + V_{y_i} \dot{\psi}_{v_i} S(\psi_{v_{i-1}} - \psi_{v_i}) - \dot{V}_{x_i} S(\psi_{v_{i-1}} - \psi_{v_i}) + V_{x_i} \dot{\psi}_{v_i} C(\psi_{v_{i-1}} - \psi_{v_i}) \\ &\quad + (l_f + l_{fb} + L_a) \ddot{\psi}_{v_i} C(\psi_{v_{i-1}} - \psi_{v_i}) + (l_f + l_{fb} + L_a) \dot{\psi}_{v_i}^2 S(\psi_{v_{i-1}} - \psi_{v_i}) \\ &\quad - \ddot{\psi}_{v_{i-1}} (l_f + l_{fb} + L_a) C(\psi_{v_{i-1}} - \psi_{v_i}) - \ddot{\psi}_{v_{i-1}} (l_r + l_{rb}) - \dot{V}_{y_{i-1}} - V_{x_{i-1}} \dot{\psi}_{v_{i-1}} - y_{el_i} \dot{\psi}_{v_{i-1}}^2.\end{aligned}\quad (\text{D.10})$$

The rotational errors are written in the following way:

$$\psi_{el_i} = \psi_{v_i} - \psi_{v_{i-1}}, \quad (\text{D.11})$$

$$\dot{\psi}_{el_i} = \dot{\psi}_{v_i} - \dot{\psi}_{v_{i-1}}, \quad (\text{D.12})$$

$$\ddot{\psi}_{el_i} = \ddot{\psi}_{v_i} - \ddot{\psi}_{v_{i-1}}. \quad (\text{D.13})$$

Next, the non-linear single-track vehicle model from Appendix A, (A.20) is presented, where i indicates the vehicle number:

$$\dot{V}_{y_i} = -\frac{1}{m} \left(C \delta_i C_f \tan \left(\frac{-V_{x_i} S \delta_i + (V_{y_i} + l_f \dot{\psi}_{v_i}) C \delta_i}{V_{x_i} C \delta_i + (V_{y_i} + l_f \dot{\psi}_{v_i}) S \delta_i} \right) + C_r \tan \left(\frac{V_{y_i} - l_r \dot{\psi}_{v_i}}{V_{x_i}} \right) \right) - V_{x_i} \dot{\psi}_{v_i}, \quad (\text{D.14})$$

$$\ddot{\psi}_{v_i} = -\frac{1}{I_z} \left(l_f C \delta_i C_f \tan \left(\frac{-V_{x_i} S \delta_i + (V_{y_i} + l_f \dot{\psi}_{v_i}) C \delta_i}{V_{x_i} C \delta_i + (V_{y_i} + l_f \dot{\psi}_{v_i}) S \delta_i} \right) - l_r C_r \tan \left(\frac{V_{y_i} - l_r \dot{\psi}_{v_i}}{V_{x_i}} \right) \right) \quad (\text{D.15})$$

The vehicle model can now be substituted into in (D.10) and (D.13), and based on (2.6), (i.e. the velocity error in the \vec{e}_1^{i-1} -direction is equal to zero which results in $V_{x_{i-1}} = V_{x_i}$) a non-linear model of the lateral and rotational dynamics is obtained. This is non-linear model is not presented here due to the large size of the model, which compromises the readability. This non-linear model can be linearized using a state vector and input vector are chosen as $\zeta_1 = [V_{y_{i-1}} \ \dot{\psi}_{v_{i-1}} \ V_{y_i} \ \dot{\psi}_{v_i}]^T$ and $\gamma_1 = [\delta_{i-1} \ \delta_i]^T$. A linear model of the lateral and rotational dynamics can be obtained by finding an equilibrium for \ddot{y}_{el_i} and $\ddot{\psi}_{el_i}$. The origin can also be used here as a linearization. Therefore, \ddot{y}_{el_i} and $\ddot{\psi}_{el_i}$ are linearized by choosing zero for all states (ζ_1) and inputs (γ_1) as a linearization point. Furthermore, linearization also relies on the assumption that all inputs will be small ($< 10^\circ$). Moreover, in Appendix A, (A.20) the linearized vehicle model is presented. The linearized vehicle model is a Linear Parametric Varying model (LPV), with V_{x_i} as varying parameter. A consequence of linearization is, that for the linearized vehicle model and thereby the model of the error dynamics to be valid, it is necessary that $\dot{V}_{x_i} = 0$. Due to the fact that the

longitudinal is constant for all vehicles it is $V_{x_i} = V_x$. Linearization of y_{el_i} results in the following:

$$\begin{aligned}
\ddot{y}_{el_i} &= \frac{\partial \ddot{y}_{el_i}}{\partial V_{y_i}} \Big|_{\substack{\zeta_1 = \underline{\alpha} \\ \gamma_1 = \underline{\alpha}}} \bar{V}_{y_i} + \frac{\partial \ddot{y}_{el_i}}{\partial \dot{\psi}_{v_i}} \Big|_{\substack{\zeta_1 = \underline{\alpha} \\ \gamma_1 = \underline{\alpha}}} \dot{\psi}_{v_i} + \frac{\partial \ddot{y}_{el_i}}{\partial V_{y_{i-1}}} \Big|_{\substack{\zeta_1 = \underline{\alpha} \\ \gamma_1 = \underline{\alpha}}} \bar{V}_{y_{i-1}} + \frac{\partial \ddot{y}_{el_i}}{\partial \dot{\psi}_{v_{i-1}}} \Big|_{\substack{\zeta_1 = \underline{\alpha} \\ \gamma_1 = \underline{\alpha}}} \dot{\psi}_{v_{i-1}} + \frac{\partial \ddot{y}_{el_i}}{\partial \delta_i} \Big|_{\substack{\zeta_1 = \underline{\alpha} \\ \gamma_1 = \underline{\alpha}}} \bar{\delta}_i \\
&\quad + \frac{\partial \ddot{y}_{el_i}}{\partial \delta_{i-1}} \Big|_{\substack{\zeta_1 = \underline{\alpha} \\ \gamma_1 = \underline{\alpha}}} \bar{\delta}_{i-1}, \\
&= - \left(\frac{C_f + C_r}{m \bar{V}_x} + \frac{(l_f + l_{fb} + L_a)(C_f l_f - C_r l_r)}{I_z \bar{V}_x} \right) \bar{V}_{y_i} \\
&\quad - \left(\frac{C_f l_f - C_r l_r}{m \bar{V}_x} + \frac{(l_f + l_{fb} + L_a)(C_f l_f^2 + C_r l_r^2)}{I_z \bar{V}_x} \right) \dot{\psi}_{v_i} \\
&\quad + \left(\frac{C_f + C_r}{m \bar{V}_x} + \frac{(l_f + l_{fb} + L_a)(C_f l_f - C_r l_r)}{I_z \bar{V}_x} + \frac{(l_r + l_{rb})(C_f l_f - C_r l_r)}{I_z \bar{V}_x} \right) \bar{V}_{y_{i-1}} \\
&\quad + \left(\frac{C_f l_f - C_r l_r}{m \bar{V}_x} + \frac{(l_f + l_{fb} + L_a)(C_f l_f^2 + C_r l_r^2)}{I_z \bar{V}_x} + \frac{(l_r + l_{rb})(C_f l_f^2 + C_r l_r^2)}{I_z \bar{V}_x} \right) \dot{\psi}_{v_{i-1}} \\
&\quad + C_f \left(\frac{1}{m} + \frac{l_f(l_f + l_{fb} + L_a)}{I_z} \right) \bar{\delta}_i - C_f \left(\frac{1}{m} + \frac{l_f(l_f + l_{fb} + L_a)}{I_z} + \frac{l_f(l_r + l_{rb})}{I_z} \right) \bar{\delta}_{i-1},
\end{aligned} \tag{D.16}$$

where \bar{V}_x is the longitudinal velocity for which $\dot{V}_x = 0$. When ψ_{el_i} is linearized the following result is obtained:

$$\begin{aligned}
\ddot{\psi}_{el_i} &= \frac{\partial \ddot{\psi}_{el_i}}{\partial V_{y_i}} \Big|_{\substack{\zeta_1 = \underline{\alpha} \\ \gamma_1 = \underline{\alpha}}} \bar{V}_{y_i} + \frac{\partial \ddot{\psi}_{el_i}}{\partial \dot{\psi}_{v_i}} \Big|_{\substack{\zeta_1 = \underline{\alpha} \\ \gamma_1 = \underline{\alpha}}} \dot{\psi}_{v_i} + \frac{\partial \ddot{\psi}_{el_i}}{\partial V_{y_{i-1}}} \Big|_{\substack{\zeta_1 = \underline{\alpha} \\ \gamma_1 = \underline{\alpha}}} \bar{V}_{y_{i-1}} + \frac{\partial \ddot{\psi}_{el_i}}{\partial \dot{\psi}_{v_{i-1}}} \Big|_{\substack{\zeta_1 = \underline{\alpha} \\ \gamma_1 = \underline{\alpha}}} \dot{\psi}_{v_{i-1}} + \frac{\partial \ddot{\psi}_{el_i}}{\partial \delta_i} \Big|_{\substack{\zeta_1 = \underline{\alpha} \\ \gamma_1 = \underline{\alpha}}} \bar{\delta}_i \\
&\quad + \frac{\partial \ddot{\psi}_{el_i}}{\partial \delta_{i-1}} \Big|_{\substack{\zeta_1 = \underline{\alpha} \\ \gamma_1 = \underline{\alpha}}} \bar{\delta}_{i-1}, \\
&= - \frac{C_f l_f - C_r l_r}{I_z \bar{V}_x} \bar{V}_{y_i} - \frac{C_f l_f^2 + C_r l_r^2}{I_z \bar{V}_x} \dot{\psi}_{v_i} + \frac{C_f l_f - C_r l_r}{I_z \bar{V}_x} \bar{V}_{y_{i-1}} + \frac{C_f l_f^2 + C_r l_r^2}{I_z \bar{V}_x} \dot{\psi}_{v_{i-1}} + \frac{C_f l_f}{I_z} \bar{\delta}_i \\
&\quad - \frac{C_f l_f}{I_z} \bar{\delta}_{i-1}.
\end{aligned} \tag{D.17}$$

Next, from linearized vehicle model the following relation, $\bar{V}_{y_i} = \bar{y}_i - \bar{V}_{x_2} \bar{\psi}_i$, can be substituted into (D.16) and (D.17), which results in:

$$\begin{aligned}
\ddot{\bar{y}}_{el_i} &= - \left(\frac{C_f + C_r}{m \bar{V}_x} + \frac{(l_f + l_{fb} + L_a)(C_f l_f - C_r l_r)}{I_z \bar{V}_x} \right) (\dot{\bar{y}}_{v_i} - V_x \dot{\bar{\psi}}_{v_i}) \\
&- \left(\frac{C_f l_f - C_r l_r}{m \bar{V}_x} + \frac{(l_f + l_{fb} + L_a)(C_f l_f^2 + C_r l_r^2)}{I_z \bar{V}_x} \right) \dot{\bar{\psi}}_{v_i} \\
&+ \left(\frac{C_f + C_r}{m \bar{V}_x} + \frac{(l_f + l_{fb} + L_a)(C_f l_f - C_r l_r)}{I_z \bar{V}_x} + \frac{(l_r + l_{rb})(C_f l_f - C_r l_r)}{I_z \bar{V}_x} \right) (\dot{\bar{y}}_{v_{i-1}} - \bar{V}_x \dot{\bar{\psi}}_{v_{i-1}}) \\
&+ \left(\frac{C_f l_f - C_r l_r}{m \bar{V}_x} + \frac{(l_f + l_{fb} + L_a)(C_f l_f^2 + C_r l_r^2)}{I_z \bar{V}_x} + \frac{(l_r + l_{rb})(C_f l_f^2 + C_r l_r^2)}{I_z \bar{V}_x} \right) \dot{\bar{\psi}}_{v_{i-1}} \\
&+ C_f \left(\frac{1}{m} + \frac{l_f(l_f + l_{fb} + L_a)}{I_z} \right) \bar{\delta}_i - C_f \left(\frac{1}{m} + \frac{l_f(l_f + l_{fb} + L_a)}{I_z} + \frac{l_f(l_r + l_{rb})}{I_z} \right) \bar{\delta}_{i-1}.
\end{aligned} \tag{D.18}$$

and

$$\begin{aligned}
\ddot{\bar{\psi}}_{el_i} &= - \frac{C_f l_f - C_r l_r}{I_z \bar{V}_x} (\dot{\bar{y}}_{v_i} - \bar{V}_x \dot{\bar{\psi}}_{v_i}) - \frac{C_f l_f^2 + C_r l_r^2}{I_z \bar{V}_x} \dot{\bar{\psi}}_{v_i} + \frac{C_f l_f - C_r l_r}{I_z \bar{V}_x} (\dot{\bar{y}}_{v_{i-1}} - \bar{V}_x \dot{\bar{\psi}}_{v_{i-1}}) \\
&+ \frac{C_f l_f^2 + C_r l_r^2}{I_z \bar{V}_x} \dot{\bar{\psi}}_{v_{i-1}} + \frac{C_f l_f}{I_z} \bar{\delta}_i - \frac{C_f l_f}{I_z} \bar{\delta}_{i-1}.
\end{aligned} \tag{D.19}$$

Next, the dynamics of the errors between the look-ahead point v_l and rear bumper r_l can be written as a function of the states of vehicle i and vehicle $i-1$. The errors at the look-ahead point are written in the following state vector $x_{el_i} = [\bar{y}_{el_i} \quad \dot{\bar{y}}_{el_i} \quad \bar{\psi}_{el_i} \quad \dot{\bar{\psi}}_{el_i}]^T$, equation (D.18) and (D.19) can be written in the following state space representation:

$$\dot{x}_{el_i} = A_{el} x_{el_i} - A_{v_{i-1}} x_{i-1} + B_{v_l} \bar{\delta}_i - B_{r_l} \bar{\delta}_{i-1},$$

where $\bar{\delta}_i$ is the input and $\bar{\delta}_{i-1}$ the exogenous disturbance to the system and

$$\begin{aligned}
A_{el} &= \begin{bmatrix} 0 & 1 & 0 & 0 \\ 0 & -\frac{\kappa_1 + \kappa_2}{V_x} & \kappa_1 + \kappa_2 & \frac{\kappa_1(l_{fb} + L_a) + \kappa_2(l_f + l_{fb} + L_a + l_r)}{V_x} \\ 0 & 0 & 0 & 1 \\ 0 & -\frac{C_f l_f - C_r l_r}{I_z \bar{V}_x} & \frac{C_f l_f - C_r l_r}{I_z} & \frac{C_f l_f(l_{fb} + L_a) - C_r l_r(l_f + l_{fb} + L_a + l_r)}{I_z \bar{V}_x} \end{bmatrix}, \\
A_{v_{i-1}} &= \begin{bmatrix} 0 & 0 & 0 & 0 \\ 0 & -(l_r + l_{rb}) \left(\frac{C_f l_f - C_r l_r}{I_z \bar{V}_x} \right) & (l_r + l_{rb}) \left(\frac{C_f l_f - C_r l_r}{I_z} \right) & -(l_r + l_{rb}) \left(\frac{C_f l_f^2 + C_r l_r^2}{I_z \bar{V}_x} \right) \\ 0 & 0 & 0 & 0 \\ 0 & 0 & 0 & 0 \end{bmatrix}, \\
B_{v_l} &= \begin{bmatrix} 0 \\ C_f \left(\frac{1}{m} + \frac{l_f(l_f + l_{fb} + L_a)}{I_z} \right) \\ 0 \\ \frac{C_f l_f}{I_z} \end{bmatrix}, B_{r_l} = \begin{bmatrix} 0 \\ C_f \left(\frac{1}{m} + \frac{l_f(l_f + l_{fb} + L_a + l_r + l_{rb})}{I_z} \right) \\ 0 \\ \frac{C_f l_f}{I_z} \end{bmatrix}, \\
\kappa_1 &= C_f \left(\frac{1}{m} + \frac{l_f(l_f + l_{fb} + L_a)}{I_z} \right) \quad \text{and} \quad \kappa_2 = C_r \left(\frac{1}{m} - \frac{l_r(l_f + l_{fb} + L_a)}{I_z} \right).
\end{aligned}$$

Appendix E

Time-domain simulation results of a lane change manoeuver

In this appendix, time-domain simulation results of a lane change manoeuver are presented for $\bar{V}_x = 15\text{m/s}$, $L_a = 2\text{m}$, duration of lane change manoeuver=8s and with and without the use of feedforward. Furthermore, time-domain simulation results of a lane change manoeuver are presented for $\bar{V}_x = 15\text{m/s}$, $L_a \in \mathcal{T}_1$, duration of lane change manoeuver=4s and with and without the use of feedforward.

Lane change with $\bar{V}_x = 15\text{m/s}$, $L_a = 2\text{m}$, duration manoeuvre=8s and without feed-forward

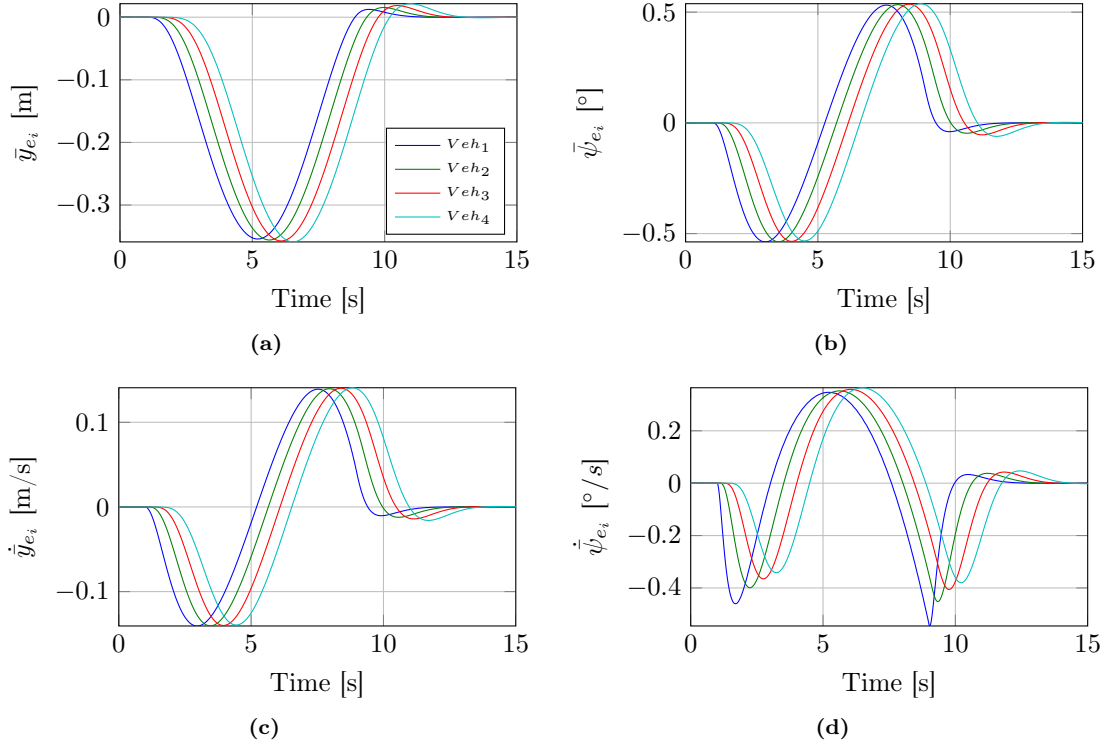


Figure E.1: Error responses of (4.16) when only feedback control is used for $\bar{V}_x = 15\text{m/s}$ and $L_a = 2\text{m}$.

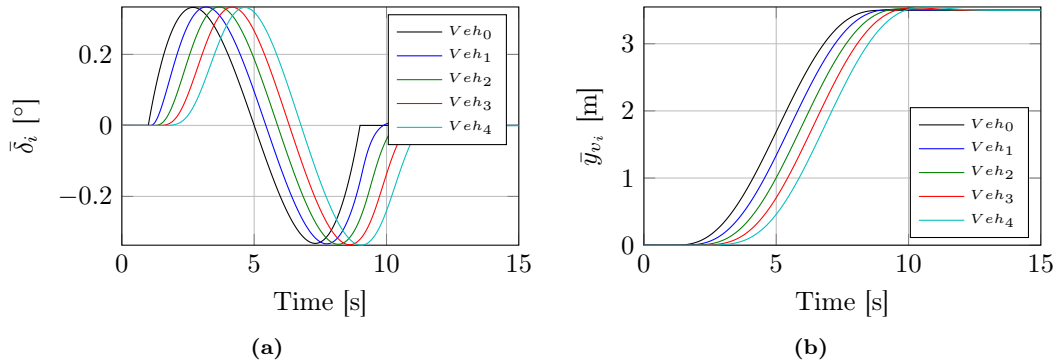


Figure E.2: (a) Control inputs. (b) Lateral global positions.

Lane change with $\bar{V}_x = 15\text{m/s}$, $L_a = 2\text{m}$, duration manoeuvre=8s and with feed-forward

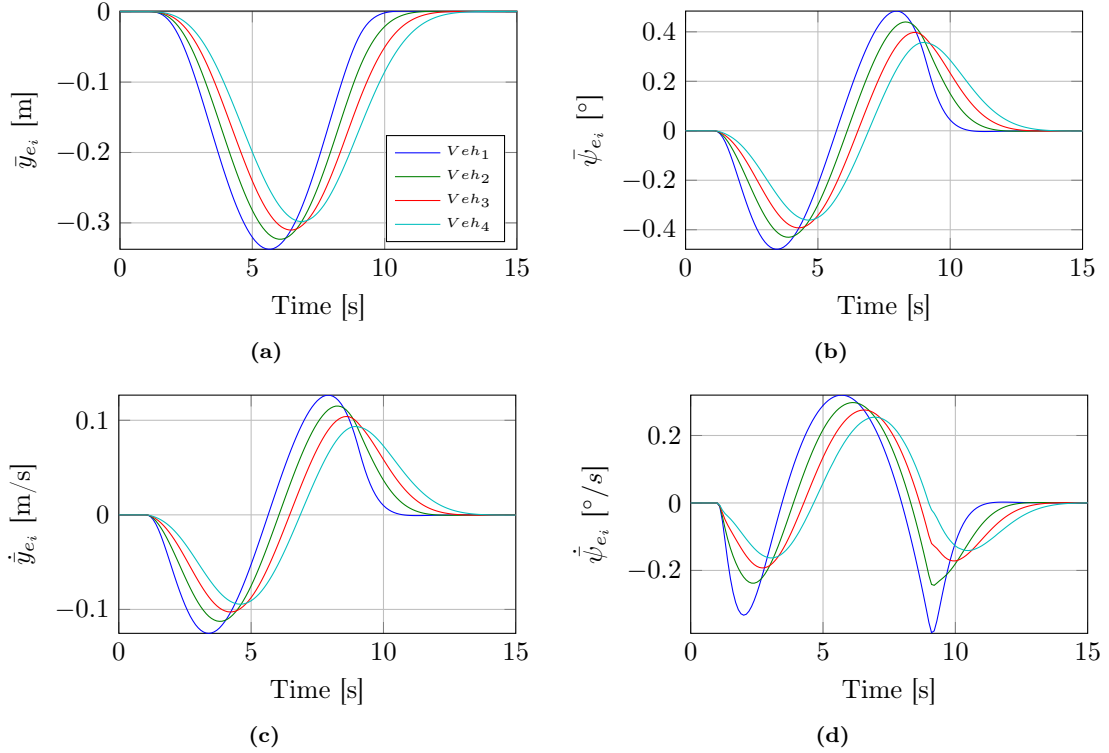


Figure E.3: Error responses of (4.16) when feedback and feed-forward control is used for $\bar{V}_x = 15\text{m/s}$ and $L_a = 2\text{m}$.

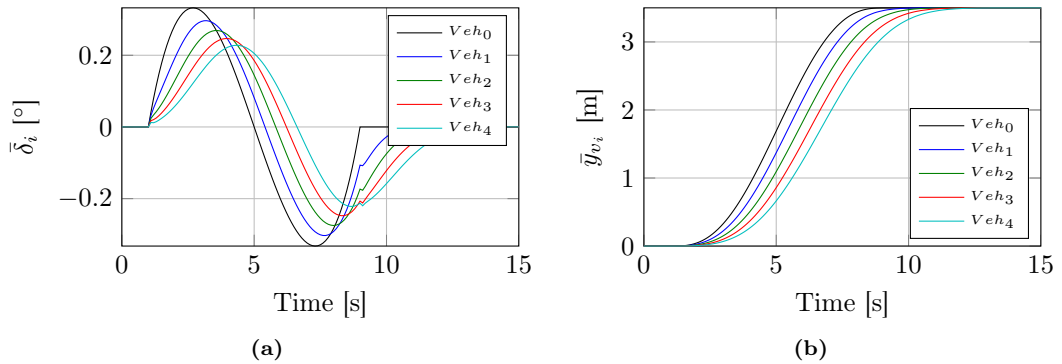


Figure E.4: (a) Control inputs. (b) Lateral global positions.

Lane change with $\bar{V}_x = 15\text{m/s}$, $L_a = 2\text{m}$, duration manoeuvre=4s and without feed-forward

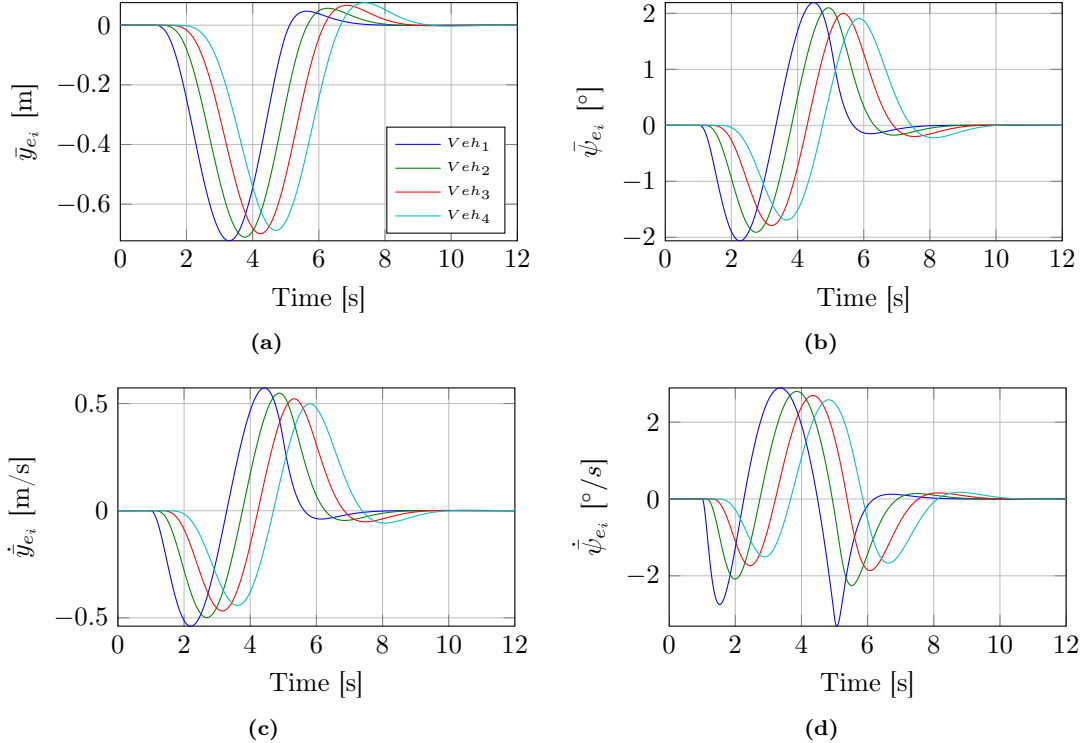


Figure E.5: Error responses of (4.16) when only feedback control is used for $\bar{V}_x = 15\text{m/s}$ and $L_a = 2\text{m}$.

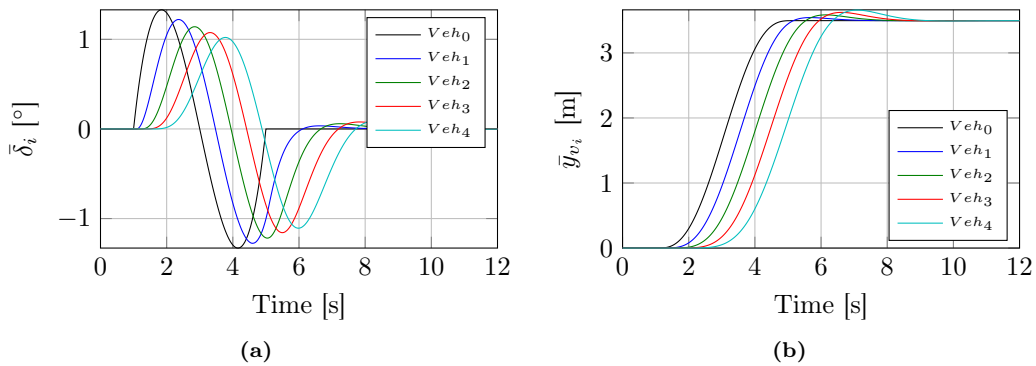


Figure E.6: (a) Control inputs. (b) Lateral global positions.

Lane change with $\bar{V}_x = 15\text{m/s}$, $L_a = 2\text{m}$, duration manoeuvre=4s and with feed-forward

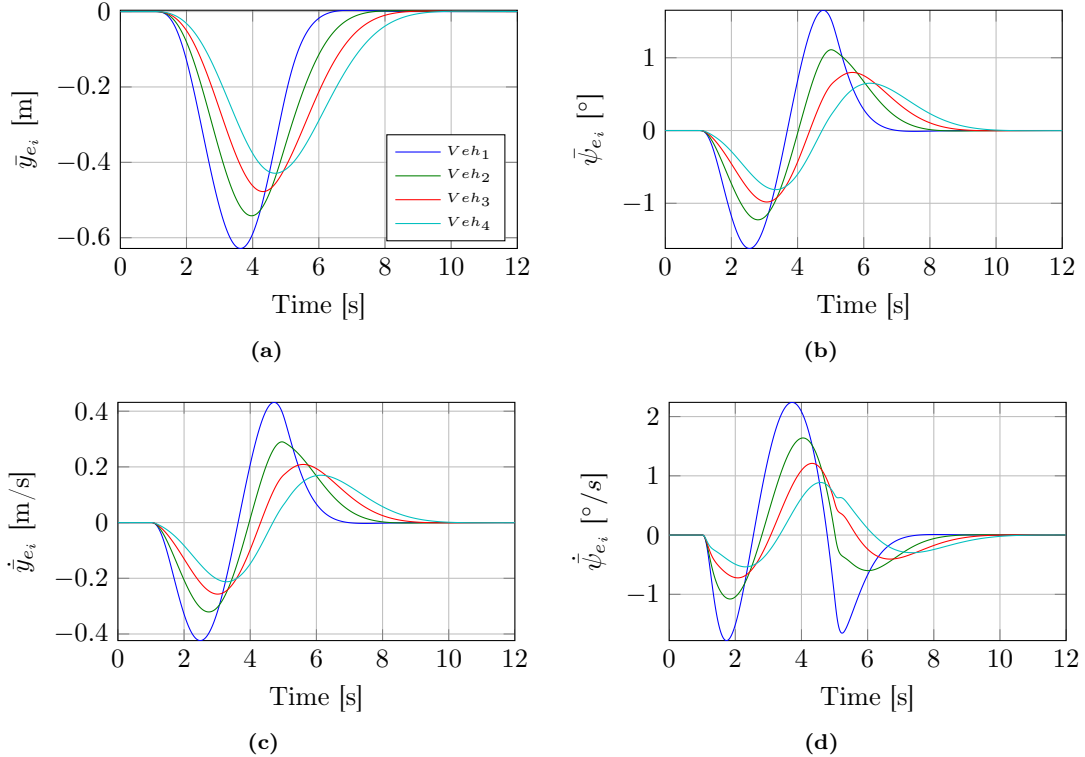


Figure E.7: Error responses of (4.16) when only feedback control is used for $\bar{V}_x = 15\text{m/s}$ and $L_a = 2\text{m}$.

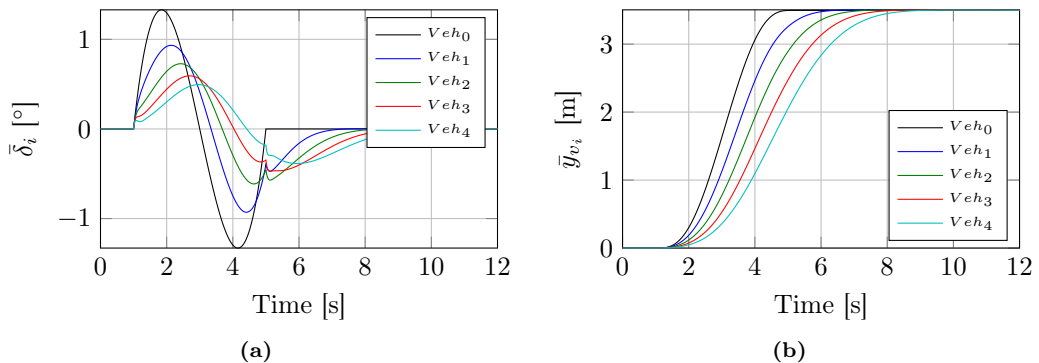


Figure E.8: (a) Control inputs. (b) Lateral global positions.

Lane change with $\bar{V}_x = 15\text{m/s}$, $L_a = 6\text{m}$, duration manoeuvre=4s and without feed-forward

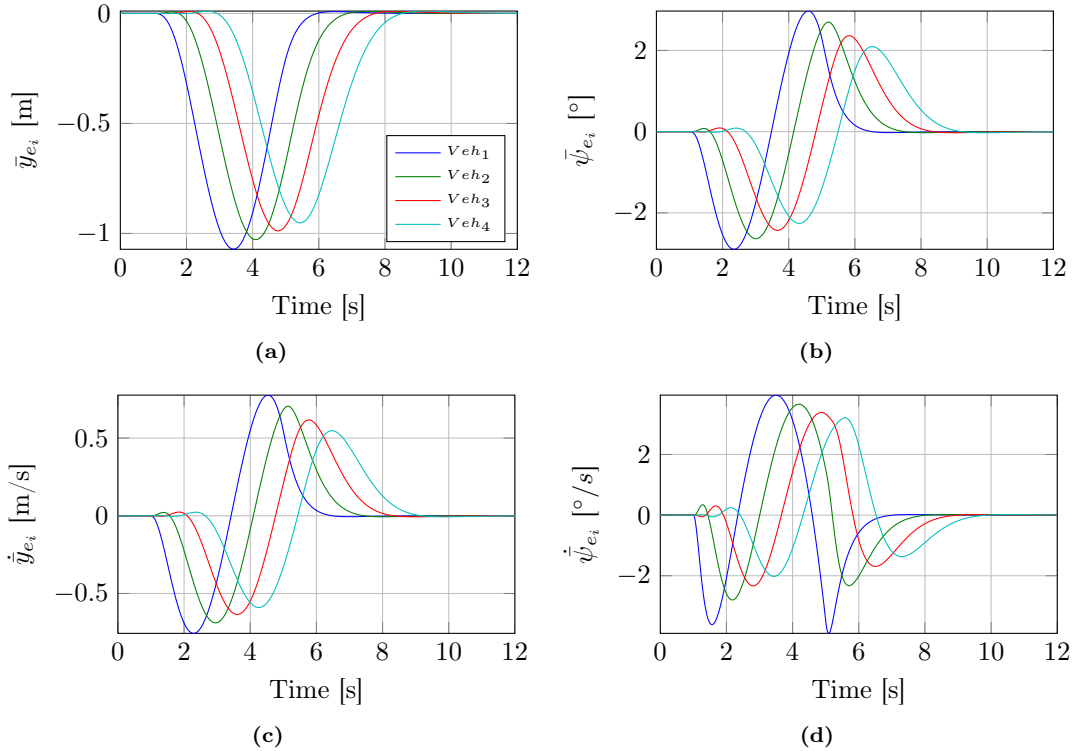


Figure E.9: Error responses of (4.16) when only feedback control is used for $\bar{V}_x = 15\text{m/s}$ and $L_a = 6\text{m}$.

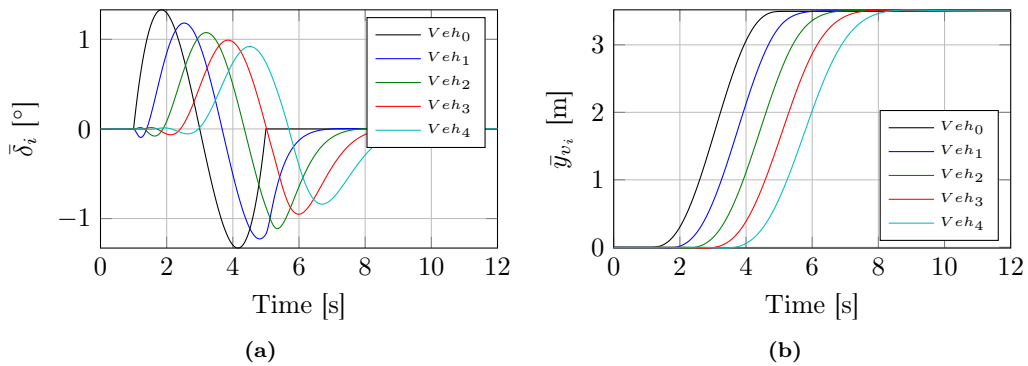


Figure E.10: (a) Control inputs. (b) Lateral global positions.

Lane change with $\bar{V}_x = 15\text{m/s}$, $L_a = 6\text{m}$, duration manoeuvre=4s and with feed-forward

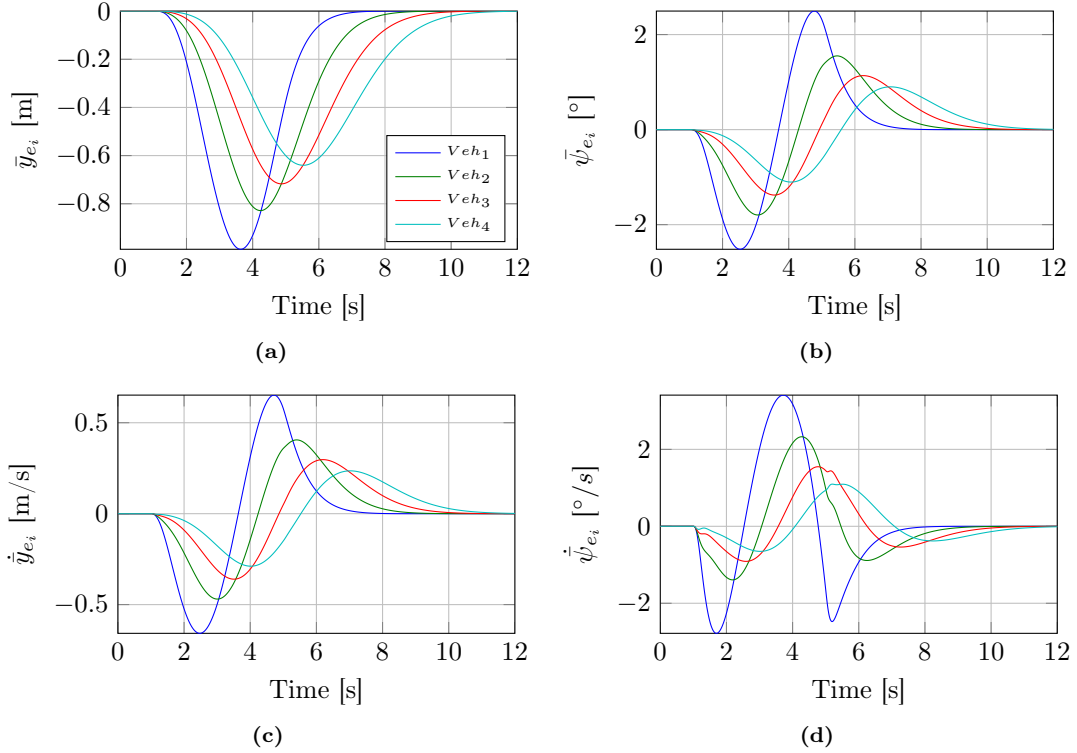


Figure E.11: Error responses of (4.16) when feedback and feed-forward control is used for $\bar{V}_x = 15$ and $L_a = 6$.

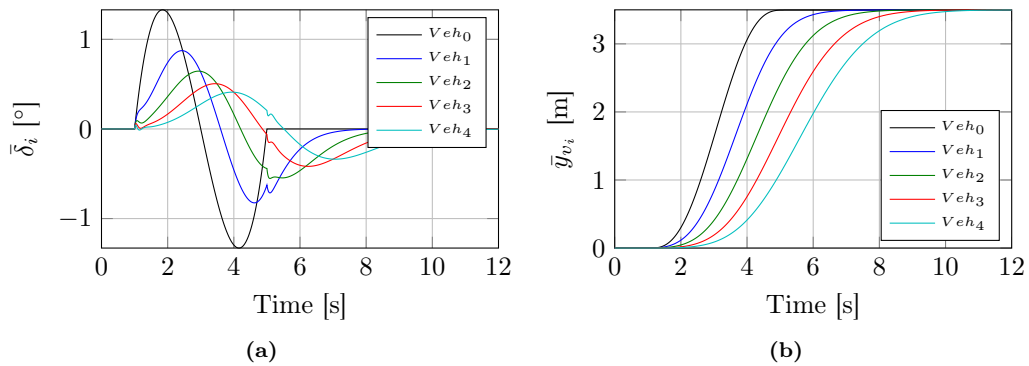


Figure E.12: (a) Control inputs. (b) Lateral global positions.

Lane change with $\bar{V}_x = 15\text{m/s}$, $L_a = 10\text{m}$, duration manoeuvre=4s and without feed-forward

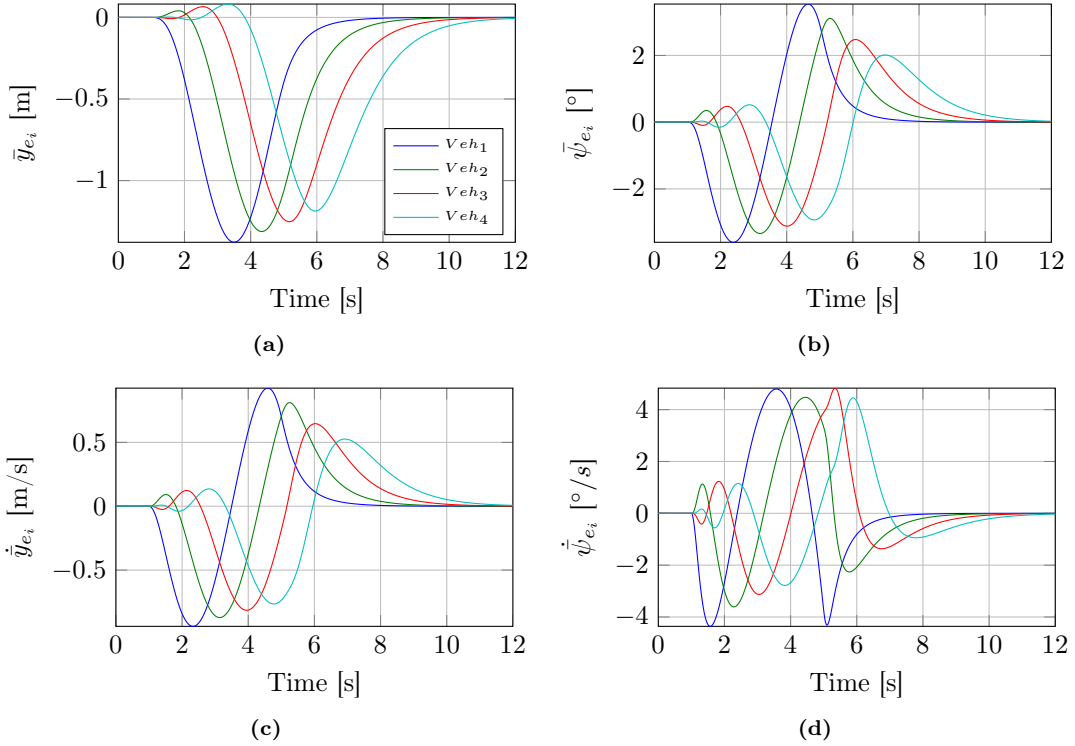


Figure E.13: Error responses of (4.16) when only feedback control is used for $\bar{V}_x = 15\text{m/s}$ and $L_a = 10\text{m}$.

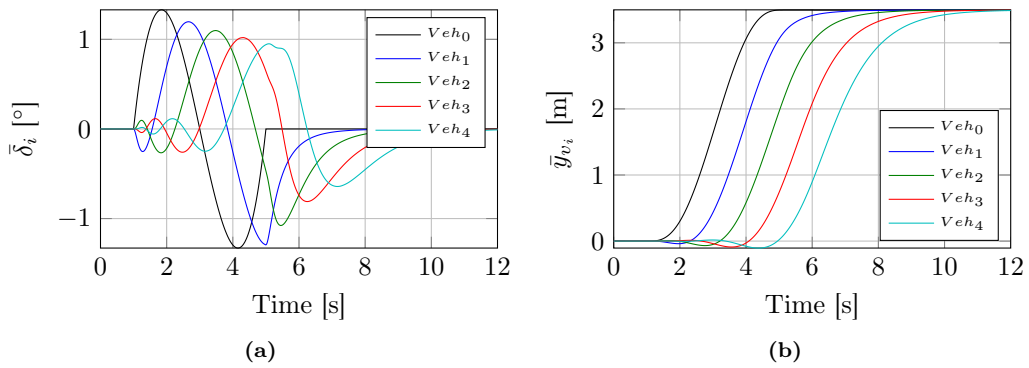


Figure E.14: (a) Control inputs. (b) Lateral global positions.

Lane change with $\bar{V}_x = 15\text{m/s}$, $L_a = 10\text{m}$, duration manoeuvre=4s and with feed-forward

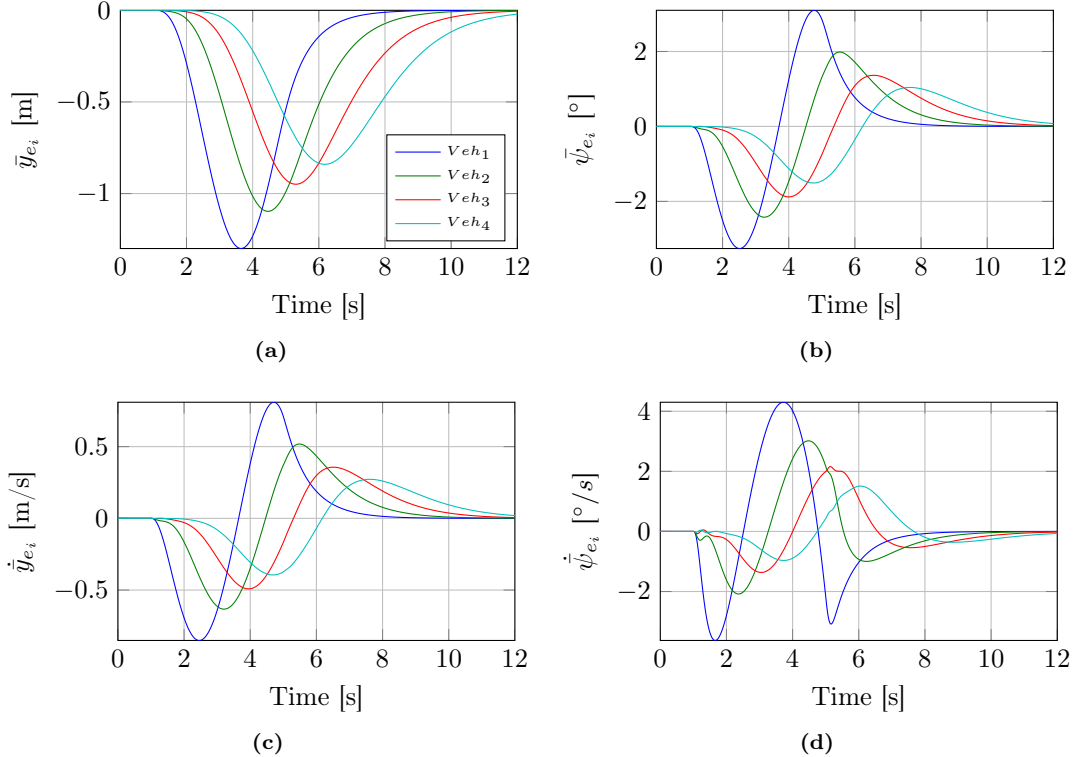


Figure E.15: Error responses of (4.16) when feedback and feed-forward control is used for $\bar{V}_x = 15\text{m/s}$ and $L_a = 10\text{m}$.

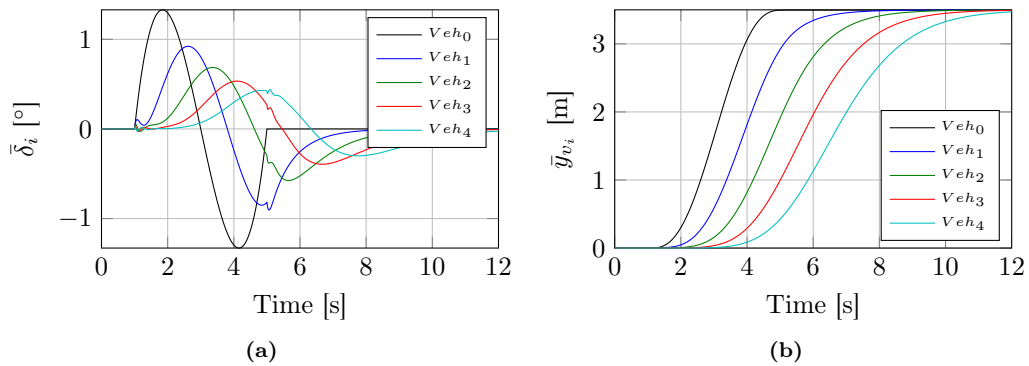


Figure E.16: (a) Control inputs. (b) Lateral global positions.